



City Research Online

City, University of London Institutional Repository

Citation: Gatcombe, C.P. (1990). Computer modelling of high resolution ultrasonic transducers. (Unpublished Doctoral thesis, City, University of London)

This is the accepted version of the paper.

This version of the publication may differ from the final published version.

Permanent repository link: <https://openaccess.city.ac.uk/id/eprint/28503/>

Link to published version:

Copyright: City Research Online aims to make research outputs of City, University of London available to a wider audience. Copyright and Moral Rights remain with the author(s) and/or copyright holders. URLs from City Research Online may be freely distributed and linked to.

Reuse: Copies of full items can be used for personal research or study, educational, or not-for-profit purposes without prior permission or charge. Provided that the authors, title and full bibliographic details are credited, a hyperlink and/or URL is given for the original metadata page and the content is not changed in any way.

COMPUTER MODELLING OF HIGH RESOLUTION ULTRASONIC TRANSDUCERS

by

**CHRISTOPHER PETER
GATCOMBE**

Thesis submitted for the degree of
DOCTOR OF PHILOSOPHY

Measurement and Instrumentation Centre
Department of Electrical, Electronic and Information Engineering
The City University
London
January 1990

Contents

	Page
<u>List of illustrations</u>	4
<u>Acknowledgements</u>	7
<u>Copyright declaration</u>	8
<u>Abstract</u>	9
<u>List of symbols</u>	10
1 <u>Introduction</u>	13
2 <u>Theory</u>	16
2.1 Continuous wave propagation in fluids.....	16
2.2 Plane- and edge-wave model.....	20
2.3 Pulsed wave propagation in fluids.....	21
2.4 Impulse response method.....	22
2.5 Transmit-receive mode.....	32
2.6 Resolution and its limitations.....	38
2.7 Non-uniform excitation.....	41
2.8 Finite-size targets.....	47
2.9 Off-axis finite-size targets.....	55
2.10 Transducers.....	59
2.10.1 Conventional uniformly-excited transducer.....	59
2.10.2 Non-uniformly-excited transducers.....	61
2.10.3 Non-uniform relationship between range and time.....	62
2.11 Application to solids.....	66
2.12 Computational methods.....	68
2.12.1 General details.....	68
2.12.2 Implementation of the equations on the computer.....	73
3 <u>Results</u>	75
3.1 Computed results for point targets.....	77

3.1.1	Velocity potential impulse responses.....	78
3.1.2	Spatial velocity potential impulse responses.....	82
3.1.3	Numerical visualisation of pressure waveforms.....	86
3.1.4	Directivity of edge waves.....	91
3.1.5	Transmit-receive waveforms.....	93
3.1.6	Transmit-receive beam profiles.....	97
3.2	Computed results for finite-size targets.....	102
3.2.1	0.8mm diameter target.....	102
3.2.2	4mm diameter target.....	106
3.2.3	Velocity potential impulse responses.....	109
3.3	Experimental results for point targets.....	111
3.3.1	Conventional transducer.....	113
3.3.2	Edge-wave-only transducer.....	115
3.3.3	Plane-wave-only transducer.....	120
3.4	Experimental results for finite-size targets.....	122
3.4.1	Flat targets.....	123
3.4.2	Cone-shaped targets.....	125
3.5	B-scan imaging results.....	140
4	<u>Discussion</u>	145
4.1	Resolution.....	145
4.2	Target size and front face shape.....	148
4.3	Non-uniform relationship between range and time.....	152
5	<u>Conclusions</u>	153
6	<u>Future work</u>	157
	<u>Appendix</u>	158
	<u>References</u>	163

List of illustrations

	Page
Fig (2.1.1) Geometry and pressure distribution for a circular source emitting cw.....	19
Fig (2.4.1) Geometry of a circular source and a point target at an arbitrary position in the field.....	25
Fig (2.4.2) Graphical derivation of the velocity potential impulse response, pressure impulse response and pressure in the field of a circular source.....	29
Fig (2.5.1) Graphical derivation of the transmit-receive echo responses of a target in the field of a circular source.....	35
Fig (2.5.2) Pressure and transmit-receive beam profiles.....	37
Fig (2.6.1) Axial pressure and transmit-receive waveforms for a circular transducer.....	40
Fig (2.7.1) Schematic diagram showing how source velocity profiles are built up by using plane wave contributions.....	44
Fig (2.7.2) Source velocity profiles.....	46
Fig (2.8.1) Schematic diagram for the finite-size target scattering medium.....	48
Fig (2.9.1) Geometry of a circular source and a finite-size target at an arbitrary position in the field.....	56
Fig (2.10.1.1) Schematic diagram of transducer construction.....	60
Fig (2.10.3.1) Range and time relationships.....	64
Fig (2.10.3.2) Target depth and positional error.....	65
Fig (2.12.1.1) Schematic diagram of cone-shaped target.....	72
Fig (3.1.1.1) Velocity potential impulse response for point targets.....	81
Fig (3.1.2.1) Spatial velocity potential impulse response for conventional transducer.....	84
Fig (3.1.2.2) Spatial velocity potential impulse responses for non-uniformly-excited transducers.....	85
Fig (3.1.3.1) Numerical visualisation of a pulse radiated by a conventional transducer.....	88

Fig (3.1.3.2)	Numerical visualisation of a pulse radiated by an edge-wave-only transducer.....	89
Fig (3.1.3.3)	Numerical visualisation of a pulse radiated by a plane-wave-only transducer.....	90
Fig (3.1.4.1)	Calculated edge wave directivity pattern.....	92
Fig (3.1.5.1)	Transmit-receive waveforms for point targets.....	96
Fig (3.1.6.1)	Transmit-receive beam profiles for point targets.....	100,101
Fig (3.2.1.1)	Transmit-receive impulse responses for 0.8mm target.....	104
Fig (3.2.1.2)	Transmit-receive waveforms for 0.8mm target.....	105
Fig (3.2.2.1)	Transmit-receive impulse responses for 4mm target...	107
Fig (3.2.2.2)	Transmit-receive waveforms for 4mm target.....	108
Fig (3.2.3.1)	Velocity potential impulse responses for 0.8mm target.....	110
Fig (3.2.3.2)	Velocity potential impulse responses for 4mm target.....	110
Fig (3.3.1.1)	Calculated and measured transmit-receive waveforms for a 0.8mm point-like target.....	114
Fig (3.3.2.1)	Measured and calculated transmit-receive waveforms for point target and edge-wave-only transducer, on axis.....	116
Fig (3.3.2.2)	Measured and calculated transmit-receive waveforms for point target and edge-wave-only transducer, off axis.....	117
Fig (3.3.2.3)	Calculated transmit-receive beam profiles for point target and edge-wave-only transducer.....	118
Fig (3.3.2.4)	Measured transmit-receive beam profiles for point target and edge-wave-only transducer.....	119
Fig (3.3.3.1)	Measured and calculated transmit-receive waveforms for point target and plane-wave-only transducer.....	121
Fig (3.4.1.1)	Measured and calculated transmit-receive waveforms for 4mm flat target and conventional transducer.....	124
Fig (3.4.2.1)	Measured and calculated transmit-receive waveforms for 2mm axial cone-shaped targets, at 35mm range.....	128,129

Fig (3.4.2.2)	Measured and calculated transmit-receive waveforms for 2mm axial cone-shaped targets, at 120mm range.....	130,131
Fig (3.4.2.3)	Measured and calculated transmit-receive waveforms for 4mm axial cone-shaped targets, at 35mm range.....	132,133
Fig (3.4.2.4)	Measured and calculated transmit-receive waveforms for 4mm axial cone-shaped targets, at 120mm range.....	134,135
Fig (3.4.2.5)	Measured and calculated transmit-receive waveforms for 10mm axial cone-shaped targets, at 35mm range.....	136,137
Fig (3.4.2.6)	Measured and calculated transmit-receive waveforms for 10mm axial cone-shaped targets, at 120mm range.....	138,139
Fig (3.5.1)	B-scans of an array of nylon threads.....	142
Fig (3.5.2)	B-scans of a metal block with holes.....	144

Acknowledgements

I am indebted to Dr. J.P. Weight for his encouragement and advice, to Professor A.F. Brown for his comments on the manuscript.

The modelling work described in this thesis formed part of an on-going research programme to design, manufacture and evaluate new types of ultrasonic transducer. I would like to thank Dr. R. Brittain for his work in designing the new transducers based on the modelling results described here, and Dr. S. McLaren for his help in evaluating the new transducers, and comparing experimentally obtained results with calculated results obtained using the modelling.

Financial support was provided by the Science and Engineering Research Council, grant number GR/B/9289.8.

Copyright declaration

I grant powers of discretion to the University Librarian to allow this thesis ("Computer modelling of high resolution ultrasonic transducers") to be copied in whole or in part without further reference to me. This permission covers only single copies made for study purposes, subject to normal conditions of acknowledgement.

Abstract

A model for the propagation of ultrasonic pulses in fluids using a conventional circular transducer is discussed, and it is shown that diffraction effects limit the range and lateral resolution of such pulse-echo systems. The variation in amplitude and shape of the echo responses which result, can make interpretation of the results difficult.

The diffraction effects are explained in terms of a model which sees a circular transducer as a piston source radiating a direct plane wave in the geometric region straight ahead of the source, together with diffracted toroidal waves from the edge of the source.

An impulse response method is used to make calculations of the echo waveforms reflected from point targets. The forms of the echo responses are used to demonstrate the effects of diffraction on the overall resolution of the transducer. The impulse response method is extended so that the echo response from any arbitrary geometry targets, including non-planar, can be modelled.

New high-resolution transducers are designed to overcome some of the limitations due to the diffraction effects, by radiating either solely plane waves, or solely edge waves, in a non-uniform manner across the transducer's surface. The results show that such non-uniformly excited transducers have both improved resolution and simpler field structures than conventional transducers.

List of symbols

a	Transducer radius
$c, \Delta c$	Speed of sound, or its change
$e(t)$	Transmit-receive echo waveform
$e_i(t)$	Transmit-receive echo impulse response
$e_{it}(\underline{r}, t)$	Transmit-receive echo "impulse response" for finite-size target
$e_t(t)$	Transmit-receive echo waveform for finite- size target
K	Arbitrary constant
$P(\underline{r}, t)$	Pressure waveform
$P_i(\underline{r}, t)$	Pressure impulse response
$P_{in}(\underline{r}, t)$	Incident pressure waveform
$P_{sc}(\underline{r}, t)$	Scattered pressure waveform
\underline{r}	General point in space
S	General surface
t	Time
T	Radius of a finite-size target
$u(t), U(\omega)$	Transducer velocity
V	General volume
y	Y-axis
y_0	Axial separation of target from transducer
z	Z-axis
z_0	Target range
$Z, \Delta Z$	Specific acoustic impedance, or its change
$\rho, \Delta\rho$	Density, or its change
$\phi(\underline{r}, t), \phi(\underline{r}, \omega)$	General velocity potential
$\phi_i(\underline{r}, t)$	Velocity potential impulse response

$$\frac{\partial \phi(\underline{r}, t)}{\partial t}$$

"Impulse response" of medium

$$\frac{\partial \phi(\underline{r}, t)}{\partial z}$$

Spatial "impulse response" of medium

ω

Angular frequency

COMPUTER MODELLING OF HIGH RESOLUTION
ULTRASONIC TRANSDUCERS

1 INTRODUCTION

Ultrasonic pulse-echo techniques are widely used as a means of quality control of products as well as in-service inspection of machinery. In medicine, ultrasound is used to image bodily organs. These applications of non-destructive evaluation (NDE) require transducers of high quality to transmit and receive pulses of ultrasound.

The target resolution of the transducer being used must be high enough to discriminate between two targets which are close together. By "resolution", two types of resolution are actually meant: range resolution and lateral resolution, which refer to the transducer's discrimination ability either along, or perpendicular to, the transducer's axis, respectively. Conventional transducers suffer from both poor range resolution, and poor lateral resolution, as will be explained later. If the ultrasonic pulses are continuous waves (cw) then variations in amplitude occur throughout the field due to diffraction effects. Ultrasonic techniques now require shorter pulses to be emitted, in order to improve the range resolution. Whereas with cw, the diffraction effects could be explained using classic, steady-state cw theory, with short pulses this is no longer true. Impulse response methods have recently been developed, which provide a general theory for arbitrary motion of the transducer. This theory forms the basis of all the modelling work described in this thesis.

A prerequisite of good range resolution is for the transducer to be able to emit short pulses, ie. it must be a wideband device. An added advantage of using a wideband transducer is that it makes measuring frequency dependent effects such as attenuation easier. This

is because the frequency spectrum of the received signal can be instantly displayed on a spectrum analyser. Changing the conditions under test produces an instant change in the frequency spectrum. In most systems it is the transducer which limits the bandwidth.

New types of non-uniformly excited transducers have been developed which reduce the diffraction effects and so improve both the range resolution and lateral resolution.

This thesis describes my part of the work of an on-going research group. My work was to provide computer models of various transducer and target configurations based on the impulse response method, so that improved transducers could be designed. It fell to my colleagues, Dr. R. Brittain, to produce the new transducers, and Dr. S. McLaren, to compare their performance with my predicted results. The impulse response method is reviewed and it is shown how it is used to model the behaviour of conventional transducers interrogating point targets in fluids. The impulse response method is extended to cater for non-uniformly excited types of transducer, and also to allow for larger planar (flat-faced) targets. A simple extension to the model is introduced, to enable targets with non-planar (pointed) faces to be included in the modelling.

Chapter 2 starts by describing the theory of continuous and pulsed wave propagation in fluids for point targets in terms of plane and edge waves, and the impulse response method is introduced. The theory for finite-sized targets on the axis of a transducer is also described, and its extension for off-axis targets is presented. There then follows a section on the construction of the transducers described, in terms of radiating plane waves only or edge waves only,

and the non-uniform relationship between range and time which exists for edge-wave-only transducers. Chapter 2 finishes with two sections on the application of the fluid model to solids, and computational methods.

The results section, chapter 3, is essentially divided into three parts. The first part contains computed results from the modelling, assuming ideal conditions. The second part contains experimental results and computed results obtained for the purpose of comparison. The third part shows B-scan images of some test targets, included to show how transducers perform under more realistic testing situations.

Chapters 4 and 5 discuss the results and some conclusions are drawn, and then chapter 6 describes how this work could be extended in future.

2 Theory

2.1 Continuous-wave propagation in fluids

There is a wide body of literature (for example Rayleigh, 1896, chapters 11 and 14, and Hunter, 1957, chapter 4) which deals with the theory of propagation of acoustic waves. The waves in question are mostly treated as being simple harmonic waves, or continuous waves extending to infinity.

The usual mathematical simplification is used, whereby irrotational vector quantities are expressed as the gradient of a single scalar potential, which is then differentiated to produce the vector components. Thus the vector particle velocity \underline{v} is given in terms of a velocity potential ϕ :-

$$\underline{v} = - \nabla \phi . \quad (2.1.1)$$

The instantaneous pressure at a point in the field is then given by:-

$$P(\underline{r}, t) = \rho \frac{\partial \phi}{\partial t} . \quad (2.1.2)$$

where ρ is the density of the medium. The velocity potential ϕ is the solution of the wave equation:-

$$\nabla^2 \phi = - \frac{1}{c^2} \frac{\partial^2 \phi}{\partial t^2} . \quad (2.1.3)$$

Rayleigh (1896) showed that a solution of eqn. (2.1.3) for the case of a perfectly rigid piston source in an infinite baffle is:-

$$\phi = - \frac{1}{2\pi} \int_S u(t) \frac{ds}{r} , \quad (2.1.4)$$

where r is the point in the field, S is the source surface, c is the speed of sound in the medium, and $u(t) = e^{j\omega(t - r/c)}$ is the

velocity of the source. This equation has become known as the Rayleigh integral.

Other assumptions that Rayleigh used to obtain eqn. (2.1.4) are that the fluid medium is homogeneous, there is no vortex motion, displacements are small, and that there is no net loss or gain of fluid in the given volume.

Physically, the Rayleigh integral represents Huygens' principle, which says that each point on the source acts as a tiny point source contributing a hemispherical wave. The field at an arbitrary point is given by the superposition of these waves.

As is the case for optical diffraction, the cw sound field is divided into two regions. The near-field region (Fresnel region) is characterised by interference effects which give rise to large amplitude changes. The far-field region (Fraunhofer region) is smoother and more uniform.

In general, eqn. (2.1.4) can only be integrated analytically for a few special cases. For instance, on the axis of a circular source excited by cw (figure (2.1.1a)), eqn. (2.1.4) can be solved (Hunter, 1957 and Kinsler and Frey, 1962) to obtain the intensity, and hence pressure distribution, which is of the form:-

$$P = P_{\max} \sin \left[(\pi/\lambda) (\sqrt{a^2 + z^2}) - z \right], \quad (2.1.5)$$

where a is the source radius, λ is the wavelength of the sound and z is the axial distance from the source. This is shown plotted in figure (2.1.1b). A simple derivation using the existence of plane and edge waves will be shown later, in section 2.4.

Off-axis, in the far-field, it can be shown (Kinsler and Frey,

1962) that the pressure varies with angle from the centre of the source in the form of a Bessel function:-

$$P = P_{\max} \frac{J_1(x)}{x} \quad (2.1.6)$$

where $x = ka \sin(\theta)$, $k = 2\pi/\lambda$, and θ is the angle subtended at the transducer's centre.

As mentioned above, integral expressions for velocity potential (and hence pressure) such as eqn. (2.1.4) cannot be integrated analytically. By using suitable approximations such as assuming the source is much larger than the wavelength of the sound, and the position of the point of interest is further away than the size of the source, numerical solutions to these equations can be made. Because of the assumptions made, such solutions are only valid in the far-field of the source.

Zemanek (1971) has shown that it is possible to numerically integrate such equations without approximations, to obtain numerical values for the pressure, which are valid in both the near- and far-field.

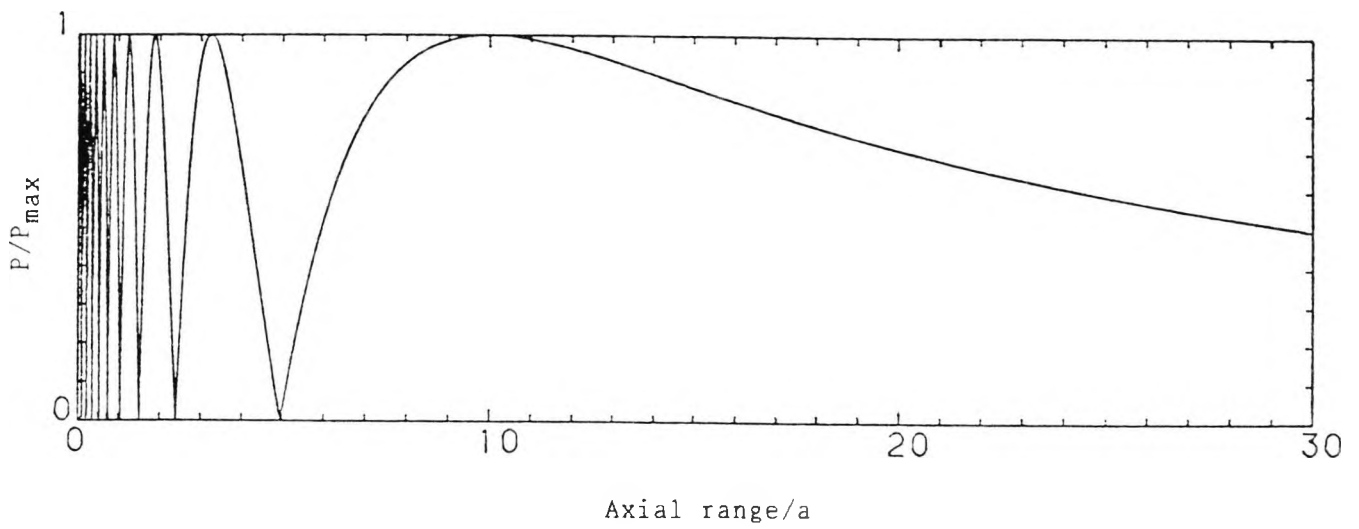
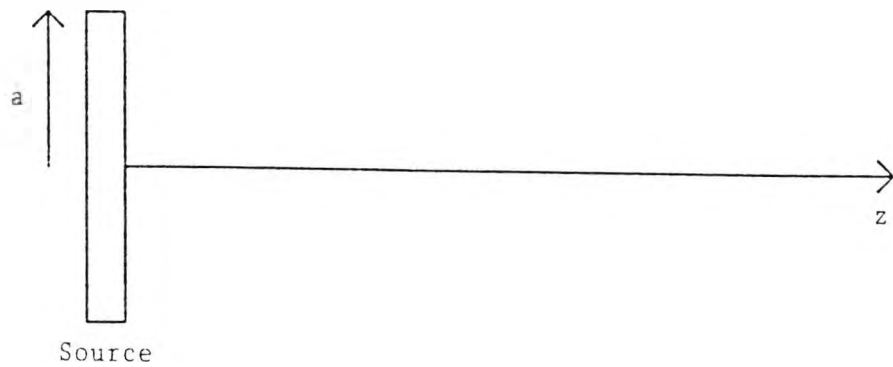


Figure (2.1.1): a: Geometry of a circular source emitting cw.
 b: Axial pressure distribution for same source ($a=10\lambda$).

2.2 Plane- and edge-wave model

Pursuing the optical analogy, the diffraction theory of Thomas Young (1802) explains diffraction fringes as being produced by the interaction of a diverging wave from the edge of the aperture (an edge wave) and the direct wave from the middle of the aperture.

Dehn (1960) shows how Schoch separated the Rayleigh integral into two parts. One of these has the form of a plane wave, while the other depends on the distance from the piston edge, and is called the disturbing, or edge wave.

Dehn discusses how radiation from a circular source can be represented by three 'rays' passing through the field point. One proceeds perpendicularly from the piston face (the "plane wave" contribution), and one from each of the extreme edge points (the "edge wave" contribution). With cw excitation of the source, these rays interfere with one another to produce the amplitude fluctuations described by eqns. (2.1.5) and (2.1.6). In the geometric region straight ahead of the source, all three rays interfere with one another, producing a complicated field structure. Outside the geometric region, only the two edge rays can interfere with each other, forming side lobes. In the near field, the path difference between the rays can be several wavelengths, so there are rapid changes of amplitude with field point position. The fluctuations are less rapid in the far field because the path differences change more slowly with range than in the near field. Experimental confirmation of this has been shown by Weight and Restori (1986), using a stroboscopic schlieren system to visualise pulses propagating in water (Hayman 1977).

2.3 Pulsed wave propagation in fluids

With continuous wave propagation, we are concerned with the steady-state distribution of the field. With pulsed wave propagation other factors are also of interest such as short pulse length and pulse shape.

In order to obtain the full transient solution giving the time waveforms of pressure at any point in the field, it is necessary to solve Rayleigh's integral, eqn. (2.1.4) in terms of an arbitrary motion of the source. As Rayleigh has treated the case for harmonic motion of the source, due to the Fourier theorem, Rayleigh's results can also be used for arbitrary motion of the source. This can be done in theory by harmonic synthesis from the steady-state continuous wave solution - if there is one.

Beaver (1971) has shown that it is possible to numerically integrate the Rayleigh integral, for arbitrary motion of the source. Such techniques have since led to the development of an impulse response method most prominently by Stepanishen (1971a, 1971b), which allows the Rayleigh integral to be solved for an impulsive source motion, and this result is then convolved with the actual motion of the source to obtain the pressure waveform. This is explained more fully in the next section.

Detailed numerical calculations of a source radiating a short pulse into a fluid will be shown in section 3.1.3.

2.4 Impulse response method

Impulse response methods have been developed (Stepanishen, 1971b) whereby the pressure due to an impulsive motion of the source can be calculated. This has the advantage that the theory of linear (time invariant) systems may be used, the pressure due to an arbitrary transducer motion being obtained by convolution.

The Rayleigh integral of eqn. (2.1.4) can be written in the form:-

$$\phi(\underline{r}, t) = \int_S \frac{u_n(\underline{r}, t)}{2\pi r} ds, \quad (2.4.1)$$

where \underline{r} is the point in the field, S is the source surface, and $u_n(\underline{r}, t)$ is the (arbitrary) motion of the source, normal to the source surface.

The pressure is then given by:-

$$P(\underline{r}, t) = \rho \frac{\partial}{\partial t} \int_S \frac{u_n(\underline{r}, t)}{2\pi r} ds. \quad (2.4.2)$$

If the source velocity is expressed as:-

$$u_n(\underline{r}, t) = u(t - r/c), \quad (2.4.3)$$

or as a convolution integral:-

$$u_n(\underline{r}, t) = \int_{-\infty}^{\infty} u(\tau) \delta(t - r/c - \tau) d\tau, \quad (2.4.4)$$

where $\delta(t - r/c - \tau)$ represents a delta function, and τ the dummy integration variable of the convolution, then eqn. (2.4.1) becomes:-

$$\phi(\underline{r}, t) = \int_{-\infty}^{\infty} u(\tau) \int_S \frac{\delta(t - r/c - \tau)}{2\pi r} ds d\tau . \quad (2.4.5)$$

As this is in the form of a convolution integral, it can be simplified as:-

$$\phi(\underline{r}, t) = u(t) * \phi_i(\underline{r}, t) , \quad (2.4.6)$$

where

$$\phi_i(\underline{r}, t) = \int_S \frac{\delta(t - r/c)}{2\pi r} ds , \quad (2.4.7)$$

and the symbol '*' denotes the convolution operation. Eqn. (2.4.7) represents the velocity potential impulse response due to an impulsive motion of the source. $\phi_i(\underline{r}, t)$ has been expressed simply by Stepanishen (1971b):-

$$\phi_i(\underline{r}, t) = c\Omega/2\pi . \quad (2.4.8)$$

Ω represents the angle of the equidistant circular arc which is projected from the field point on to the source surface, as shown in figure (2.4.1). This circular arc passes through all points on the source surface which are at an equal distance ct from the field point. Ω is therefore proportional to the length of the arc which actually lies on the source surface. Hence to calculate the velocity potential impulse response, $\phi_i(\underline{r}, t)$ at an arbitrary field point position and time, a simple geometric expression can be used. An analytic expression (in cylindrical co-ordinates) for Ω was first given by Miles (1953), although Oberhettinger (1963) and Stepanishen (1971b) have also derived expressions in cartesian co-ordinates, and these are conveniently tabulated by Robinson et. al. (1974):-

$$\Omega = \cos^{-1} \left[\frac{c^2 t^2 - z_0^2 + y_0^2 - a^2}{2 y_0 \sqrt{(c^2 t^2 - z_0^2)}} \right] . \quad (2.4.9)$$

Thus, the velocity potential impulse response eqn. (2.4.8) becomes:-

$$\phi_i(\underline{r}, t) = \frac{c}{2\pi} \cos^{-1} \left[\frac{c^2 t^2 - z_0^2 + y_0^2 - a^2}{2 y_0 \sqrt{(c^2 t^2 - z_0^2)}} \right] . \quad (2.4.10)$$

Note that Robinson actually gives expressions for θ , but here Ω is used, where $\Omega = 2\theta$.

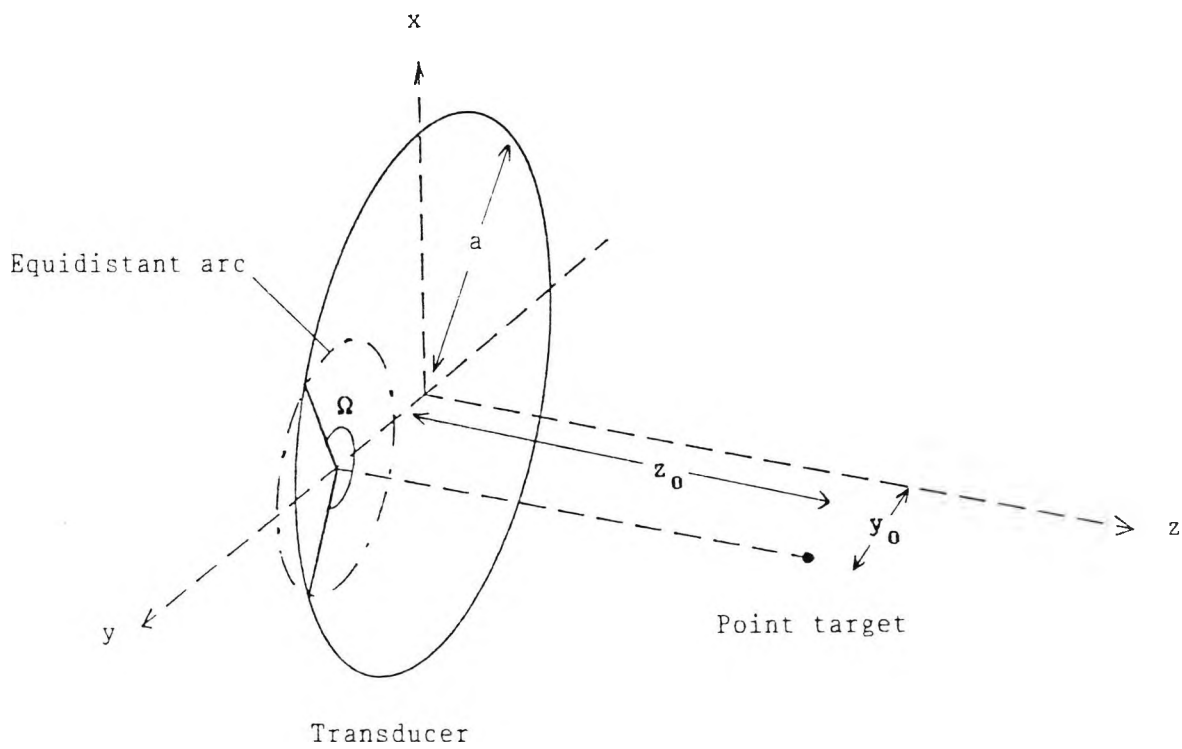


Figure (2.4.1): Geometry of a circular source and a point target at an arbitrary position in the field.

Figure (2.4.2) shows graphical solutions for the velocity potential, for a transducer undergoing an impulsive motion. On axis, figure (2.4.2a), the projection of the field point is at the centre of the transducer. At time t_0 , (the time it takes for the wave from the centre of the transducer to reach the field point) the velocity potential impulse response jumps up to a maximum value. At successive time intervals, because the arcs are all complete circles, the velocity potential impulse response remains constant. At time t_1 (the time from the edge of the transducer to the field point) the arcs suddenly become zero, because they are outside the transducer's geometric region. Thus the velocity potential impulse response also drops to zero.

When the field point is slightly off-axis of the transducer (figure (2.4.2b)), the velocity potential impulse response again jumps up to a maximum value at time t_0 . However at time t_1 (the nearer edge time) the circular arcs begin to go outside the transducer's geometric region, and so the velocity potential impulse response begins to fall. It falls quite suddenly at first, then slower and finally faster as it approaches time t_2 (the farther edge time), after which it is zero.

Outside the transducer's geometric region (figure (2.4.2c)), there is no velocity potential impulse response until time t_1 (the nearer edge time). The arcs are never complete circles, so the velocity potential impulse response only rises to a small maximum. It then falls as it approaches time t_2 (the farther edge time) and is zero afterwards.

Note that the exact form of the velocity potential impulse response curve is given by eqn. (2.4.10).

The pressure impulse response is obtained by differentiating eqn. (2.4.7):-

$$P_i(\underline{r}, t) = \rho \frac{\partial \phi_i(\underline{r}, t)}{\partial t} \quad (2.4.11)$$

From Robinson, eqn. (2.4.11) can be expressed directly:-

$$P_i(\underline{r}, t) = -\frac{\rho c}{2\pi} \frac{c^2 t (c^2 t^2 - z_0^2 - y_0^2 + a^2)}{(c^2 t^2 - z_0^2) \sqrt{(2(c^2 t^2 - z_0^2)(y_0^2 + a^2) - (c^2 t^2 - z_0^2)^2 - (y_0^2 - a^2)^2)}} \quad (2.4.12)$$

To get the pressure waveform radiated by the transducer, the pressure impulse response is convolved with the transducer velocity:-

$$P(\underline{r}, t) = u(t) * P_i(\underline{r}, t) \quad (2.4.13)$$

$$= u(t) * \rho \frac{\partial \phi_i(\underline{r}, t)}{\partial t} \quad (2.4.14)$$

The form of the pressure wave is best described with the aid of figure (2.4.2). On axis (figure (2.4.2a)), the velocity potential impulse response has a "top hat" shape. When differentiated, the leading and trailing edges of the velocity potential impulse response produce positive and negative delta functions in the pressure impulse response. When this is convolved with the transducer source velocity (a single cycle of a sine wave for simplicity), both delta functions produce a replica pulse of the source velocity. The first pulse represents the wave travelling from the front face of the transducer - the plane wave. The second pulse (of opposite phase) represents the two waves travelling from each edge of the source and arriving together. The time difference between the two pulses is equal to the extra time the waves from the edge take to reach the field point.

Off axis, but still within the straight-ahead geometric region of the transducer, figure (2.4.2b) the velocity potential impulse

response falls off in time. When differentiated to produce the pressure impulse response, the positive delta function is still present, but the negative delta function has been replaced by two smaller negative pulses. After convolution, they produce the plane wave as before, and also two distorted and inverted replicas of the source velocity. The latter pulses represent waves travelling from the nearest and furthest edges. Again, the path differences between the waves correspond to the time differences between the pulses.

Further off axis, now outside the transducer's geometric region, (figure (2.4.2c)) the situation is as above, except there is no plane wave, and the edge waves are more spread out in time.

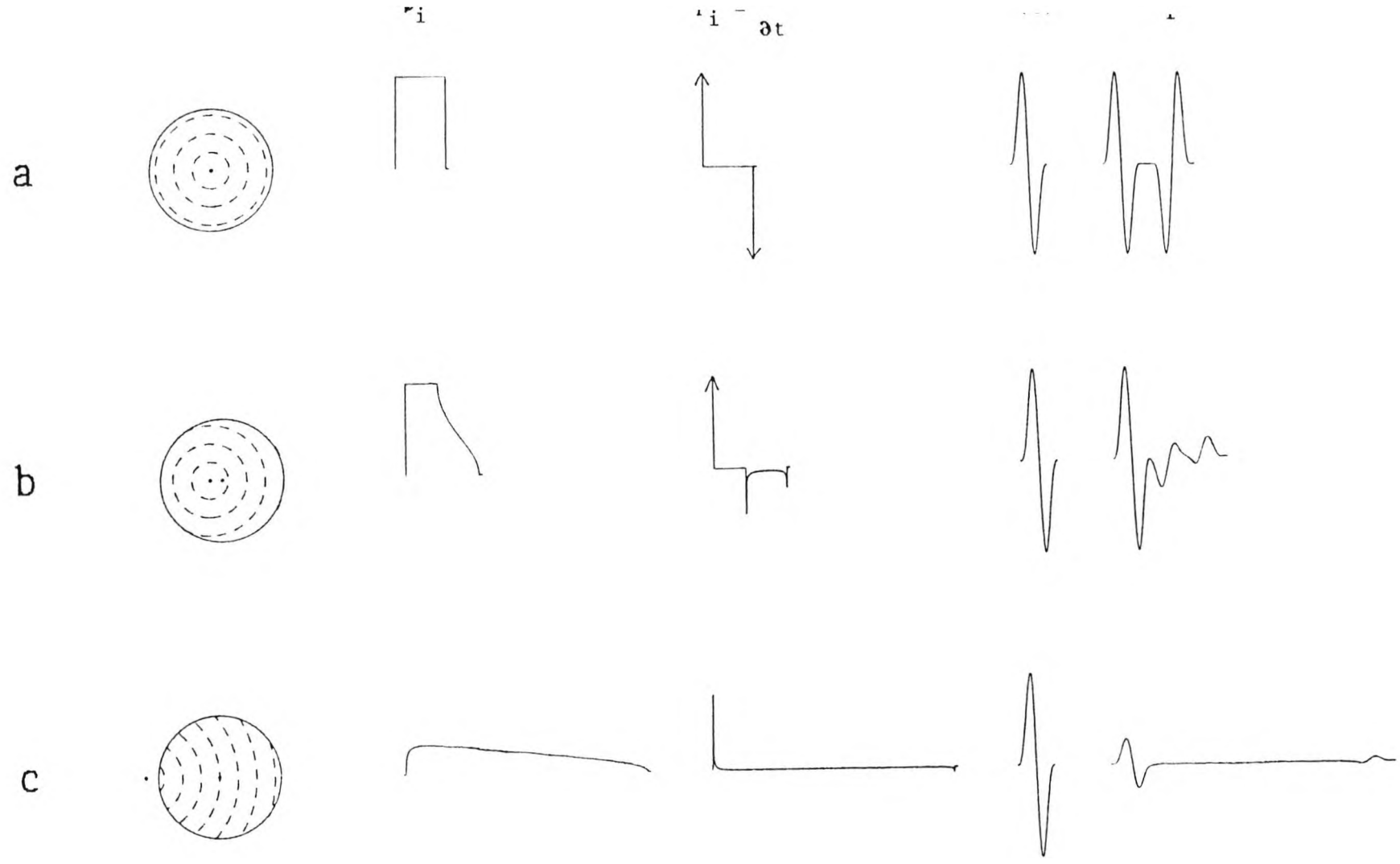


Figure (2.4.2): Graphical derivation of the velocity potential impulse response ϕ_i for a circular source, and hence the pressure impulse response P_i , which is convolved with the motion of the source $u(t)$ to obtain the pressure waveform P .
a: field point on-axis,
b: field point off-axis, but within the geometric region,
c: field point off-axis, but outside the geometric region.

To show the generality of the impulse response method, it is possible to obtain an expression for the pressure along the axis of a circular source (eqn. (2.1.5)). Note that this equation is valid only for the cw case.

On-axis, figure (2.4.2a), the expression for the pressure impulse response can be written in terms of two delta functions; the first due to the plane-wave contribution, and the second due to the edge-wave contribution:-

$$P_i(\underline{r}, t) = \rho c (\delta(t) - \delta(t - \tau)) . \quad (2.4.15)$$

$\delta(t - \tau)$ represents the edge wave component which has a time difference τ from the plane wave component $\delta(t)$. The time difference τ is given by $(\sqrt{a^2 + z^2} - z)/c$. In the frequency domain, eqn. (2.4.15) becomes:-

$$P_i(\underline{r}, \omega) = \rho c \int_{-\infty}^{\infty} (\delta(t) - \delta(t - \tau)) e^{-j\omega t} dt , \quad (2.4.16)$$

or for convenience, making $P_i(\underline{r}, \omega)$ an odd function by shifting the time origin:-

$$P_i(\underline{r}, \omega) = \rho c \int_{-\infty}^{\infty} (\delta(t + \tau/2) - \delta(t - \tau/2)) e^{-j\omega t} dt , \quad (2.4.17)$$

$$= \rho c \int_{-\infty}^{\infty} \delta(t + \tau/2) e^{-j\omega t} dt - \rho c \int_{-\infty}^{\infty} \delta(t - \tau/2) e^{-j\omega t} dt . \quad (2.4.18)$$

Since

$$\int_{-\infty}^{\infty} f(t) \delta(t - \tau) dt = f(\tau) , \quad (2.4.19)$$

eqn. (2.4.18) becomes:-

$$P_i(\underline{r}, \omega) = \rho c e^{j\omega\tau/2} - \rho c e^{-j\omega\tau/2} , \quad (2.4.20)$$

$$= \rho c (e^{j\omega\tau/2} - e^{-j\omega\tau/2}) , \quad (2.4.21)$$

$$= \rho c 2j \sin \left[\frac{\omega\tau}{2} \right] . \quad (2.4.22)$$

Taking the modulus of the pressure:-

$$|P_i(\underline{r}, \omega)| = 2\rho c \sin \left[\frac{\omega\tau}{2} \right] , \quad (2.4.23)$$

and substituting for τ :-

$$|P_i(\underline{r}, \omega)| = 2\rho c \sin \left[\frac{\omega}{2c} (\sqrt{a^2 + z^2} - z) \right] , \quad (2.4.24)$$

or, since $\omega = 2\pi c/\lambda$,

$$|P_i(\underline{r}, \omega)| = 2\rho c \sin \left[(\pi/\lambda) (\sqrt{a^2 + z^2} - z) \right] . \quad (2.4.25)$$

This is the same form as eqn. (2.1.5), showing that the plane and edge wave model gives the same result as for cw (section 2.1).

2.5 Transmit-receive mode

Weight and Hayman (1978) showed that the impulse response method of section 2.4 can be extended to cover reflections from a point target, with the transducer in transmit-receive mode.

Treating the target as if it were a tiny spherical source emitting a spherical wave, the velocity potential back at the transducer is given by:-

$$\phi'(\underline{r}, t) = \frac{q}{4\pi r} u'(t - \underline{r}/c) \quad (2.5.1)$$

where $u'(t - \underline{r}/c)$ is the velocity of the spherical wave, and q is the source strength.

The pressure impulse response back at the transducer is given by eqn. (2.4.7):-

$$P'_i(\underline{r}, t) = \frac{\partial \phi'_i(\underline{r}, t)}{\partial t} \quad (2.5.2)$$

The pressure wave at the transducer is given by eqn. (2.4.13):-

$$P'(\underline{r}, t) = u'(t) * P'_i(\underline{r}, t) \quad (2.5.3)$$

The output voltage from the transducer is proportional to the pressure:-

$$e(t) = K \int_S P'_i(\underline{r}, t) ds \quad (2.5.4)$$

$$= K \int_S \rho \frac{\partial \phi'_i(\underline{r}, t)}{\partial t} ds \quad (2.5.5)$$

$$= K\rho q \frac{\partial}{\partial t} \int_S \frac{u'(t - \underline{r}/c)}{4\pi r} ds \quad (2.5.6)$$

Eqn. (2.5.6) can be written in a form similar to eqn. (2.1.4):-

$$e(t) = \frac{Kq}{2} \rho \frac{\partial}{\partial t} \int_S \frac{u'(t - r/c)}{2\pi r} ds, \quad (2.5.7)$$

$$= u'(t) * e_i(t), \quad (2.5.8)$$

where $e_i(t) = \frac{Kq}{2} P_i'(\underline{r}, t)$.

If we now assume that the target is an ideal reflector, with a reflection coefficient of -1, then the reflector can be treated as if it were a point source, with velocity $u'(t) = -P(\underline{r}, t)/\rho c$ and pressure impulse response $P_i'(\underline{r}, t) = P_i(\underline{r}, t)$.

The electrical output of the transducer becomes (from eqn. (2.5.8)):-

$$e(t) = - \left[\frac{P(\underline{r}, t)}{\rho c} \right] * \left[\frac{Kq}{2} P_i(\underline{r}, t) \right], \quad (2.5.9)$$

$$= \frac{-1}{\rho c} \left[u(t) * P_i(\underline{r}, t) \right] * \left[\frac{Kq}{2} P_i(\underline{r}, t) \right], \quad (2.5.10)$$

$$= \frac{-Kq}{2\rho c} \left[u(t) * P_i(\underline{r}, t) * P_i(\underline{r}, t) \right]. \quad (2.5.11)$$

The double convolution in eqn. (2.5.11) means that transmit-receive echo waveforms look very different from their pressure counterparts. This is illustrated in figure (2.5.1) which shows a graphical derivation of the transmit-receive echo waveforms. This should be contrasted with the graphical derivation of the pressure waveforms, shown in figure (2.4.2). On axis, the pressure waveform consists of two pulses (figure (2.4.2a)), whereas the transmit-receive echo waveform consists of three pulses (figure (2.5.1a)). The reason

that the transmit-receive echo waveforms are a different shape is as follows. The point target (on axis (figure (2.5.1a)) for simplicity) which reflects the incident pressure waveform, can be regarded as being the source of two spherical waves - one due to the incident pressure plane wave, and the other due to the (coincident) pressure edge waves, with a time delay between the plane and edge waves due to the increased path the edge waves must travel to reach the target.

The plane wave is reflected straight back to the transducer's centre first. After a short interval, the same wave reaches the transducer's edges. During this time, the average pressure on the transducer's surface is zero. This is because as the spherical wave expands, the point of contact between the wave and the transducer's surface has both positive and negative pressures which average out to zero. All that remains is a positive pressure at the instant the wave reaches the transducer's centre, and a negative pressure when the wave finally passes past the transducer's edges.

At the same instant the plane wave reaches the transducer's edges, the edge waves reach the transducer's centre. These reinforce to give the double amplitude central pulse.

Finally, as was the case for the reflected plane wave, there is zero pressure until the edge waves pass past the transducer's edges, producing the third pulse in the transmit-receive echo waveform.

With the reflecting target moved off axis, (figure (2.5.1b-c)), the edge wave components no longer coincide, and the simple three-pulse structure becomes more complicated.

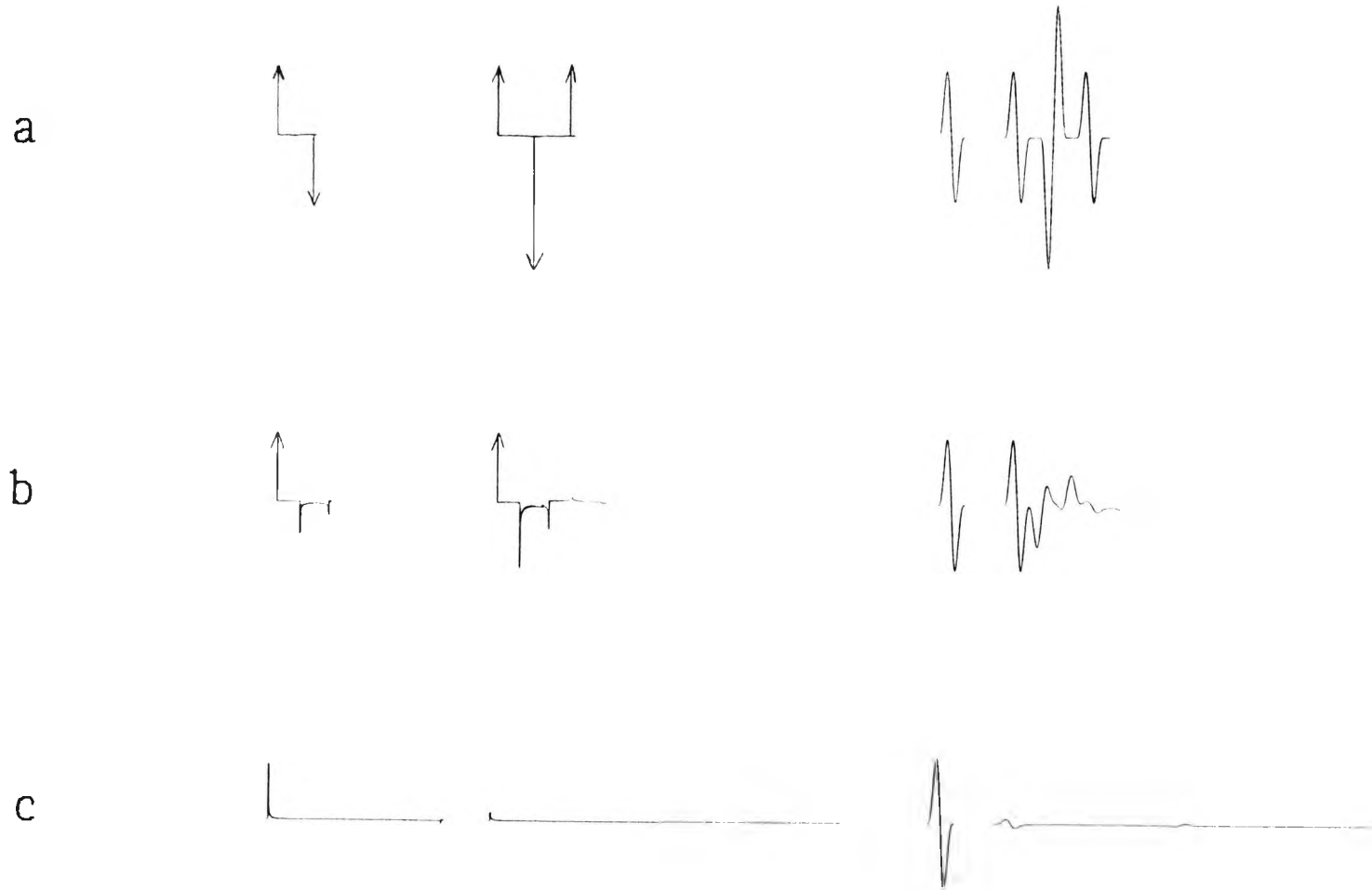



Figure (2.5.1): Graphical derivation of the transmit-receive echo response e , which is obtained from the self-convolution of the pressure impulse response P_i (see figure (2.4.2)) with the motion of the source $u(t)$.
a: target on axis,
b: target off axis, but within the geometric region,
c: target off axis, but outside the geometric region.

Theoretical beam profiles may be obtained by evaluating either eqn. (2.4.14) or eqn. (2.5.11) in a point-by-point fashion, at closely spaced intervals across the beam.

The beam profiles have been shown by Weight (1984b) to have different forms according to whether they are pressure mode (corresponding to eqn. (2.4.14)) or transmit-receive mode (corresponding to eqn. (2.5.11)). Two figures from the Weight (1984b) paper are reproduced here as figure (2.5.2). Both the pressure and transmit-receive beam profiles look similar in the far-field, consisting of a single peak centred on the axis of propagation. In the near-field however, the transmit-receive case has pronounced central maxima. This is due to the presence of the extra large pulse, as shown in figure (2.5.1a).

Transducer diameter = 19 mm

Transducer velocity =  0.5 μ s

- 37 -

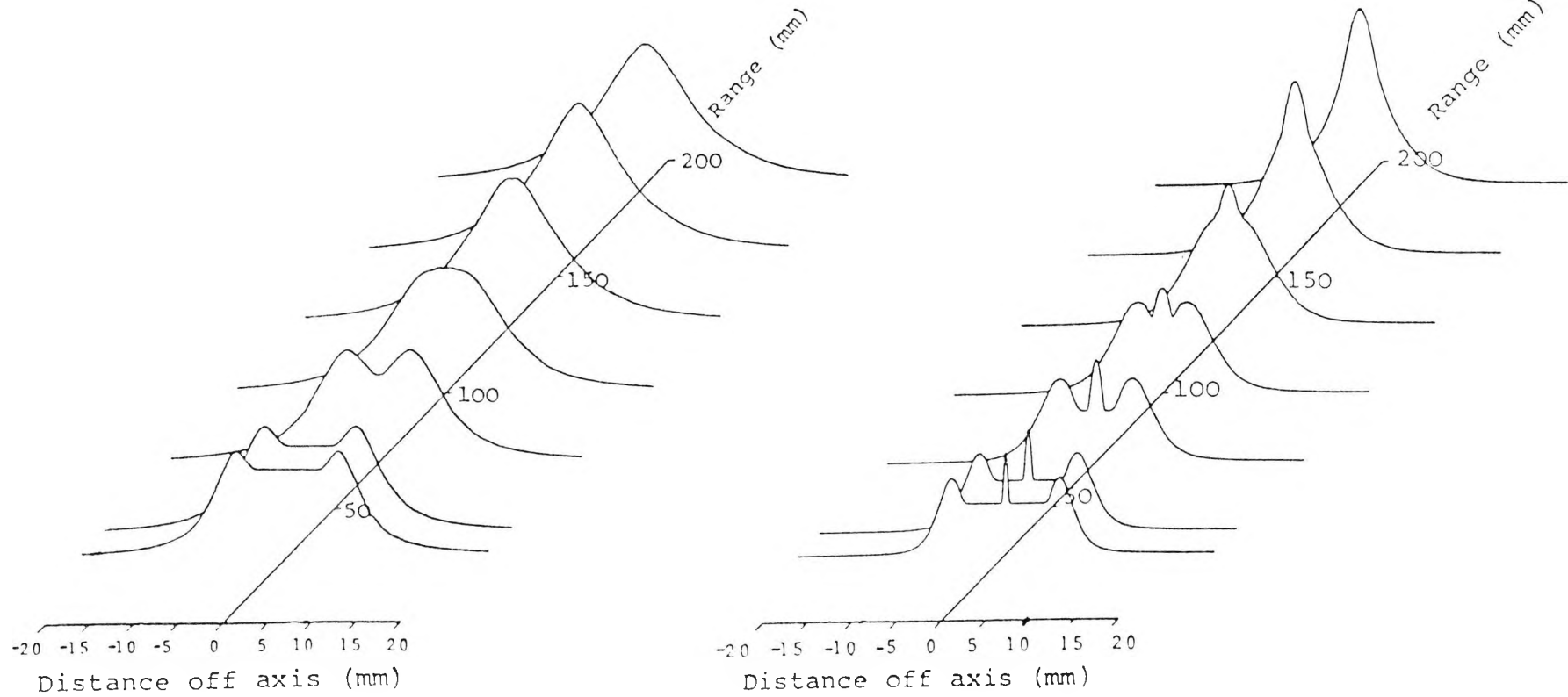


Figure (2.5.2): Pressure (*left*) and transmit-receive (*right*) beam profiles for a 19mm conventional transducer radiating into water.

2.6 Resolution and its limitations

Resolution is defined in two ways: range resolution and lateral resolution. They both refer to a transducer's ability to distinguish between closely spaced targets, and they differ only in the direction being considered.

It has been shown in section 2.4 that the plane and edge waves can be resolved at positions near to the transducer. At further ranges they merge, as shown in figure (2.6.1), to become a single pulse of varying shape. Robinson et. al. (1974) have shown that in the far field the pressure waveform is of the form of the time differential of the plane wave pulse. This can be seen in figure (2.6.1), although smoothed sine functions are used here (with a smoother start and finish, unlike the pure sine function), to prevent problems with discontinuities occurring in the computations (see section 2.12). The plane wave pulse is the left-most pulse of the left hand waveform in the upper part of the figure. Similarly for the transmit-receive mode waveforms, the far field pulse is of the form of the second time differential of the plane wave pulse. The plane wave pulse is again the left-most pulse of the left hand waveform of the lower part of the figure.

As mentioned earlier in section 2.4, the total pulse length is much longer than the length of the single sinusoidal driving pulse. The reason that the total pulse length is large (especially in the near field), is the difference in path between rays from the centre of the transducer and rays from the edge. At further ranges this path difference becomes smaller, and so the total pulse length decreases.

As figure (2.6.1) shows, the pulse shape does become relatively

constant in size and shape, in the far-field, thus giving a good range resolution. In the near-field however, because the pulse size and shape change rapidly with range, it is difficult to interpret such waveforms. The lateral resolution is not good however, as the beam profiles of figure (2.5.2) show. As they are as wide as the source, a target placed at any lateral position will produce waveforms of similar amplitude.

Targets which are very close to the transducer cannot be detected because of saturation effects in the electronic receiving equipment. This occurs because the driving pulse used to excite the transducer is also fed to the receiving amplifier, and as it is a very large amplitude, saturates the amplifier for a short time. This "dead time" translates to a minimum range a target can be at, so that the echoes from the target are able to be detected. With our current equipment, the minimum range is about 20mm.

Thus it can be seen that while short pulses of ultrasound should give good range resolution, this is only approached in the far-field. Echo responses from targets in the near-field must be interpreted with caution because of the multi-pulse structure of the echo waveforms. If results from targets at different ranges are compared, allowances must be made for the change in shape which occurs.

Since the pulse shape is the result of interaction between the plane and edge waves (ideally there should be little variation in amplitude throughout the field), an obvious way to prevent this interaction is to remove one or other of them. This is the subject of the following section.

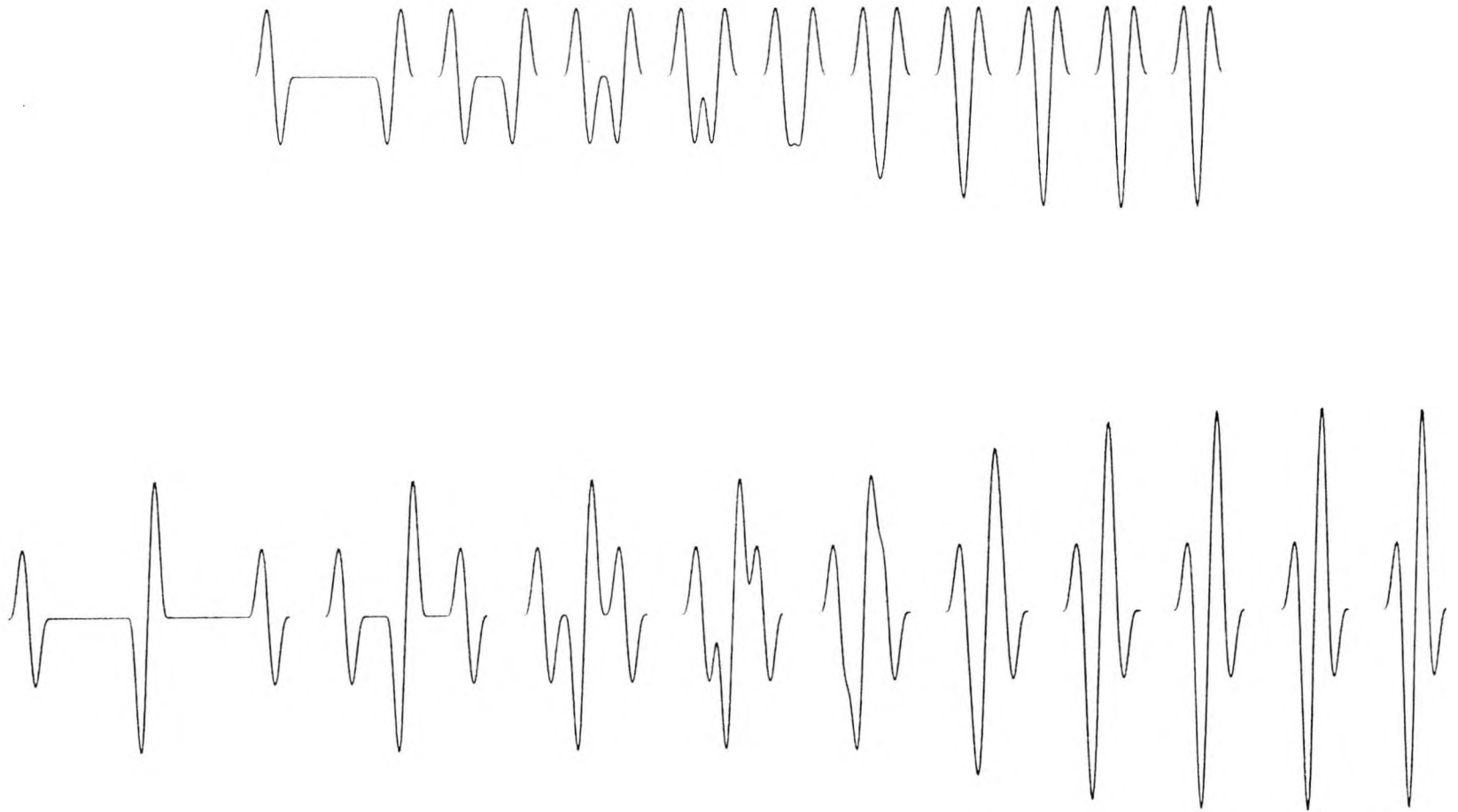


Figure (2.6.1): Axial pressure waveforms (*top*) and transmit-receive echo waveforms (*bottom*) for a 19mm diameter circular transducer. Ranges are from 50mm (*left*) to 500mm (*right*) at intervals of 50mm.

2.7 Non-uniform excitation

For continuous waves, the important factor for good resolution is that the radiated pressure waveforms should be uniform throughout the field. This leads to uniform spectra, and beam profiles with no fluctuations due to diffraction effects. One way of achieving this is to make the motion of the source non-uniform across its surface. This is similar to the method of apodising used in optics and radar (Jacquinot and Roizen-Dossier, 1964). Martin and Breazeale (1971), and other authors have shown how it is possible to excite a transducer axisymmetrically, so that the variation in the electric field across a transducer diameter is approximately Gaussian. The resulting motion of the source has a similar variation.

Several authors (for example, Harris, 1981b, Stepanishen, 1981, Weight, 1982b and 1984a, Guyomar and Powers, 1986, and Hutchins et. al., 1986) have studied the situation of a transducer which has an arbitrary velocity distribution across the transducer surface. They are mainly concerned with distribution functions which are easy to handle and have a shape not unlike a Gaussian, to obtain uniform fields.

To obtain a more uniform field, it might be thought that removing the edge waves would be all that was required. This is not easy to do in practice, since edge waves are produced as the plane waves propagate. The edge waves can only be reduced. In the results section, it will be shown (figures (3.1.5.1.d) and (3.1.6.1d)) that such a "plane-wave-only" transducer has several advantages over conventional transducers, including simpler pulse shapes and an improved lateral resolution.

If the plane waves are reduced, resulting in an "edge-wave-only" transducer, we find that such a transducer has a field which is concentrated along the axis of the transducer. This is a peculiarity of edge waves where their directivity compensates for the spreading nature of the edge waves (Weight, 1982a, and figure (3.1.4.1)) and so the axial pressure remains constant with range. This will be shown in section 3.1.4. It is very easy to model an ideal edge-wave-only transducer, by simply suppressing the initial impulse of the plane wave in the calculations. The results section will show (figures (3.1.5.1b-c) and (3.1.6.1b-c)) how these edge-wave-only transducers have order of magnitude improvements in lateral resolution, and much simpler echo waveforms than conventional transducers.

In order to calculate the pressure for these non-uniformly-excited transducers, the source may be regarded as a concentric collection of uniformly-excited sources, whose individual pressures are added together (Weight, 1982b and Hutchins et. al., 1986). From eqn. (2.4.13), the pressure is given by:-

$$P(y,t) = u(y,t) * P_i(\underline{r},t) , \quad (2.7.1)$$

where $u(y,t)$ is now a function of radial distance y . The total pressure $P_w(\underline{r},t)$ at a point in the field in the limit, is given by:-

$$P_w(\underline{r},t) = \int_0^a P(y,t) dy , \quad (2.7.2)$$

where a is the transducer radius.

Theoretically, it is the velocity potential impulse response which is calculated in this way. The simplest example of this is for

an annular transducer, of radius a , and annulus width W . The total velocity potential impulse response is given by first calculating the velocity potential impulse response for a hypothetical source of radius a . From this is subtracted the velocity potential impulse response for a smaller hypothetical source of radius $a-W$ as shown in figure (2.7.1a). This annular transducer is described simply to illustrate the method of building up a non-uniform velocity profile. An annular transducer does not produce edge waves alone because the width of the ring will still produce plane waves. A narrow ring, although producing a uniform toroidal wave, does not have the sensitivity, or constant sensitivity with range, that an edge-wave-only source would have (Weight, 1984a).

For more complicated transducer types, the velocity profile is used to weight the individual velocity potential impulse responses (Weight, 1982b, and Hutchins et. al., 1986). They are then either added up to produce plane-wave-only type transducers (figure (2.7.1b)), or subtracted to produce edge-wave-only type transducers (figure (2.7.1c)).

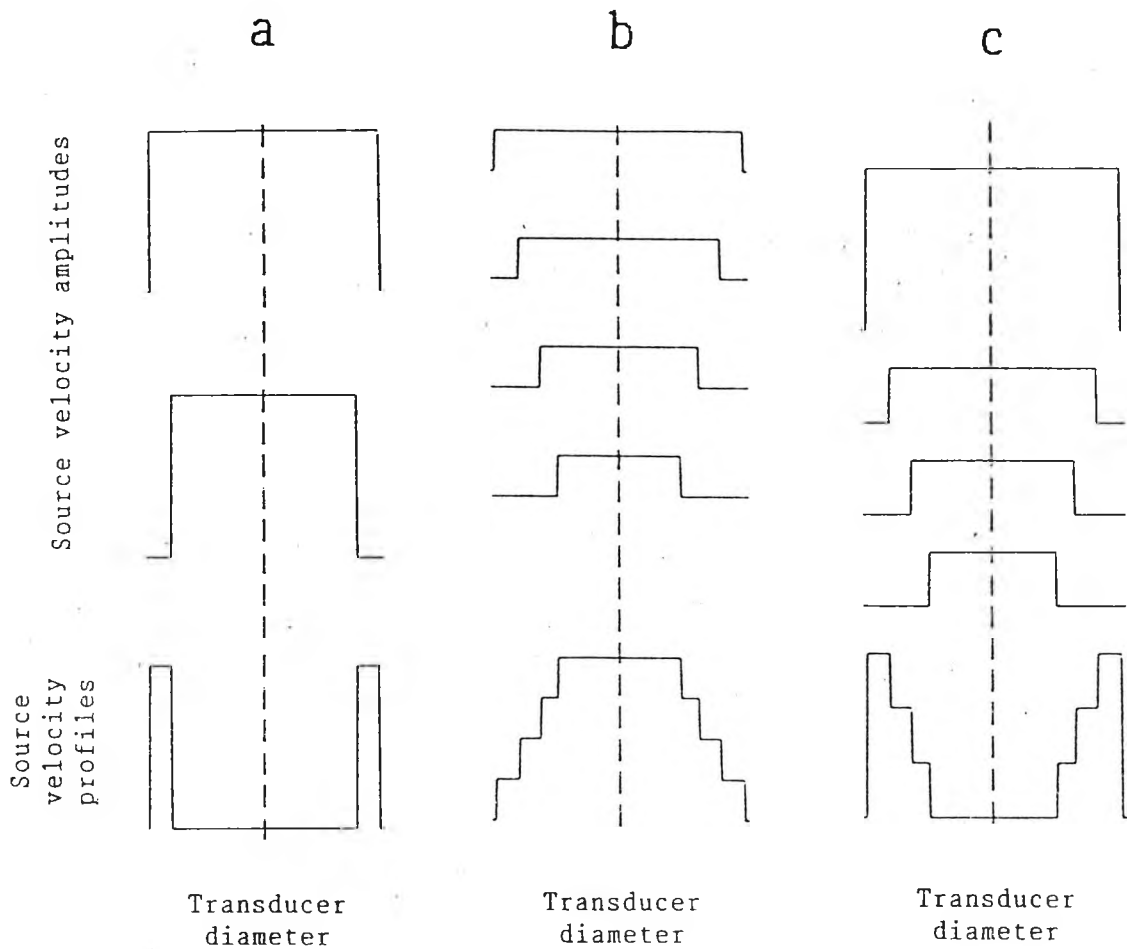


Figure (2.7.1): Schematic diagram showing how source velocity profiles (*bottom*) are built up using plane wave contributions.

- a: An ideal annular source, where the contributions are subtracted from each other.
- b: A plane-wave-only source, where the contributions are added together.
- c: An edge-wave-only source, where the contributions are subtracted from each other.

The velocity weighting function chosen for edge-wave-only transducers, V_{ewo} , was of a Gaussian form:-

$$V_{ewo}(y) = e^{-(yk)^2}, \quad (2.7.3)$$

where $k = (\sqrt{-\ln(0.5)})/W$, and W represents the 'half-width' of the weighting function, which represents the distance from the edge of the transducer, where the Gaussian function has fallen to a value of 0.5.

For plane-wave-only transducers, the weighting function chosen, V_{pwo} , was similar, being an inverted version of eqn. (2.7.3):-

$$V_{pwo}(y) = 1 - e^{-(yk)^2}. \quad (2.7.4)$$

The half-widths chosen for subsequent calculations were $W = 0.75\text{mm}$ for edge-wave-only type transducers, and $W = 4.0\text{mm}$ for plane-wave-only type transducers. These values were chosen after several runs on the computer to give the best compromise between simple pulse shapes and resolution for the transducer being modelled, which was a 19mm diameter type. For the edge-wave-only transducer, making the half-width smaller tended to reduce the effective range of the transducer, and making the half-width larger broadened the beam profiles and introduced side lobes in the near field. For the plane-wave-only transducer, making the half-width smaller produced maxima and minima in the beam profiles.

Plots of the functions used are shown in figure (2.7.2).

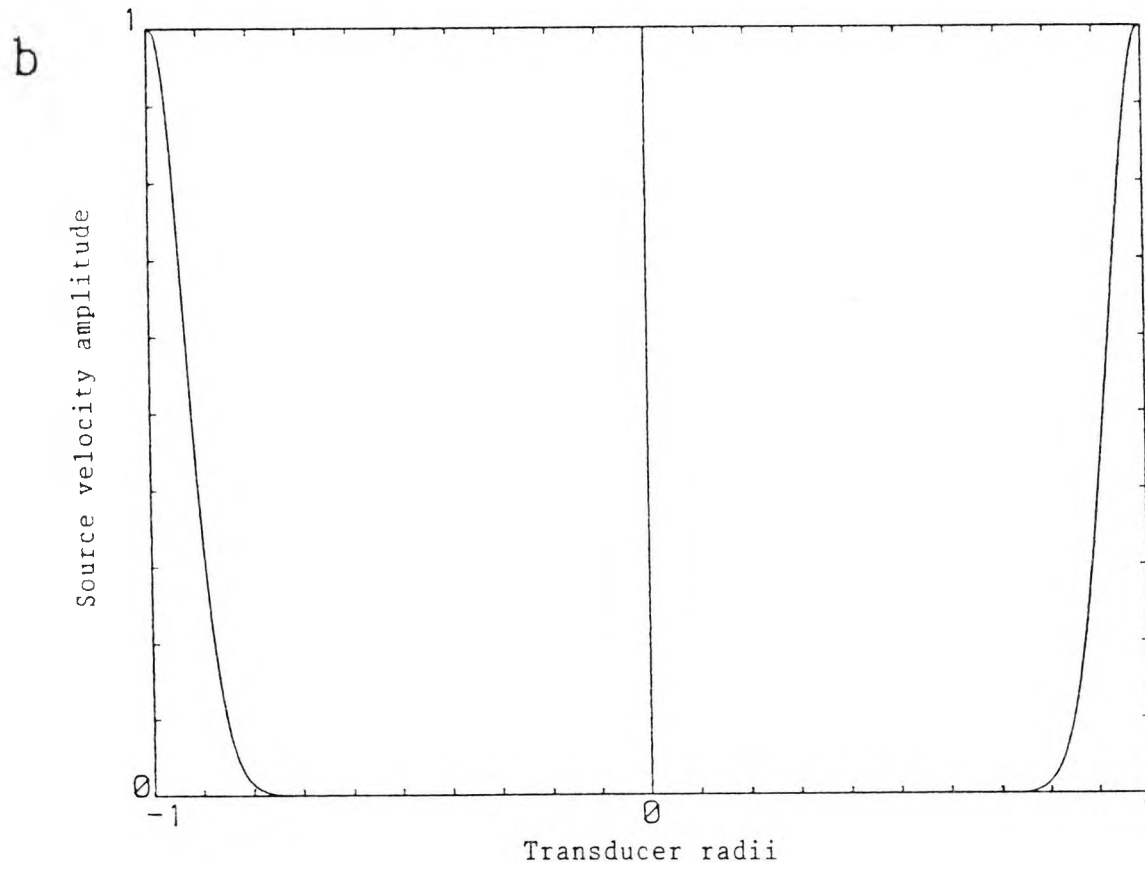
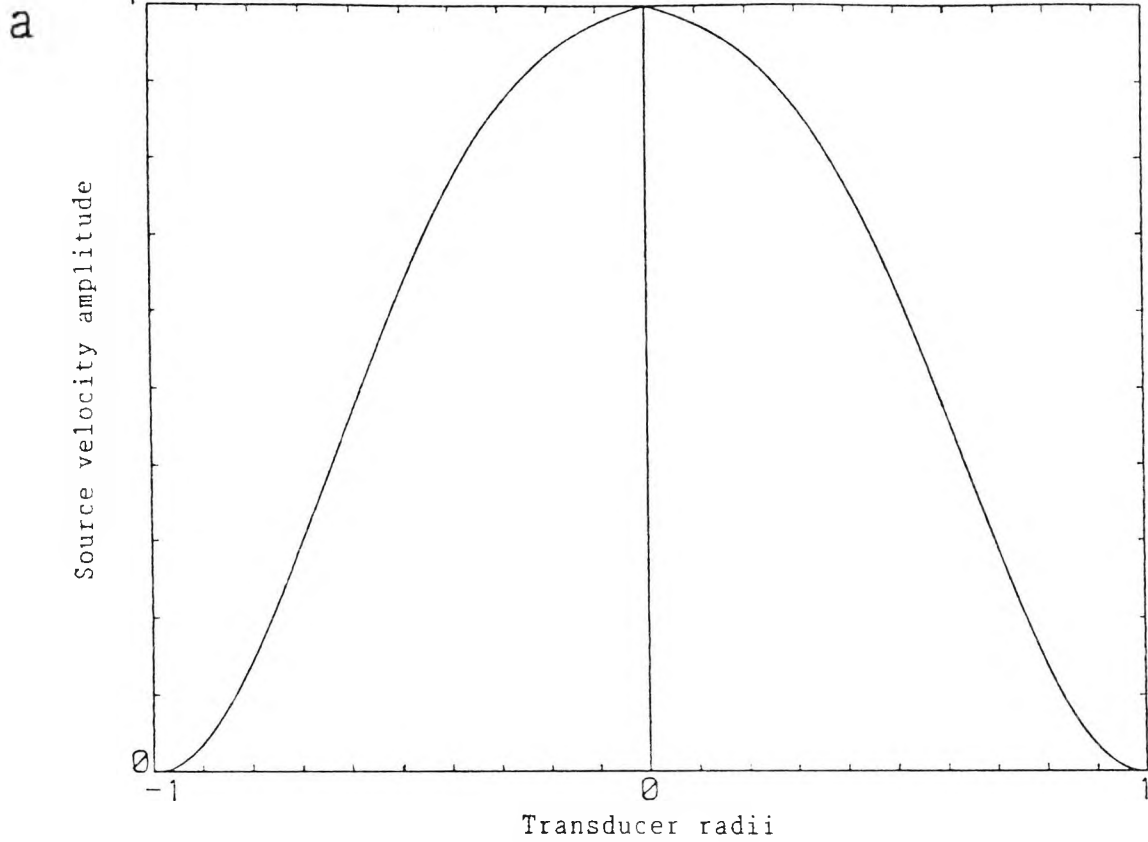


Figure (2.7.2): Source velocity profiles for:
 a: a plane-wave-only source,
 b: an edge-wave-only source.

2.8 Finite-size targets

Ueda and Ichikawa (1981) have shown how the impulse response method can be used to model echo signals reflected by weakly scattering, cylindrical, finite-sized targets on the axis of a circular piston source. It has recently been shown (McLaren and Weight, 1987) that their model is valid for strong scatterers. Ueda and Ichikawa's analysis is repeated here for completeness, but the symbols have been changed to be consistent with the present work, and some extra explanatory comments have been given.

The starting point is the inhomogeneous wave equation:-

$$\frac{1}{c^2} \frac{\partial^2 P}{\partial t^2} - \nabla^2 P = \frac{2\Delta c}{c^3} \frac{\partial^2 P}{\partial t^2} - \frac{1}{\rho} \nabla(\Delta\rho) \cdot \nabla P, \quad (2.8.1)$$

where P is the sound pressure, Δc and $\Delta\rho$ are the fluctuations in sound velocity and density from their mean values c and ρ . It is assumed that the scattering volume V is embedded in a uniform medium of density ρ and sound velocity c . The incident wave is $P_{in}(\underline{r}, t)$ and the scattered wave is $P_{sc}(\underline{r}, t)$, (figure (2.8.1)).

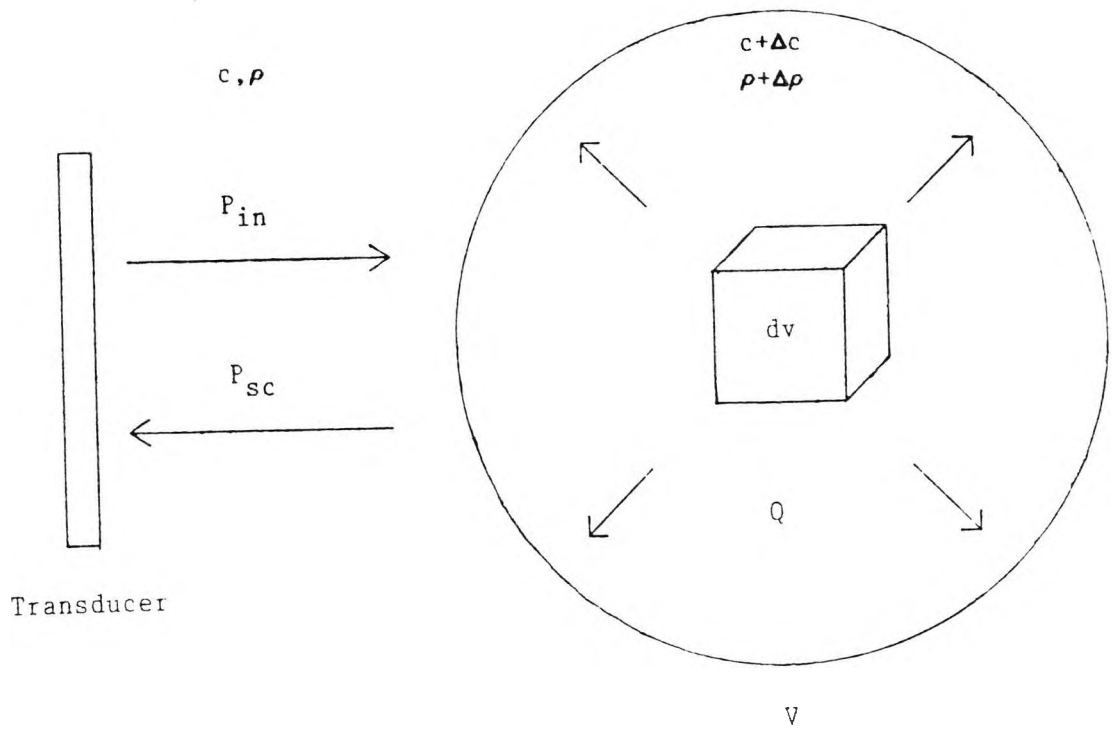


Figure (2.8.1): Schematic diagram for the finite-size target scattering medium.

The scattered wave is represented as:-

$$P_{sc}(\underline{r}, t) = \int_V \frac{Q(\underline{s}, t - |\underline{r} - \underline{s}|/c)}{4\pi|\underline{r} - \underline{s}|} dv , \quad (2.8.2)$$

where dv is a volume element of the volume V , \underline{r} is the position vector of the volume V from the transducer, \underline{s} is the position vector of the volume element dv , and $Q(\underline{r}, t)$ is the scattering strength of the scatterer and is given by:-

$$Q(\underline{r}, t) = \left[\frac{2\Delta c}{c^3} \right] \left[\frac{\partial^2 P_{in}(\underline{r}, t)}{\partial t^2} \right] - \left[\frac{1}{\rho} \right] \nabla(\Delta\rho) \cdot \nabla P_{in}(\underline{r}, t) . \quad (2.8.3)$$

The first term of eqn. (2.8.3) shows the contribution due to the velocity fluctuation Δc , and the second term shows the contribution due to the density fluctuation $\Delta\rho$.

The incident wave is represented as:-

$$P_{in}(\underline{r}, t) = u(t) * \rho \frac{\partial \phi(\underline{r}, t)}{\partial t} , \quad (2.8.4)$$

where $\phi(\underline{r}, t)$ is the velocity potential of the medium, given by:-

$$\phi(\underline{r}, t) = \frac{1}{2\pi} \int_{-\infty}^{\infty} \Phi(\underline{r}, \omega) e^{j\omega t} d\omega , \quad (2.8.5)$$

and $\partial\phi(\underline{r}, t)/\partial t$ is the impulse response of the medium given by:-

$$\frac{\partial\phi(\underline{r}, t)}{\partial t} = \frac{1}{2\pi} \int_{-\infty}^{\infty} j\omega \Phi(\underline{r}, \omega) e^{j\omega t} d\omega . \quad (2.8.6)$$

$\Phi(\underline{r}, \omega)$ is the Fourier transform of $\phi(\underline{r}, t)$ and is given by:-

$$\phi(\underline{r}, \omega) = \frac{1}{2\pi} \int_S \frac{e^{-j\omega|\underline{r} - \underline{s}|/c}}{|\underline{r} - \underline{s}|} ds, \quad (2.8.7)$$

where ds is a surface element on the transducer's surface S . Transformed to the frequency domain, eqn. (2.8.4) can be expressed as:-

$$P_{in}(\underline{r}, t) = \frac{1}{2\pi} \int_{-\infty}^{\infty} U(\omega) j\omega \rho \phi(\underline{r}, \omega) e^{j\omega t} d\omega, \quad (2.8.8)$$

where $U(\omega)$ is the Fourier transform of $u(t)$, the transducer velocity. By considering separately, velocity fluctuations and density fluctuations, Ueda and Ichikawa obtain two expressions for the frequency responses of the medium (see appendix):-

$$F_c(\omega) = \int_V \frac{(j\omega)^2 \Delta c \phi^2(\underline{r}, \omega)}{c^3} dv, \quad (2.8.9)$$

$$F_\rho(\omega) = \int_V \frac{-\nabla(\Delta\rho) \cdot \nabla\phi(\underline{r}, \omega) \phi(\underline{r}, \omega)}{2\rho} dv, \quad (2.8.10)$$

Eqns. (2.8.9) and (2.8.10) are difficult to compare directly, because of their different forms, so Ueda and Ichikawa resort to a discrete model of the scattering medium, to enable eqn. (2.8.10) to be cast into a form suitable for comparison with eqn. (2.8.9).

If the scatterer is regarded as a collection of m small cubes, each of which has a frequency response given by eqn. (2.8.10), then the total frequency response of the whole scatterer is the summation of eqn. (2.8.10) over all the m cubes:-

$$F_{\rho}(\omega) = \sum_{i=1}^m \left[\int_{V_i} \frac{[-\nabla(\Delta\rho) \cdot \nabla\phi(\underline{r}, \omega)] \phi(\underline{r}, \omega)}{2\rho} dv \right] . \quad (2.8.11)$$

The term $\nabla(\Delta\rho)/\rho$ represents the change in density throughout the elementary cube. Since this is assumed only to change at the cube's edges, the term can be rewritten as $-\Delta\rho_i \underline{N}_i \delta(\underline{r} - \underline{s})/\rho$ where $\Delta\rho_i$ is the density throughout the i^{th} cube, \underline{N}_i is a normal unit vector to the cube's surface, and $\delta(\underline{r} - \underline{s})$ is a delta function to represent the discontinuity of change at the edges of the cube. This can now be substituted into eqn. (2.8.11) and it becomes a surface integral due to the delta function:-

$$F_{\rho}(\omega) = \sum_{i=1}^m - \int_{V_i} \frac{[-\Delta\rho_i \underline{N}_i \delta(\underline{r} - \underline{s}) \cdot \nabla\phi(\underline{r}, \omega)] \phi(\underline{r}, \omega)}{2\rho} dv , \quad (2.8.12)$$

$$= \sum_{i=1}^m \int_{V_i} \frac{\Delta\rho_i \phi(\underline{r}, \omega) \underline{N}_i \cdot \nabla\phi(\underline{r}, \omega) \delta(\underline{r} - \underline{s})}{2\rho} dv , \quad (2.8.13)$$

$$= \sum_{i=1}^m \int_{S_i} \frac{\Delta\rho_i \phi(\underline{r}, \omega) \underline{N}_i \cdot \nabla\phi(\underline{r}, \omega)}{2\rho} ds , \quad (2.8.14)$$

where ds is a surface element on the scatterer's surface S_i .

If the identity:

$$\int_V (\nabla h \cdot \nabla h + h \nabla^2 h) dv = \int_S \underline{N} \cdot h \nabla h ds , \quad (2.8.15)$$

where h is a differentiable scalar function, is substituted into eqn. (2.8.14), we obtain:

$$F_{\rho}(\omega) = \sum_{i=1}^m \int_{V_i} \frac{\Delta\rho_i [\nabla\phi(\underline{r},\omega) \cdot \nabla\phi(\underline{r},\omega) + \phi(\underline{r},\omega) \nabla^2\phi(\underline{r},\omega)]}{2\rho} dv , \quad (2.8.16)$$

Since the wave is assumed to satisfy the wave equation for a uniform medium, i.e.:

$$\nabla^2\phi(\underline{r},\omega) = \frac{1}{c^2} \frac{\partial^2\phi(\underline{r},\omega)}{\partial t^2} , \quad (2.8.17)$$

or, since $\phi(\underline{r},\omega) = e^{j\omega t}$, eqn. (2.8.17) becomes:-

$$\nabla^2\phi(\underline{r},\omega) = (j\omega/c)^2\phi(\underline{r},\omega) . \quad (2.8.18)$$

Also, assuming the scatterer is homogeneous, eqn. (2.8.16) can be written as:

$$F_{\rho}(\omega) = \int_V \frac{\Delta\rho [\nabla\phi(\underline{r},\omega) \cdot \nabla\phi(\underline{r},\omega) + \phi(\underline{r},\omega) (j\omega/c)^2 \phi(\underline{r},\omega)]}{2\rho} dv . \quad (2.8.19)$$

If eqns. (2.8.9) and (2.8.19) are now compared:

$$F_c(\omega) = \int_V \frac{\Delta c}{c} \left[(j\omega/c) \phi(\underline{r},\omega) \right]^2 dv , \quad (2.8.20)$$

$$F_{\rho}(\omega) = \int_V \frac{\Delta\rho}{\rho} \frac{1}{2} \left[\nabla\phi(\underline{r},\omega) \cdot \nabla\phi(\underline{r},\omega) + [(j\omega/c) \phi(\underline{r},\omega)]^2 \right] dv , \quad (2.8.21)$$

Ueda and Ichikawa conclude that eqns. (2.8.20) and (2.8.21) are equivalent, if the following relation holds:

$$\nabla\phi(\underline{r},\omega) \cdot \nabla\phi(\underline{r},\omega) = [(j\omega/c) \phi(\underline{r},\omega)]^2 . \quad (2.8.22)$$

Stacey (1989) has since shown that eqn. (2.8.22) amounts to a plane-

wave approximation. Ueda and Ichikawa also state that if the distance between the scatterer and the transducer is greater than the radius of the transducer, it is not necessary to distinguish between density changes $\Delta\rho$ and velocity changes Δc . The response of the medium can be described using only changes of specific acoustic impedance ΔZ . Eqn. (2.8.14) is used (in the continuum):

$$F(\omega) = \int_S \frac{\Delta Z \phi(\underline{r}, \omega) \underline{N} \cdot \nabla \phi(\underline{r}, \omega)}{2Z} ds . \quad (2.8.23)$$

Assuming cylindrical co-ordinates, eqn. (2.8.23) can be split up into a component from the front surface of the scatterer, and a component from the cylindrical side surface of the scatterer. Since the vector \underline{N} is always perpendicular to the relevant surfaces, $\underline{N} \cdot \nabla \phi(\underline{r}, \omega)$ simply becomes $\partial \phi(\underline{r}, \omega) / \partial \underline{r}$.

Therefore, eqn. (2.8.23) becomes:-

$$F(\omega) = \int_0^T \frac{\Delta Z}{2Z} \phi(z_0, y, \omega) \frac{\partial \phi(z_0, y, \omega)}{\partial z} 2\pi y dy + \int_{z_0}^{\infty} \frac{\Delta Z}{2Z} \phi(z, T, \omega) \frac{\partial \phi(z, T, \omega)}{\partial y} 2\pi T dz , \quad (2.8.24)$$

where T is the radius of the target face. If the edge component is assumed to be negligible, then eqn. (2.8.24) becomes:-

$$F(\omega) = \frac{\Delta Z}{2Z} \int_0^T \Phi(z_0, y, \omega) \frac{\partial \Phi(z_0, y, \omega)}{\partial z} 2\pi y \, dy . \quad (2.8.25)$$

In the time domain, this becomes a convolution:-

$$f(t) = \frac{\Delta Z}{2Z} \int_0^T \phi(z_0, y, t) * \frac{\partial \phi(z_0, y, t)}{\partial z} 2\pi y \, dy . \quad (2.8.26)$$

Thus the total echo impulse response of the target, $e_{it}(\underline{r}, t) = \partial f(t)/\partial t$ is given by:-

$$e_{it}(\underline{r}, t) = \frac{\Delta Z}{2Z} \int_0^T \frac{\partial \phi(z_0, y, t)}{\partial t} * \frac{\partial \phi(z_0, y, t)}{\partial z} 2\pi y \, dy . \quad (2.8.27)$$

The expression $\partial \phi(z_0, y, t)/\partial t$ is simply $\partial \phi_i(\underline{r}, t)/\partial t$ as given in eqn. (2.4.11). The expression $\partial \phi(z_0, y, t)/\partial z$ is obtained by replacing

∂z by $c\partial t$, and this gives $\frac{1}{c} \frac{\partial \phi_i(\underline{r}, t)}{\partial t}$.

Thus eqn. (2.8.27) becomes:-

$$e_{it}(\underline{r}, t) = K \int_0^T \left[\frac{\partial \phi_i(\underline{r}, t)}{\partial t} * \frac{\partial \phi_i(\underline{r}, t)}{\partial t} \right] 2\pi y \, dy , \quad (2.8.28)$$

where K is just a constant.

2.9 Off-axis finite-size targets

McLaren and Weight (1987) have also shown how the Ueda and Ichikawa method can be extended very easily to cater for off-axis targets.

If the geometry for the finite-sized target is drawn in a similar manner to that for a point target, (i.e. figure (2.4.1)), figure (2.9.1), (except that now the circular arcs emanate from a point on the target's face), we note that on axis, the $2\pi y$ term in eqn. (2.8.28) represents a complete arc (on the target's surface). I.e. we have $\Omega = 2\pi$. In general, for targets at arbitrary positions in the field, Ω_t is given by:-

$$\Omega_t = \cos^{-1} \left[\frac{c^2 t^2 - z_0^2 + y_0^2 - T^2}{2 y_0 \sqrt{(c^2 t^2 - z_0^2)}} \right], \quad (2.9.1)$$

which is the same as eqn. (2.4.9) but with a , the transducer radius, replaced by T , the target radius.

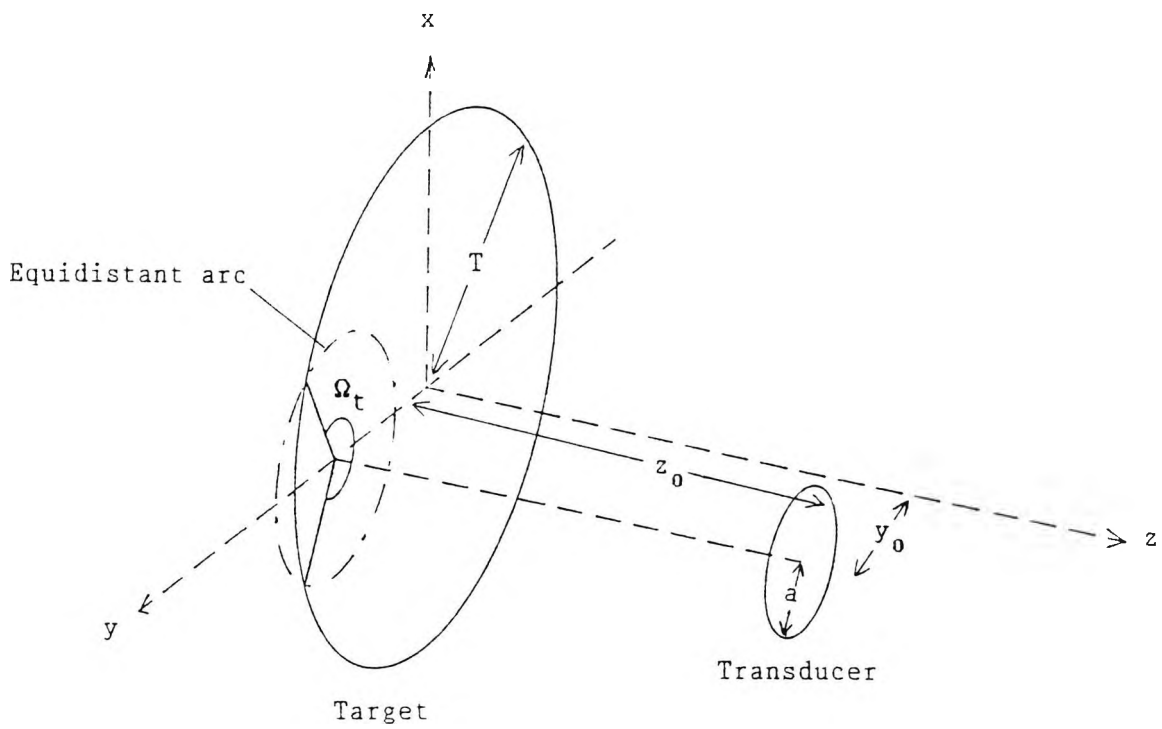


Figure (2.9.1): Geometry of a circular source and a finite-sized target at an arbitrary position in the field.

Thus eqn. (2.8.28) becomes for the case of any circular finite-sized target anywhere in the field:-

$$e_{it}(\underline{r}, t) = K \int_{y_0 - T}^{y_0 + T} \left[\frac{\partial \phi_i(\underline{r}, t)}{\partial t} * \frac{\partial \phi_i(\underline{r}, t)}{\partial t} \right] \Omega_t y dy . \quad (2.9.2)$$

Note that the integration is carried out from the nearest edge of the target to the furthest edge. If the target is in a position such that $y_0 < T$, then the integration is started at zero, and not at $y_0 - T$, which would be negative.

To obtain the transmit-receive echo signal, $e_t(t)$, an expression of the form of eqn. (2.4.13) is used:-

$$e_t(t) = u(t) * e_{it}(\underline{r}, t) . \quad (2.9.3)$$

To calculate the velocity potential, eqn. (2.9.2) is assumed to have a form like eqn. (2.5.11):-

$$e_{it}(\underline{r}, t) = P_{it}(\underline{r}, t) * P_{it}(\underline{r}, t) . \quad (2.9.4)$$

By moving to the frequency domain, the convolution becomes a multiplication:-

$$e_{it}(\underline{r}, \omega) = P_{it}(\underline{r}, \omega) P_{it}(\underline{r}, \omega) . \quad (2.9.5)$$

So that

$$P_{it}(\underline{r}, \omega) = \sqrt{e_{it}(\underline{r}, \omega)} , \quad (2.9.6)$$

or

$$P_{it}(\underline{r}, t) = \frac{1}{2\pi} \int_{-\infty}^{\infty} P_{it}(\underline{r}, \omega) e^{j\omega t} d\omega . \quad (2.9.7)$$

These last steps can easily be calculated on a computer by taking Fourier transforms, complex square-rooting, and taking the inverse

Fourier transform. To obtain the velocity potential impulse response, eqn. (2.4.11) is used:-

$$P_{it}(\underline{r}, t) = \rho \frac{\partial \phi(\underline{r}, t)}{\partial t} . \quad (2.9.8)$$

Thus the velocity potential impulse response for finite-sized targets is given by:-

$$\phi_{it}(\underline{r}, t) = \int_{t_{near}}^{t_{far}} (1/\rho) P_{it}(\underline{r}, t) dt , \quad (2.9.9)$$

where t_{near} and t_{far} are the go and return times between the closest parts and the furthest parts, respectively, of the transducer and target.

When the target is within the transducer's geometric region, t_{near} is given by:-

$$t_{near} = (2/c) z_0 , \quad (2.9.10)$$

and outside the transducer's geometric region:-

$$t_{near} = (2/c) \sqrt{ \{ z_0^2 + (y_0 - a - T)^2 \} } , \quad (2.9.11)$$

and t_{far} is given by:-

$$t_{far} = (2/c) \sqrt{ \{ z_0^2 + (y_0 + a + T)^2 \} } , \quad (2.9.12)$$

where the symbols are as defined in figure (2.9.1).

2.10 Transducers

Recent experimental work carried out at City University by Dr. R. Brittain has led to the development of practical versions of non-uniformly-excited transducers (Weight 1982a, and Brittain and Weight, 1987). These transducers and conventional uniformly-excited transducers have been used to obtain all the experimental results. Their construction is described briefly in the following sections.

2.10.1 Conventional uniformly-excited transducer

The conventional transducer was a commercially available Panametrics V3289, with a 9.5mm radius aperture. These are manufactured from heavily damped discs of lead metaniobate (PMN) with a 10MHz half wavelength thickness, equivalent to $c/2f = 3300/2 \times 10^7 = 0.16\text{mm}$.

A schematic diagram of the construction of such a transducer is shown in figure (2.10.1.1). The piezo-electric disc has electrodes on the front and rear surfaces. The front electrode is connected to the transducer case, and forms an earth screen. The rear electrode is connected to a conductive backing, and the excitation signal is applied to this. When excited with a short, high-voltage pulse, the transducer generates a short pulse of ultrasound which has a useful frequency content from 1 to 10 MHz.

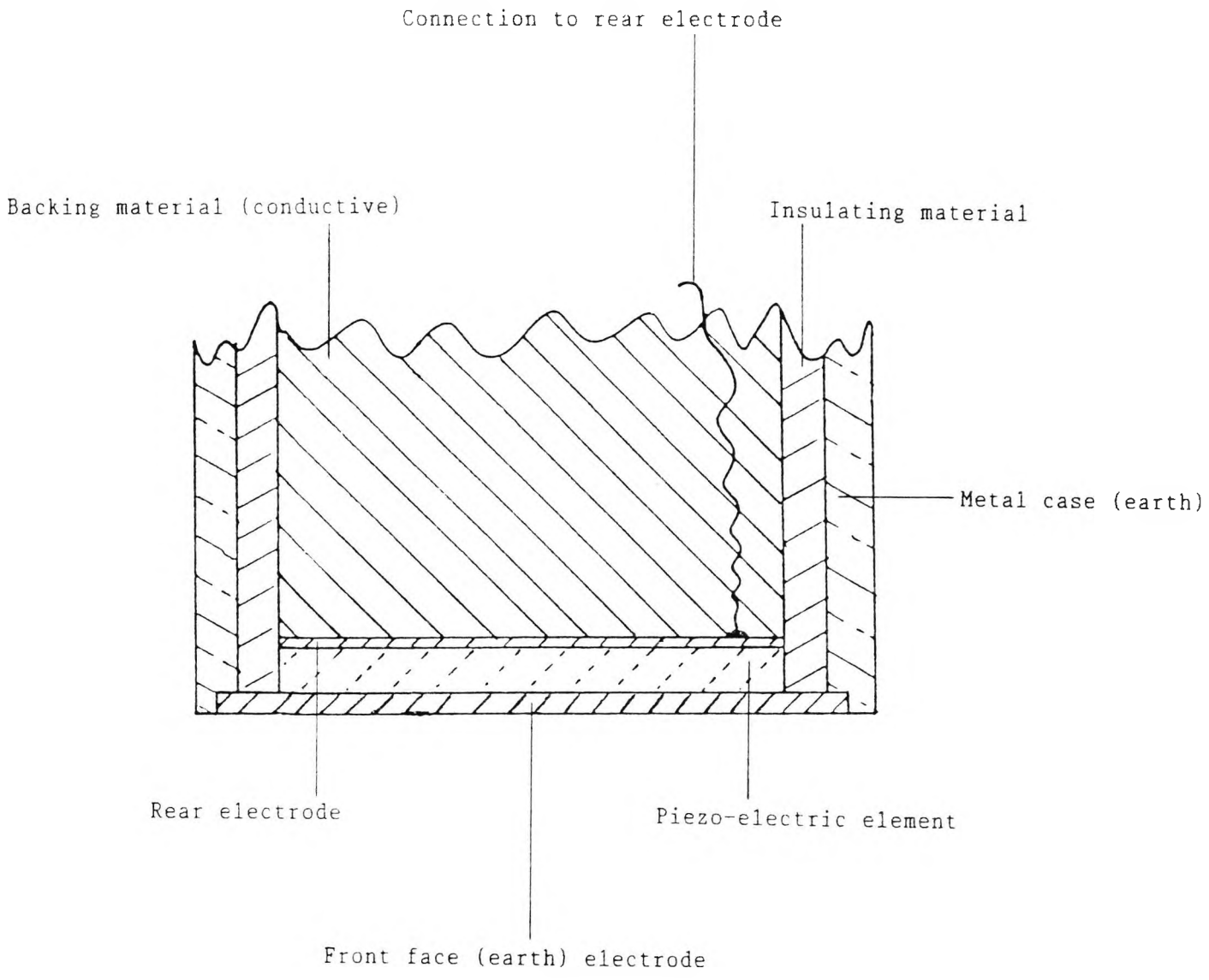


Figure (2.10.1.1): Schematic diagram of the construction of a conventional uniformly-excited transducer.

2.10.2 Non-uniformly-excited transducers

The method currently used to produce non-uniformly-excited transducers in our laboratory is described more fully in Brittain and Weight (1987) and is only briefly described here. Physically, non-uniformly-excited transducers look the same as conventional uniformly excited transducers (section 2.10)). The difference is that specially poled piezo-electric elements are used to give the transducer its desired properties. The poling process is a method of changing the piezo-electric element's intrinsic piezo-electric characteristics as a function of distance from the centre of the element. This produces an axisymmetric variation of piezo-electric strength. The degree of poling is controlled by using a series of concentric electrode rings in conjunction with a suitable potential divider network to vary the strength of the electric field applied across a de-poled element during its re-polarisation. Such a method allows various theoretical weighting functions, such as those shown in figure (2.7.2), to be applied to produce edge-wave-only and plane-wave-only transducers. Using a number of electrode rings, produces a coarse, step-wise approximation to the required weighting function. Field fringing (Weight, 1984a and Brittain and Weight, 1987) tends to smooth this out to give a closer approximation. The construction and performance of edge-wave-only and plane-wave-only transducers is described more fully in Brittain and Weight (1987 and 1990).

2.10.3 Non-uniform relationship between range and time

With uniformly-excited transducers, waves are emitted from the face of the transducer, and so it is assumed there is a linear relationship between range and time, which for the transmit-receive case, figure (2.10.3.1a), is:-

$$z = ct/2 . \quad (2.10.3.1)$$

However, at short ranges, there are three pulses (on axis), figure (2.5.1a), the latter two pulses arising from edge waves, and so they do not follow the linear relationship of eqn. (2.10.3.1) like the first (plane) wave does. When the three pulses are displayed on a time-series display, such as an oscilloscope, this means that they are shown shifted in time. The range/time relationship for edge waves is given by simple application of Pythagoras' theorem:-

$$z = \sqrt{\{(ct/2)^2 - a^2\}} , \quad (2.10.3.2)$$

This is important in the case of edge-wave-only transducers, figure (2.10.3.1b), since only edge waves are produced. If accurate measurements of range are required when using edge-wave-only transducers, it is a simple matter to calculate the time-of-flight and use eqn. (2.10.3.2) to obtain the exact range.

For the case of a water coupled target being interrogated by an edge-wave-only transducer, (figure (2.10.3.1c)), it is a much more complicated situation, because refraction occurs at the liquid/solid interface. As there are no exact expressions for refraction at the liquid/solid boundary, this means that errors can occur when calculating a target's range from its go-and-return time. I have developed an iterative method to overcome this problem and determine the error which would occur in indicated target range that would arise

if a linear time-base were used to display the target echoes. The algorithm works by using as a first guess the straight path from transducer edge to target, disregarding the refraction at the liquid/solid boundary. The algorithm then iterates to give a better approximation to the actual path, now taking into account the refraction at the liquid/solid boundary. The algorithm converges quickly to give a good approximation of the true path, and hence the time-of-flight to a target at a given depth can be calculated. Figure (2.10.3.2) shows the results of a typical situation, of an edge-wave-only transducer interrogating an 80mm deep aluminium block in water, using a 40mm coupling range. The solid line represents the actual error occurring for a given depth of target. There is assumed to be zero error at the front and rear faces of the target block, since on an oscilloscope the timebase and time delay can be adjusted to make this so. The figure shows that there is a single maximum error for this experimental set-up, of about 2.2mm at 20mm target depth. Experimental measurements taken using a non-uniformly excited edge-wave-only transducer are plotted on the graph, and confirm the theoretical curve.

The above error correction obviously depends on the length of the water coupling path to the solid target block, since rays from the transducer's edge are refracted more with a short coupling range, than with a long coupling range. This becomes an important consideration when interrogating targets embedded in solid blocks. However, as this thesis is concerned with targets in fluid media, this error correction is not required.

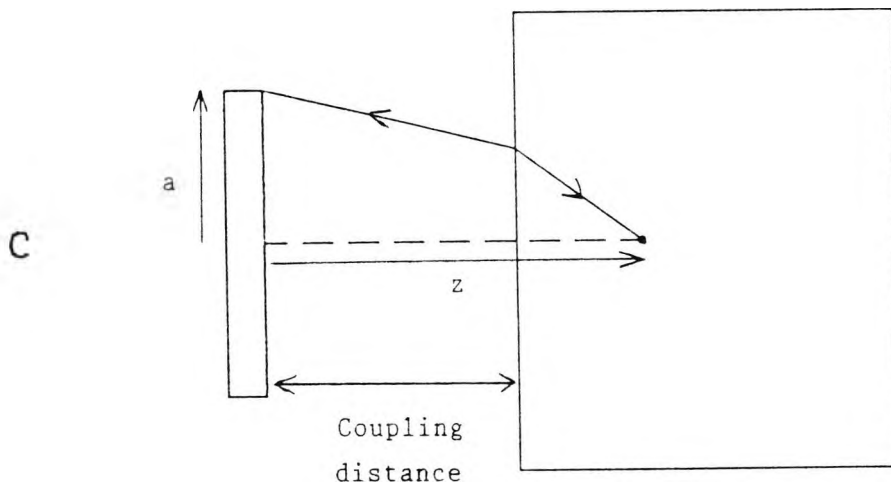
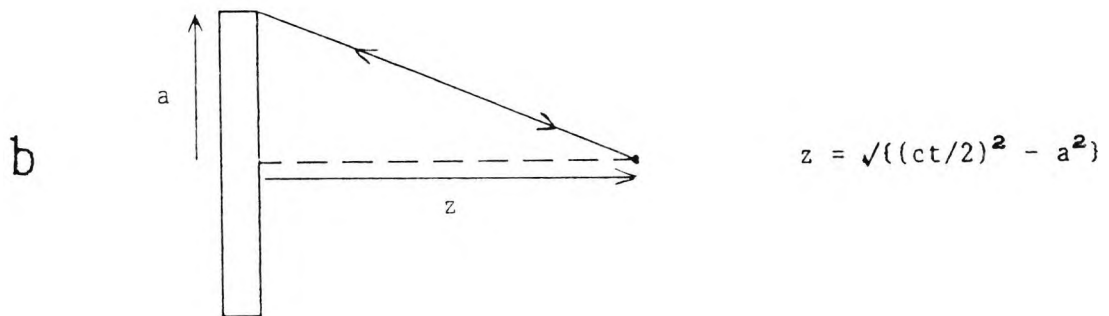
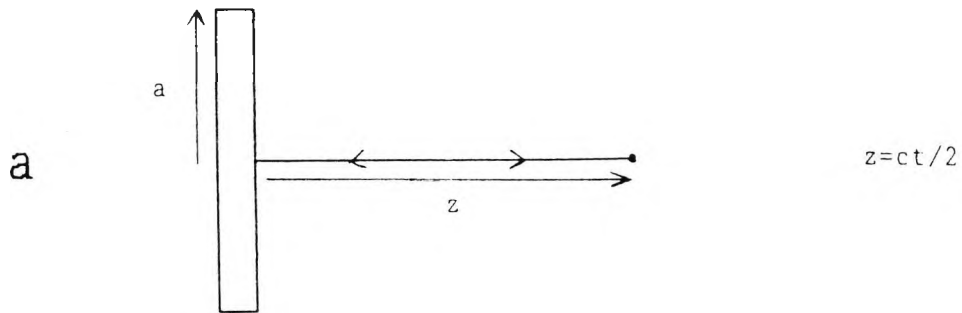


Figure (2.10.3.1): Range and time relationships for:
 a: Uniformly-excited transducer,
 b: Ideal edge-wave-only transducer,
 c: Water coupled target and ideal edge-wave-only transducer.

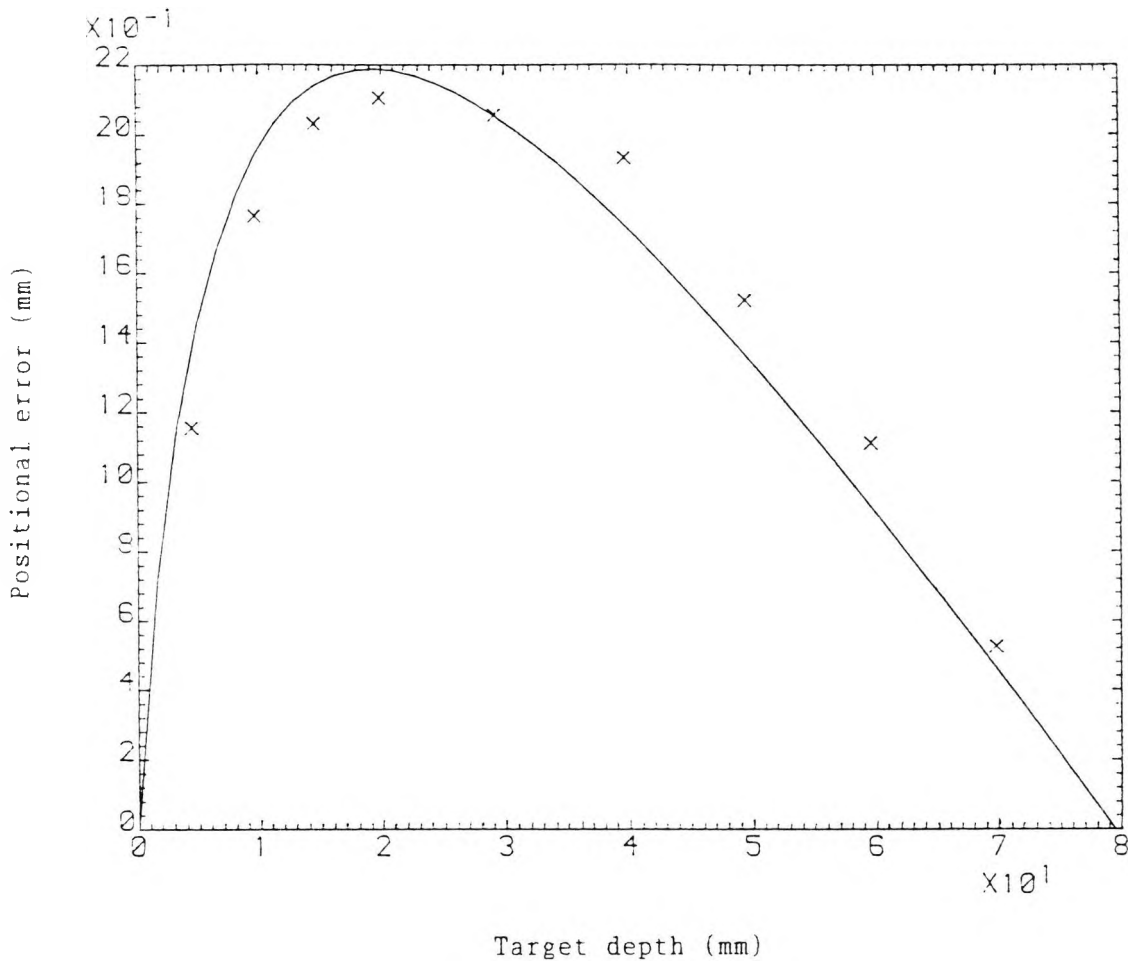


Figure (2.10.3.2): Relationship between target depth and positional error for a water coupled target block.

2.11 Application to solids

In fluids we need only be concerned with the propagation of compressional (longitudinal) waves. In solids, shear (transverse) waves and Rayleigh (surface) waves can also be propagated. Remembering that mode conversion between the various types of waves can occur at the liquid/solid interface, the mathematical treatment of a source propagating into a solid is much more difficult (see for example, Graff, 1975).

The transducers described previously in section 2.10 can be used immersed in water, or directly coupled to the surface of a solid, using a coupling jelly.

A new simple model for a source directly coupled to a solid surface based on the impulse response methods given previously, has been developed (Weight, 1982b and 1987). Hayman (1977) and Weight (1982b) consider that the shear waves which propagate in solids are mode converted edge waves. Briefly, the model calculates the velocity potential impulse response in two parts. One part is calculated at the compression wave velocity, and the other is calculated at the shear wave velocity. The individual velocity potential impulse responses then have to be weighted by empirically determined "mode conversion factors" (Weight, 1987). The shear wave velocity potential impulse response is then appended (after the appropriate time delay) to the compression wave velocity potential impulse response, to give the total velocity potential impulse response.

On axis, the pressure waveform consists of a compression plane wave, a compression edge wave, and a shear edge wave. Both edge waves split into two parts as the receiver moves off axis.

Of the non-uniformly-excited transducers in section 2.10, the plane-wave-only type is likely to be most useful, since there are no edge waves to mode convert into shear waves, resulting in simpler waveforms. The edge-wave-only transducer could also be useful, since as the compression and shear edge waves travel at different velocities, they are well time separated (except for very close ranges) and the shear edge wave can be gated out.

This work in fluids could be adapted to allow for the case of solids by modifying the single subroutine which calculates the impulse response. However, this is left as future work.

With the exception of a single B-scan result (figure (3.5.2), included in order to compare transducer performance), no results are presented using targets within solid materials.

2.12 Computational methods

2.12.1 General details

The computations employed numerical integration, differentiation, and convolution, and so the increments used had to be chosen with care to ensure that numerical errors were small and that displayed waveforms were smooth.

The convolutions involve dealing with delta functions in the impulse responses, and at first sight would appear to be a problem, since they have an infinite amplitude and must be convolved with the transducer velocity function. A delta function has zero time duration and hence infinite bandwidth, but the transducer velocity function (a single cycle of a 5MHz sine wave, say) has only a finite bandwidth. This is not a problem if the delta function is approximated by setting its amplitude to $1/\delta t$ (where δt is the time increment), so that there is unit area beneath the delta function. δt is then chosen so that the bandwidth of the delta function is wider than the bandwidth of the transducer velocity function. A suitable approach is to choose a maximum frequency, f_{\max} , beyond which there is little contribution to the frequency spectrum of the transducer velocity function, and use the Nyquist criterion:-

$$\delta t = \frac{1}{2 f_{\max}}, \quad (2.12.1.1)$$

to determine δt . In the above example, f_{\max} would be estimated as about three times the centre frequency, i.e. $3 \times 5 = 15\text{MHz}$, so $\delta t = 1/30 = 0.033\mu\text{s}$. In practice, smaller time increments of $0.005\mu\text{s}$ were used to ensure that the waveforms looked smooth when plotted.

Such smooth waveforms, with fine time increments δt , do of course mean coarse frequency increments, δf in the frequency domain. This occurs as a consequence of eqn. (2.12.1.1) where one increment is proportional to the reciprocal of the other. This means that spectra of convolved waveforms, if plotted directly, are not going to be smooth curves, but will be rather sharp and angular. There are two answers to this problem. One is to append large numbers of zeros to the waveforms before transforming to the frequency domain. This has the effect of reducing δf because the bandwidth f_{\max} is subdivided into many more points. The second method is to sample the convolved waveform (at the Nyquist rate) and throw several points away before transforming to the frequency domain. This has the effect of reducing δf by making δt bigger. Spectra are not shown in this thesis, but one of the above methods must be used when calculating them.

The convolutions were carried out directly in the time domain, based on the graphical method given by Bracewell (1978, chapter 3). Fast Fourier transform methods were not used, since tests showed that they did not significantly decrease the computer run-times. This was because although the maximum size of the arrays to be convolved was set in the programs to 2000 elements, in practice they were never this large (except at close range and far off-axis). It was also more convenient to use time domain convolution, as this allowed arbitrary length arrays to be used to store the waveforms. Fast Fourier transforms require the number of elements in the arrays to be exactly 2^n .

Digitised waveforms which were to be used as inputs to the programs may have had a DC level superimposed. This DC shift occurs as

a consequence of the equipment used to digitise the waveform. The required waveform has first to be displayed on an oscilloscope with an IEEE-488 interface bus. Using a personal computer connected to the interface bus, and some software written by the author, the computer can command the oscilloscope to send 1024 samples of the displayed waveform, over the interface bus back to the computer. Depending on the vertical position of the waveform with respect to the centre of the oscilloscope display, the sampled values of the waveform may be regarded as having a DC shift. This was reduced by calculating the definite integral of the waveform using the trapezium method, and then calculating the mean value. The mean value was then subtracted from the original waveform. If this were not done, then the waveform could have a step at the end which would cause a spurious pulse to appear after convolution.

As mentioned in section 2.6, the simple waveform used to show the pulse structure in the pressure and transmit-receive responses was not just an ordinary sine wave, but was a smoothed sine wave of the form:

$$\sin(\omega t) - \left[\frac{N}{N+1} \right] \sin \left\{ \left[\frac{N+1}{N} \right] \omega t \right\} , \quad (2.12.1.2)$$

where N is the number of cycles. In this work one cycle was used for simplicity, so eqn. (2.12.1.2) becomes:-

$$\sin(\omega t) - \frac{1}{2} \sin(2\omega t) . \quad (2.12.1.3)$$

Such an expression gives a waveform which is very close to a single cycle of a sine wave, and ensures that the beginning and end of the wave reach zero smoothly, preventing discontinuities from appearing after convolution.

Up to this point, the targets that have been modelled were simple

cylindrical rods with a flat front face. A modification of the finite-size target modelling of section 2.8 has been developed, to allow the model to consider a cylindrical target with a pointed front face, similar to a cone. A schematic diagram of such a target is shown in figure (2.12.1.1). The method works by treating the target as if it were a collection of flat-faced cylindrical targets of increasing diameter, at successive further ranges. This results in a step-like approximation to the pointed face of the target. The numerical increments used in the programs were chosen to give a reasonably large number of calculation steps describing the pointed face of the target. An increment of 0.01mm was used across the width of the target, and an increment of between 0.001mm and 0.005mm was used (depending on how pointed the front face was) along the axis of the target. Currently, only targets which are on-axis are considered, extension to off-axis targets being left to future work.

This method could be generalised to describe any axisymmetrically-shaped target, by simply describing the target in terms of a number of conventional flat-faced targets. However, this method does not take into account specular reflections from the surface of the target, nor refraction and internal reflections.

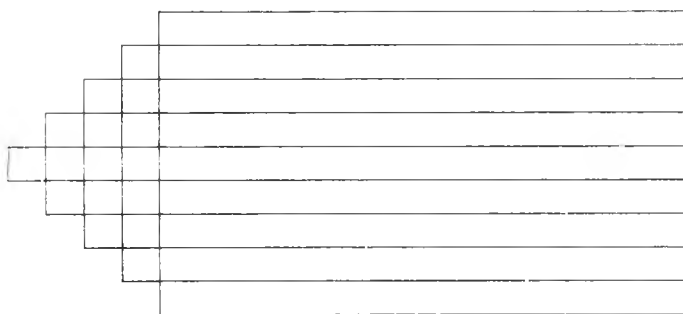
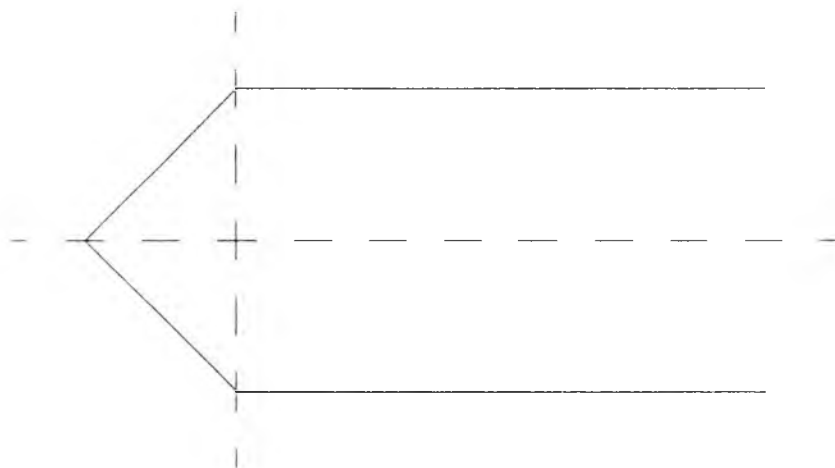


Figure (2.12.1.1): Schematic diagram of a finite-sized cone-shaped target (*top*), and how it is modelled (*bottom*).

2.12.2 Implementation of the equations on the computer

For point targets interrogated by uniformly excited transducers, the equations are implemented in a straightforward way. A single subroutine calculates the velocity potential impulse response according to eqn. (2.4.10). This is then differentiated with respect to time to give the pressure impulse response (eqn. (2.4.11)). For pressure waveforms, the pressure impulse response is simply convolved with the transducer velocity, eqn. (2.4.13). For transmit-receive waveforms, the pressure impulse response is first convolved with itself and then with the transducer velocity, eqn. (2.5.11).

For non-uniformly-excited transducers, a loop is used in the calculation of the velocity potential impulse response, to enable the building up of a total velocity potential impulse response as defined by the shape of a velocity profile (section 2.7). Each time around the loop a simple velocity potential impulse response is calculated for a progressively smaller uniform source and this is weighted by the amplitude of the velocity profile graph. Each velocity potential impulse response is then added to (for plane-wave-only transducers) or subtracted from (for edge-wave-only transducers) the total, as shown in figure (2.7.1). This total velocity potential impulse response is then used in the calculations above for the pressure and transmit-receive waveforms.

For finite-sized, targets the time differential of the velocity potential impulse response is convolved with itself within an integration laterally across the face of the target, eqn. (2.9.2). As the integration loop steps across the target face, the velocity potential impulse response is calculated at each point as if there

were just a point target at that position on the target's face. Each time around the integration loop, the values calculated after the convolution are first weighted according to the amount of circular arc which crosses the target face at that position, and then added to a running total, which ultimately becomes the value of the integral.

For cone-shaped targets (on axis only), the method for finite-sized targets above was used in a slightly modified way. As the cone-shaped target is regarded as a collection of flat-faced finite-sized targets (section 2.12.1, and figure (2.12.1.1)), the velocity potential impulse response is calculated for each flat-faced finite-sized target in turn. The collection of velocity potential impulse responses are then superposed to give a total velocity potential impulse response, which is used to obtain the subsequent waveform results.

3 Results

Several computer programs have been written over the years to produce calculated results for the various members of our research group. When different types of results are required, these programs get modified, or even rewritten, so that now, there are several programs, each designed to calculate a specific type of result, or display an existing result in a different way. It is part of the author's job to keep these programs running, modifying them as and when it becomes necessary. These programs can be divided into three main groups. The first two groups each consist of four programs set up to calculate general sets of results for impulse responses, waveforms, spectra and beam profiles. The first group calculates results for point targets, and the second group calculates results for finite-sized targets.

Each individual program was capable of modelling any size and type of circular transducer (ideal and non-uniform), excited with any arbitrary waveform, any size of circular target at any arbitrary position in the field, and in pressure or transmit-receive mode. The transducer excitation waveform and weighting profile could either be calculated, or read in from a data file containing sampled values of a real waveform or profile.

The final group of programs is a miscellaneous collection, comprising programs for calculating more specialised results, or displaying results in a more specialised manner, and for drawing some of the other figures of this thesis.

The constants which are taken into account in the following results are transducer radius, target position and radius, speed of

sound, and time. No other constants were used (density, specific acoustic impedance), since these were multiplying factors, and this thesis is mainly concerned with the relative shapes of waveforms rather than their absolute amplitudes.

The results presented in this chapter first compare theoretical results for different types of transducer interrogating ideal, point targets, and two sizes of ideal, flat-faced, finite-sized targets. Next, experimental results are presented for the same targets, and compared with the theoretical predictions. Experimental and calculated results are also presented for the pointed, cone-shaped targets. Finally, some B-scans are presented, using both a conventional, uniformly-excited transducer and a non-uniformly-excited edge-wave-only transducer, to show how much improvement in resolution the new type of transducer is capable of. The results will be described briefly as they appear, and their implications will be discussed in more detail in chapter 4.

3.1 Computed results for point targets

This section presents computed results for the four types of transducer which have been discussed previously.

Velocity potential impulse responses are shown first, so that their structure can be described in terms of rays from the transducer's centre and edges, building up to a numeric visualisation of pressure waves radiated by the transducers. This provides evidence of the plane- and edge-wave structure of the radiated pressure field. From these results, a qualitative directivity pattern for edge waves alone, is derived. Finally, transmit-receive waveforms and beam profiles are shown, for the transducers interrogating ideal point targets.

Although some of the following results have been seen before in various publications, for example, conventional transducers (Stepanishen, 1971b, Beaver, 1974, Robinson et. al., 1974, and Weight and Hayman, 1978), edge-wave-only transducers (Weight, 1982a, and Brittain and Weight, 1987, and 1990), and general axisymmetric sources (Harris, 1981b, Stepanishen, 1981, Weight, 1984a, Guyomar and Powers, 1986, Harrison and Balcer-Kubiczek, 1986 and Hutchins et. al., 1986), this section attempts to collect all these results together for completeness, presenting some in new ways, adding some new results, and finally showing how the non-uniformly-excited transducers developed in our laboratory outperform conventional transducers.

3.1.1 Velocity potential impulse responses

Figure (3.1.1.1a) shows the velocity potential impulse response of a conventional uniformly-excited circular transducer. Note that this figure (and other subsequent, similar figures) conveys both time and space information in the same picture, in a pseudo-three-dimensional manner, such that vertical overlap between waveforms is kept to a minimum. However, some long waveforms have been truncated to prevent any horizontal overlap. The dots represent the position of the target and the waveforms starting at each dot are the velocity potential impulse responses as a function of time. The waveform is plotted starting at the time corresponding to the path length from the front face of the transducer to the target point. All the waveforms take this to be the time origin for convenience.

As described in section 2.4, the on-axis responses are of the "top hat" form. The initial rise occurs at the time of arrival of the wave from the transducer's plane surface, and the trailing fall occurs at the time of arrival of the wave from the transducer's edges. At greater ranges from the transducer, the time difference between the first arrival of the wave from the plane and the wave from the edges decreases, so that the response remains the same shape, but becomes more compressed in time. As the target moves off axis, there are now two edge positions to take into account (one from the nearest part of the transducer's edge to the target, and also from the furthest part of the transducer's edge to the target) and so the response has a more complicated fall-off in time. This is because waves from each edge position take different times to reach the target point as they travel along different paths.

Figure (3.1.1.1b) shows the velocity potential impulse response for an ideal edge-wave-only transducer of the same size as in figure (3.1.1.1a). The only difference between these two figures is that the initial rise of the waveform in the edge-wave-only case, has not been calculated. This only occurs in the geometric region straight ahead of the transducer; outside, both figures are identical. As will be seen later in section 3.1.5, this is equivalent to removing the plane wave contribution.

Figures (3.1.1.1c-d) show the velocity potential impulse responses for a non-uniformly excited edge-wave-only transducer, and a non-uniformly excited plane-wave-only transducer, respectively. As a consequence of the modelling, where non-uniformly-excited transducers are regarded as the superposition of a collection of sources with an appropriate velocity weighting function (section 2.7), the velocity potential impulse response is reduced gradually from its maximum value, smoothly down to zero. It is this slope which causes the reduction in the amplitude of either the plane-wave component or the edge-wave component (depending on the transducer being modelled), since the smooth slope produces very little after the differentiation operation to give the pressure impulse response, compared to the sharp step which gives the major contribution.

For the edge-wave-only transducer, the step that causes the plane-wave component impulse after differentiation (figure (2.4.2)) is reduced to zero (figure (3.1.1.1c)) and for the plane-wave-only transducer, the step that causes the edge-wave component impulse after differentiation is reduced to zero (figure (3.1.1.1d)). Thus where the ideal edge-wave-only transducer (figure (3.1.1.1b)) simply has the

initial step suppressed, the non-uniformly-excited edge-wave-only transducer (figure (3.1.1.1c)) has a gradual increase to a maximum value.

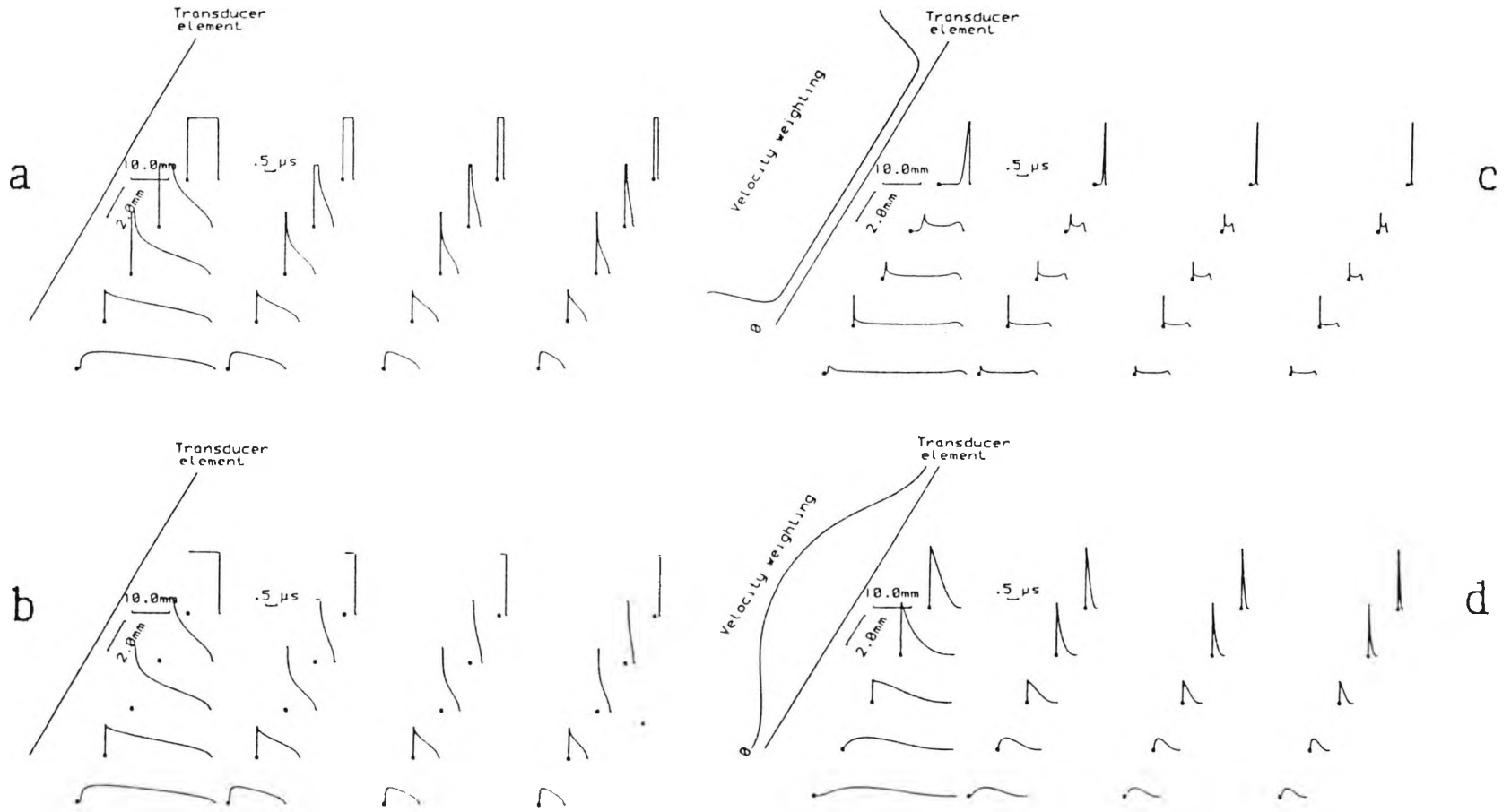


Figure (3.1.1.1): Velocity potential impulse responses at points (•) in the field of:
a: conventional ideal uniformly-excited transducer,
b: ideal edge-wave-only transducer,
c: ideal non-uniformly excited-edge-wave-only transducer,
d: ideal non-uniformly excited-plane-wave-only transducer.

3.1.2 Spatial velocity potential impulse responses

Figure (3.1.1.1) shows the velocity potential impulse responses displayed as time-series waveforms at a given point in space. An alternative way to display these results is to show the spatial form, at a given instant of time at all positions in the field, as is done by Robinson (1974). This has the effect of showing a "snapshot" of the velocity potential impulse response. Figure (3.1.2.1) shows the spatial form for a conventional uniformly-excited transducer, and figure (3.1.2.2) shows the spatial form for non-uniformly-excited transducers. These figures have been drawn in an isometric manner to enable the three-dimensional form to be displayed easily.

It can be seen that the axial range axis of figure (3.1.2.1) is a reversed form of the time axis of figure (3.1.1.1a), as time and distance always appear in the form $c^2t^2 - z_0^2$ in the defining equation, eqn. (2.4.9).

The large, angular, step-like part in the geometric region of the source will, after the differentiation and convolution operations of eqn. (2.4.14) and also figure (2.4.2), generate large pressure wavefronts. This is shown in the subsequent figure (3.1.3.1). Because the remainder of the velocity potential impulse response is smoother outside the geometric region, the pressure waves generated as a result, are of smaller amplitude. These wavefronts can both be seen in figure (3.1.3.1), where they show the plane- and edge-wave structure of the radiated pulse.

When non-uniformly-excited sources are considered, figure (3.1.2.2), two main changes are noticed. With the edge-wave-only transducer (figure (3.1.2.2a)), the structure of the velocity

potential impulse response shows clearly its dependence on the two edges of the source, resulting in semi-circular arcs emanating from the edges. When the pressure waveforms are calculated (figure (3.1.3.2)), the semi-circular wavefronts become pressure waves centred on the source's edges.

With the plane-wave-only transducer (figure (3.1.2.2b)), the velocity potential impulse response is similar to that for the uniformly-excited transducer (figure (3.1.2.1)), except that it is smoother. There is still a large step in the geometric region, and it is this step which gives the plane wave part of the pressure waveform (figure (3.1.3.3)).

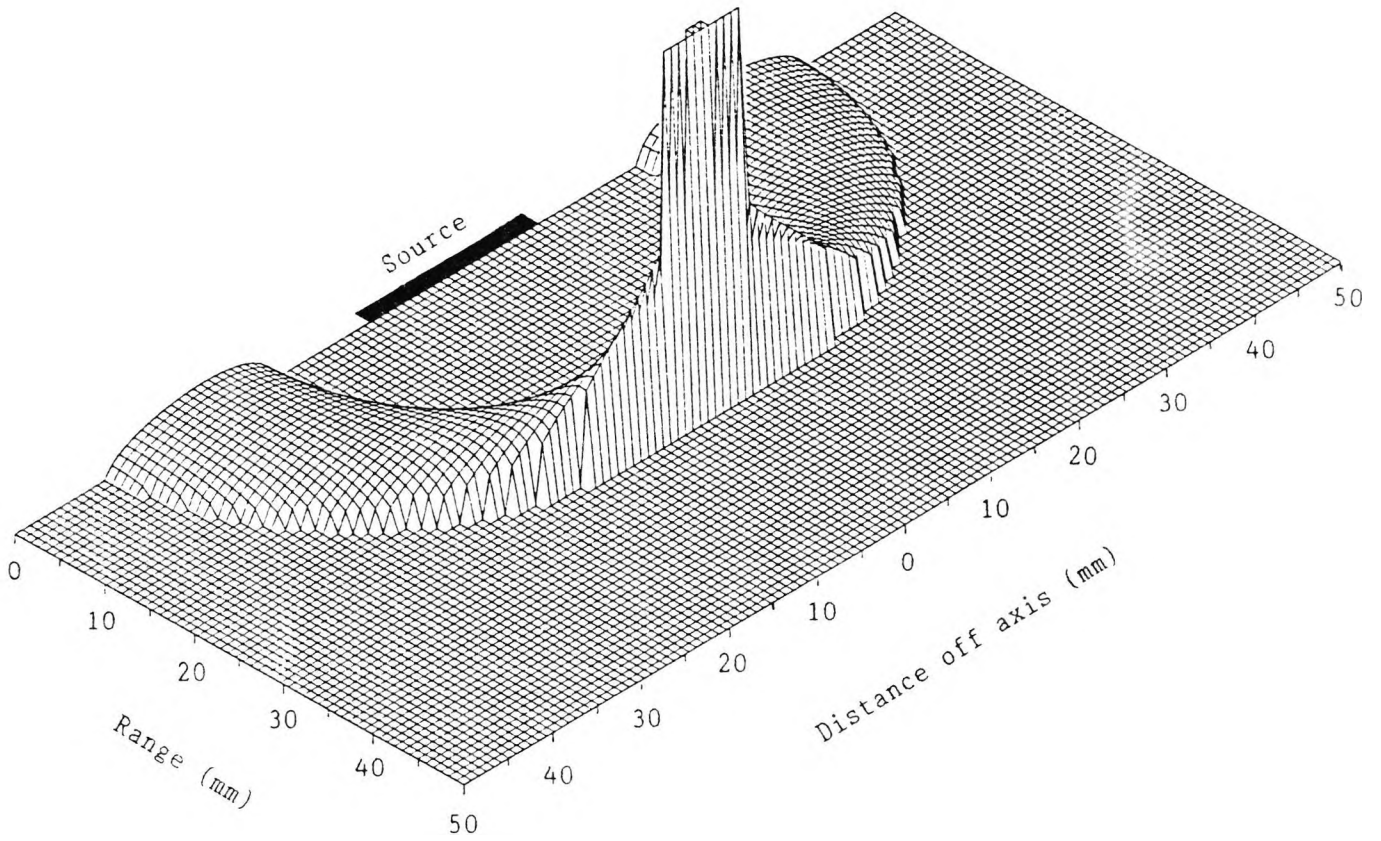


Figure (3.1.2.1): Spatial form of the velocity potential impulse response for a conventional uniformly-excited transducer.

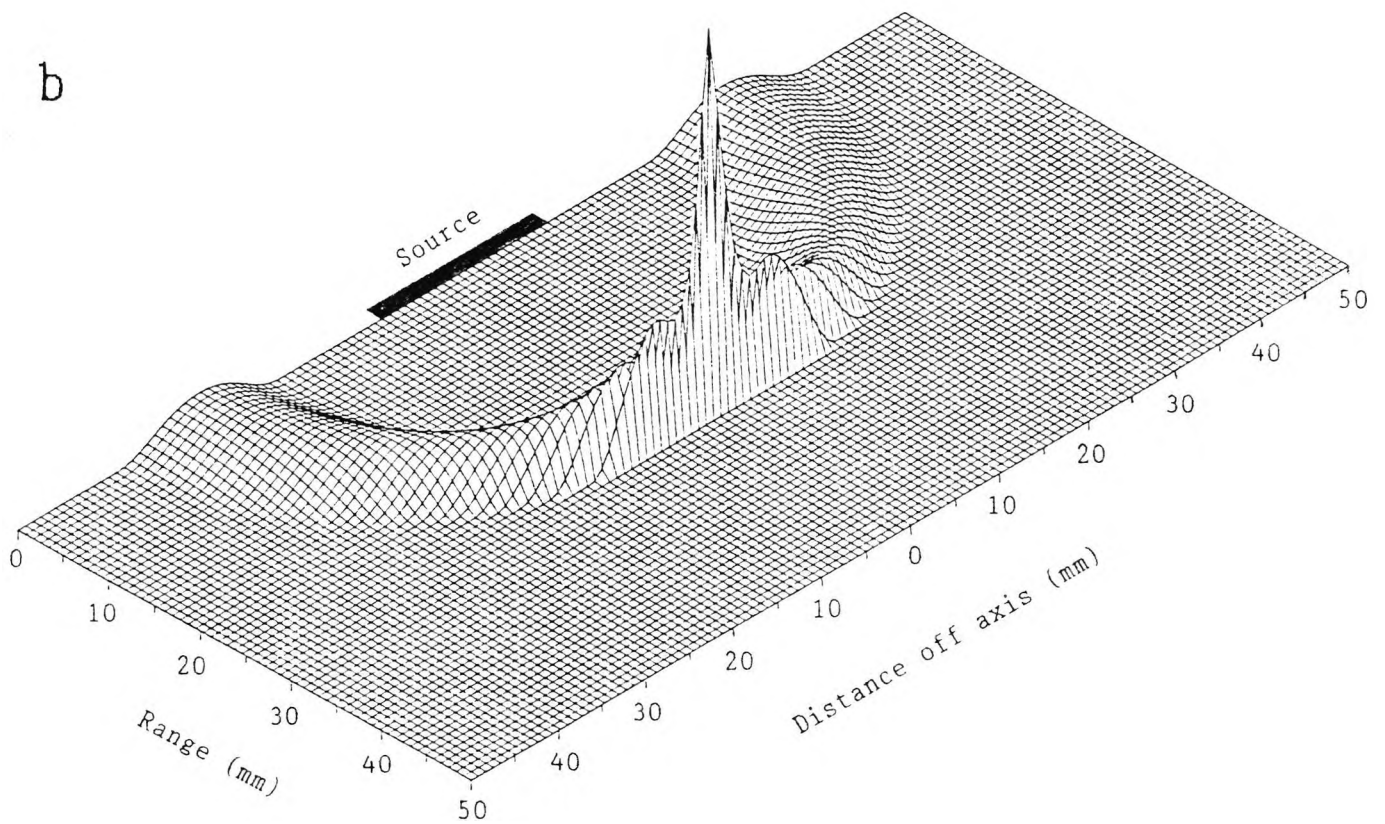
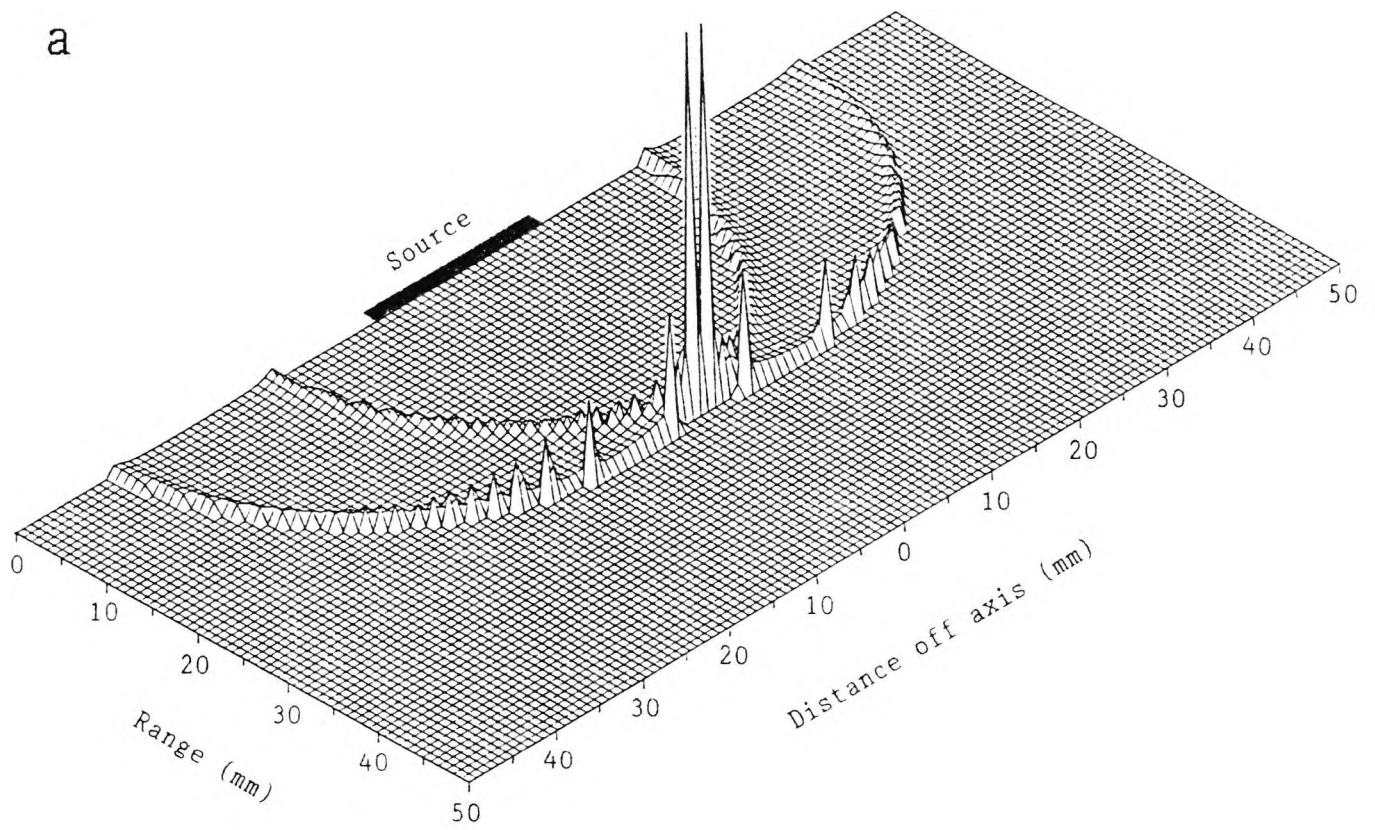


Figure (3.1.2.2): Spatial form of the velocity potential impulse response for:
 a: a non-uniformly-excited edge-wave-only transducer,
 b: a non-uniformly-excited plane-wave-only transducer.

3.1.3 Numerical visualisation of pressure waveforms

Pressure waveforms as a function of space can be calculated from the spatial form of the velocity potential impulse response, shown in figures (3.1.2.1-2), using the differentiation and convolution operations of eqn. (2.4.14). These are displayed as a sequence of four pictures which show the pressure pulse at successive times, figures (3.1.3.1-3). The figures are drawn as a sequence of closely spaced pressure waveforms, with the amplitude of each waveform plotted sideways. This results in a (numerical) visualisation of the pressure pulse as it travels away from the transducer. Two techniques have been used to enhance the figures so that the structure of the pressure field is clearer: the programs have been modelled for a transducer emitting a half-cycle of a sine wave, and also the plane-wave part has been reduced relative to the edge-wave part.

Figure (3.1.3.1) shows a pressure pulse as it travels away from a conventional, uniformly-excited transducer. What is immediately obvious from this figure is the plane- and edge-wave structure of the pressure field. This structure has also been seen in photoelastic visualisations (see for example Weight and Hayman, 1978). The plane wave is seen as a horizontal wavefront straight ahead of the transducer in the geometric region, and the edge-waves are seen as two circular arcs emanating from the edges of the transducer.

For the non-uniformly-excited edge-wave-only transducer (figure (3.1.3.2)), it is shown that the plane-wave component has been entirely suppressed, leaving just the edge waves (compare with the conventional transducer, figure (3.1.3.1)).

Similarly for the non-uniformly-excited plane-wave-only

transducer (figure (3.1.3.3)), the edge waves have been suppressed, leaving only the plane wave. Note that in section 2.7 it is stated that plane waves alone would still generate edge-waves as the plane wave propagates. This figure shows this - if it is examined carefully, small edge waves can just be seen.

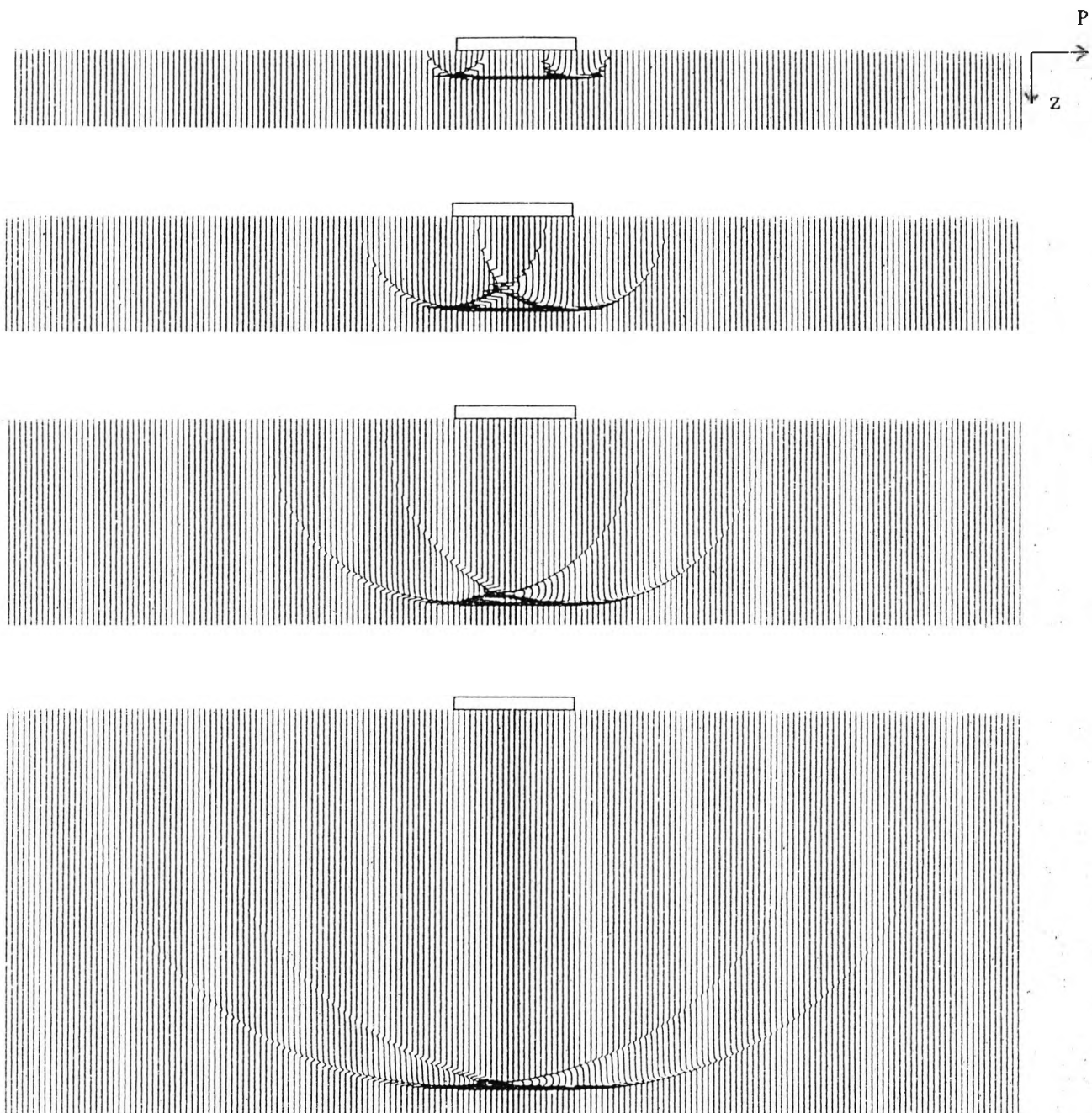


Figure (3.1.3.1): Numerical visualisation of a short pulse radiated into a fluid by a conventional uniformly-excited transducer.

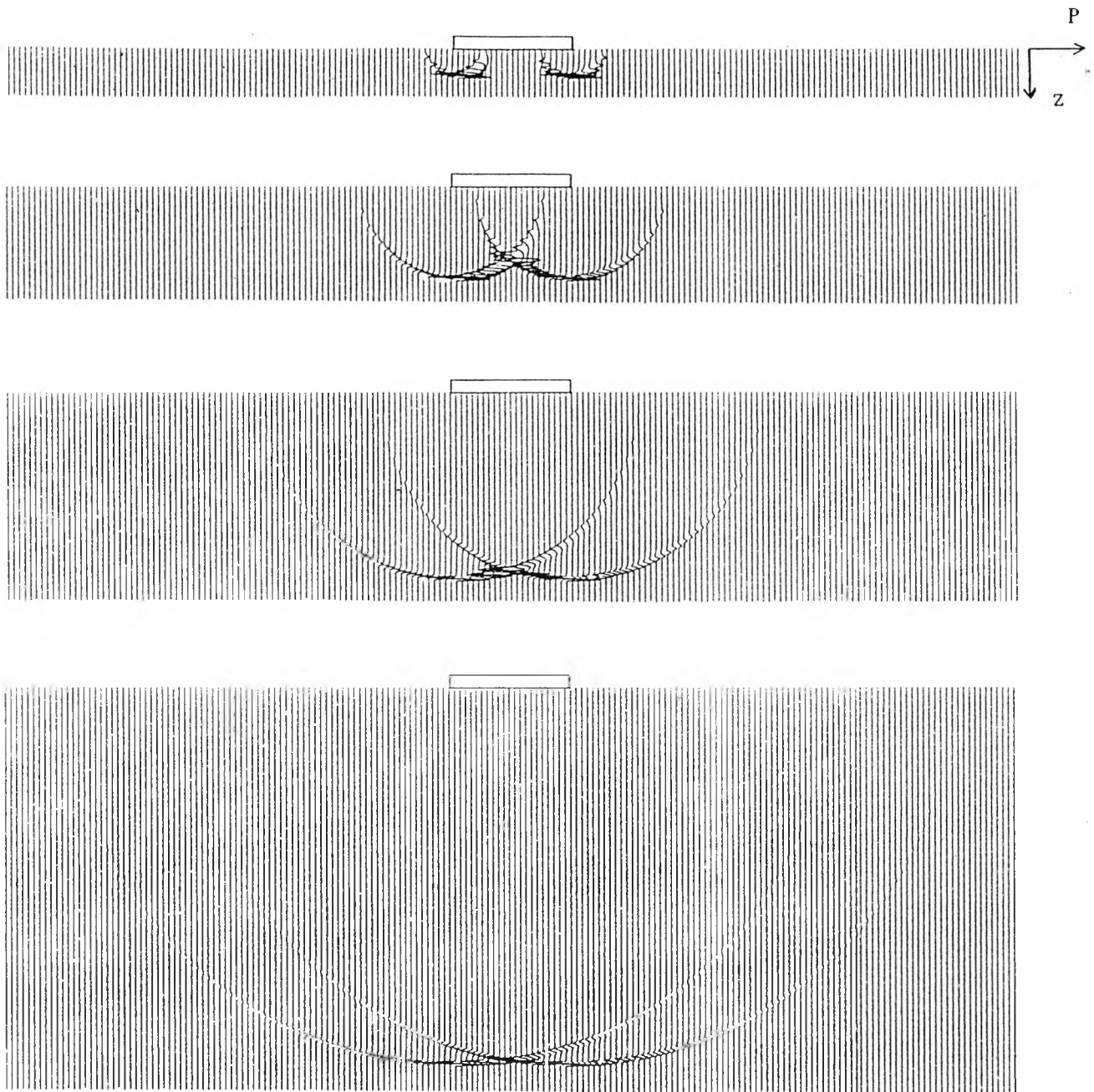
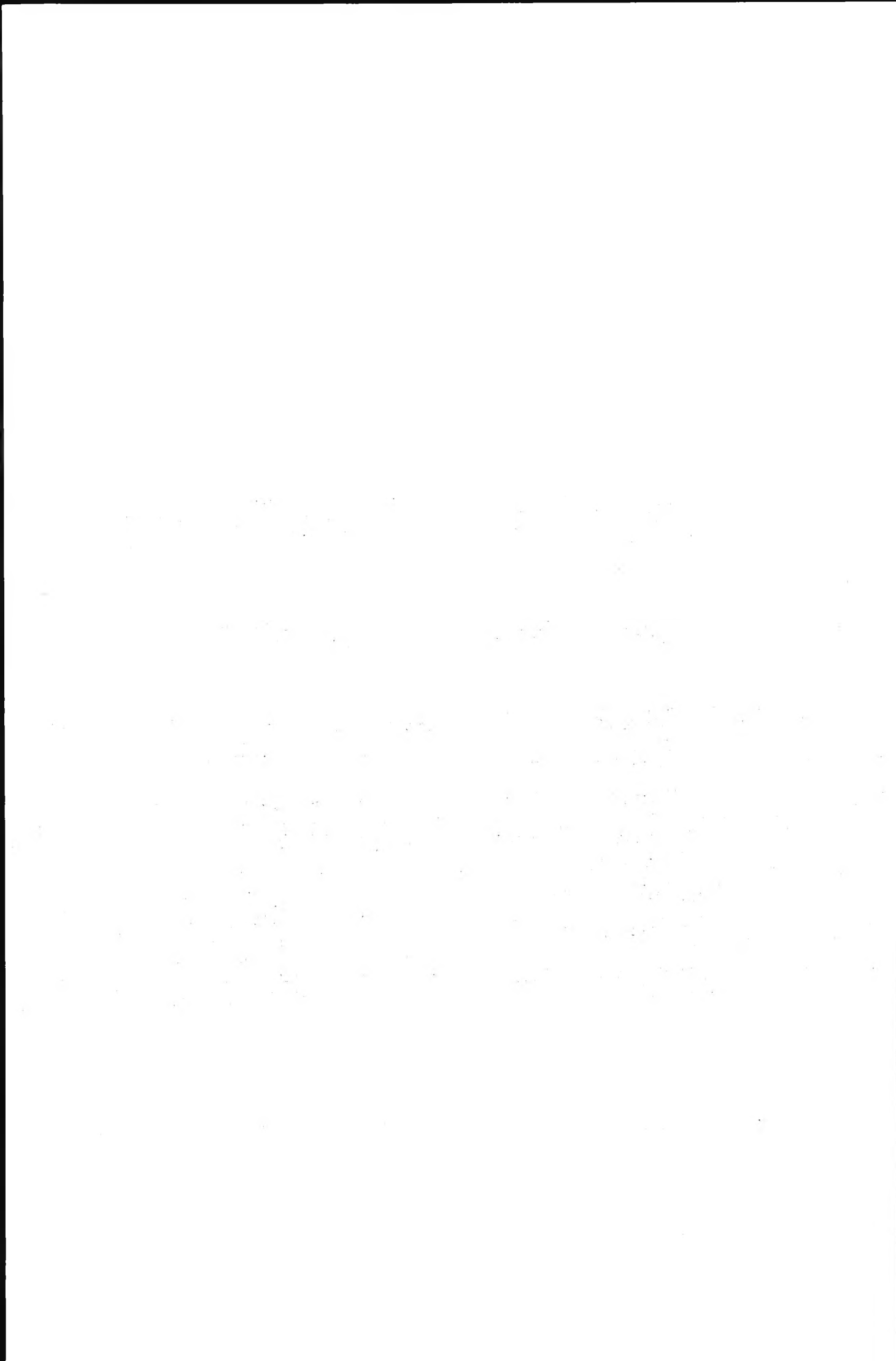


Figure (3.1.3.2): Numerical visualisation of a short pulse radiated into a fluid by a non-uniformly-excited edge-wave-only transducer.



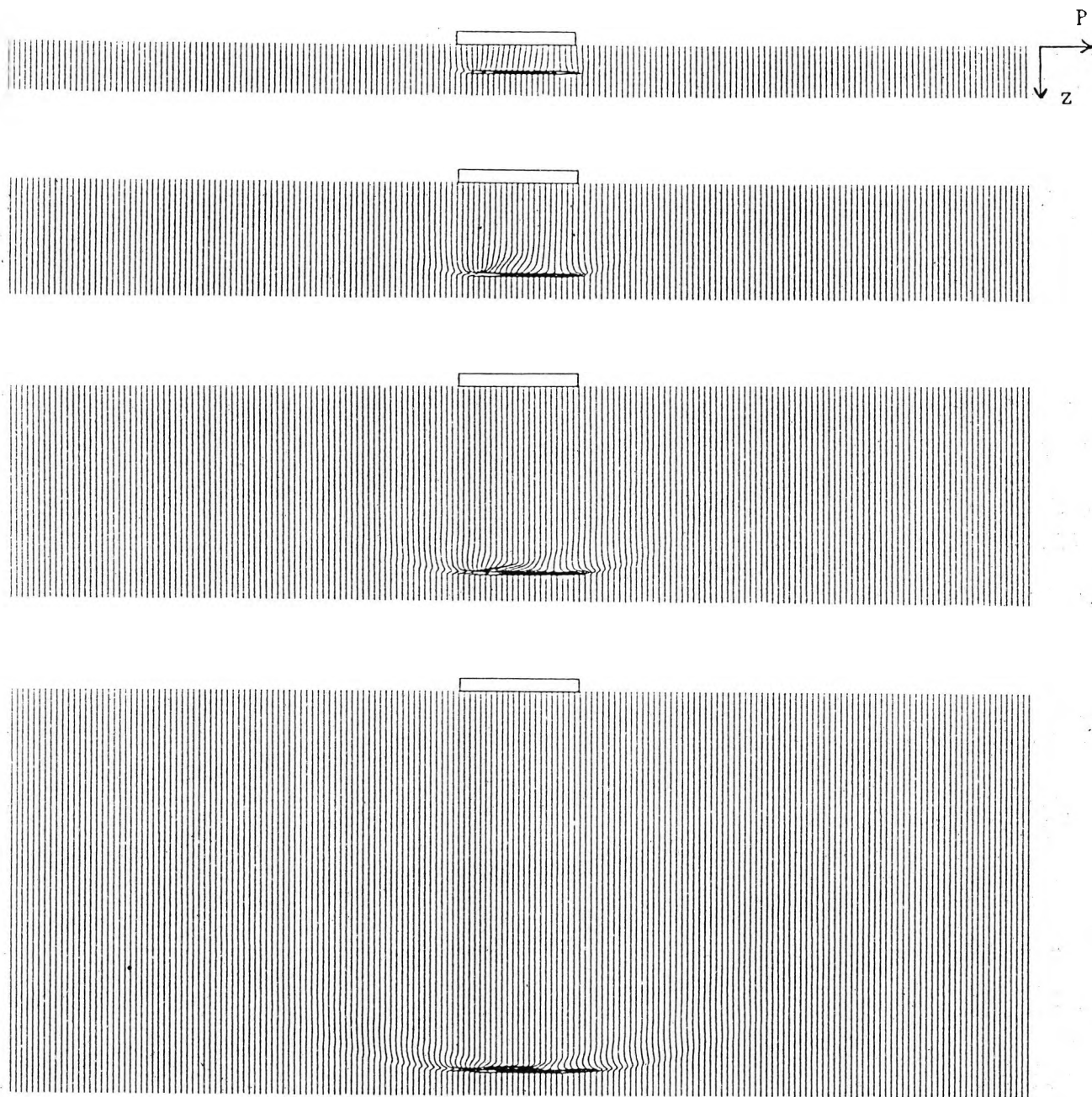


Figure (3.1.3.3): Numerical visualisation of a short pulse radiated into a fluid by a non-uniformly-excited plane-wave-only transducer.

3.1.4 Directivity of edge waves

As was stated in section 2.7, edge waves have a peculiar directivity, such that for an ideal edge-wave-only transducer, there is a constant amplitude pulse on axis. This will be seen for the transmit-receive case in figure (3.1.5.1b). This may seem strange, as the edge wave is a spreading wave, but the directivity compensates by being stronger in the direction straight ahead of the edge (figure (3.1.4.1), to be explained below).

Taking as the starting point the program which generates the numeric visualisation figures (3.1.3.1-3), but for an ideal edge-wave-only transducer, the directivity pattern for the edge waves has been calculated. It has been calculated by recording the maximum amplitude of each constituent waveform and then plotting these out as a directivity pattern. It is shown schematically in figure (3.1.4.1). As mentioned above, the directivity lobes are strongest straight ahead of the transducer's edge. They are also stronger towards the axis of the transducer than away from the axis. It is this eccentricity which compensates for the reduction in amplitude as the edge wave propagates. This result is an important result, in explaining the peculiar nature of edge waves. As was mentioned in section 2.7, their directivity exactly compensates for the reduction in amplitude of pressure and transmit-receive echo responses, producing a constant amplitude single pulse on axis. This will be shown in the next section, figure (3.1.5.1b).

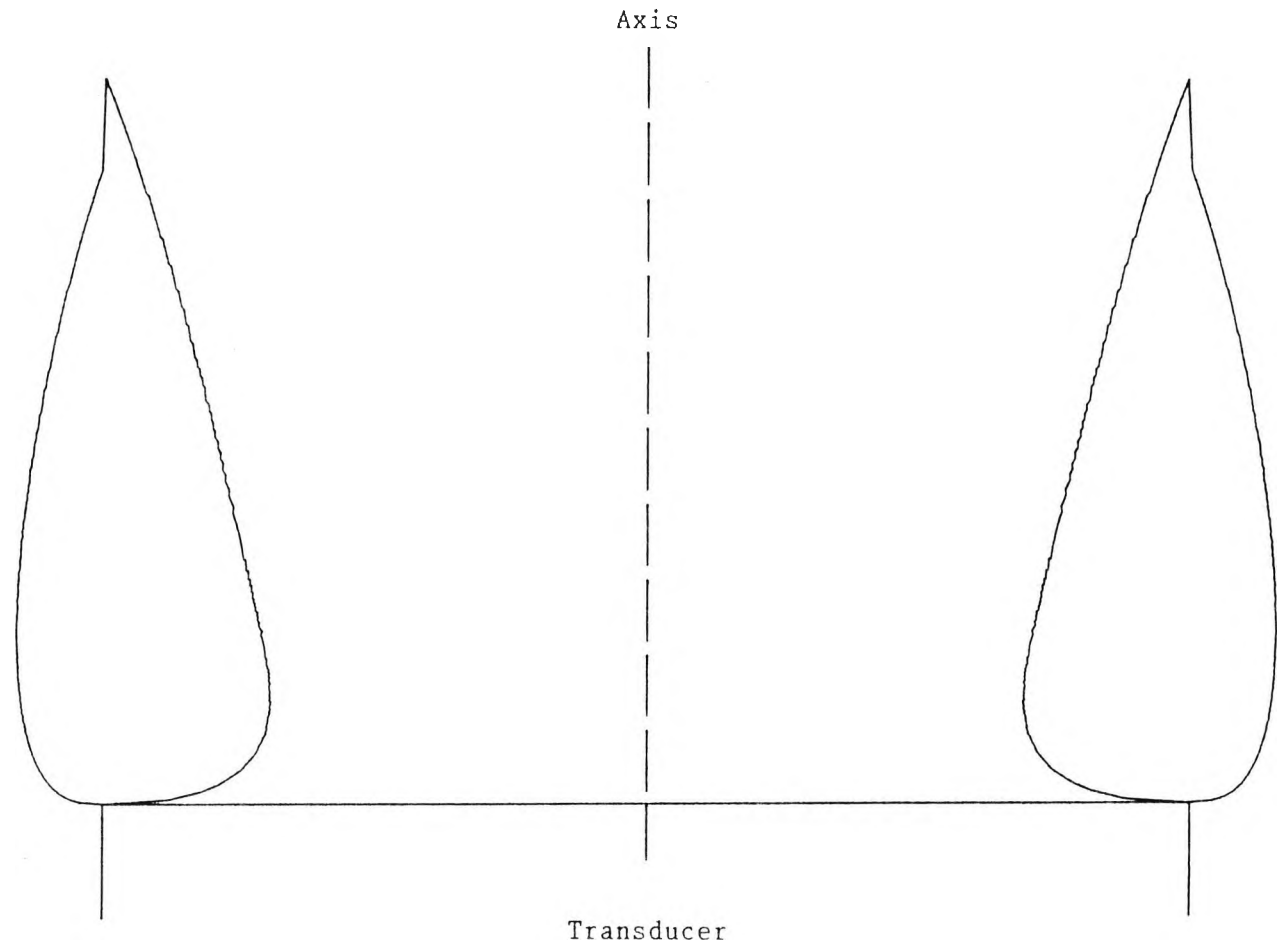


Figure (3.1.4.1): Calculated directivity pattern of an ideal edge-wave-only transducer

3.1.5 Transmit-receive waveforms

The transmit-receive waveforms are obtained after the differentiation and convolution operations given in sections 2.4 and 2.5 (eqns. (2.4.11) and (2.5.11)), and are shown in figure (3.1.5.1). This figure is drawn in the same way as figure (3.1.1.1), showing transmit-receive echo waveforms at various positions (marked by dots) in the field. Each waveform is plotted, starting from the time the plane wave takes to be received back at the transducer (or at the time the plane wave ought to be, in the case of edge-wave transducers).

The waveform used for the transducer velocity was a single cycle of a 5MHz sine wave (a smoothed sine wave - see section 2.12). This was chosen because it is short enough to allow the pulse structure of the waveforms to be seen clearly, but not so short as to be unrealistic. In practice, a transducer is not excited with a single cycle of a sine wave, but with a unidirectional pulse. This pulse tries to cause the transducer to 'ring' at its natural resonant frequency, but the damping material inside the transducer damps this resonance down so that approximately only one cycle remains.

For the uniformly-excited transducer, figure (3.1.5.1a), it can be seen how complicated the waveforms are. On axis, the three-pulse structure (section 2.5, figure (2.5.1)) telescopes together with increasing range. This is because further away from the source, the time separation between the axial plane wave and the edge waves, arriving from the centre of the source and from its rim respectively, is now less. The large central pulse on axis arises because of the overlap of the plane-wave pulse reflected from the target, and the

edge waves emitted by the transducer. This pulse has an amplitude twice that of the others. Off axis, the waveforms become even more complicated due to the edge waves being smeared out into smaller pulses. The range resolution is very limited for this transducer, since the total pulse width is large; i.e. the three component pulses are much longer than the single driving pulse.

The ideal edge-wave-only transducer (figure (3.1.5.1b)) has waveforms concentrated along the axis of propagation. As was mentioned previously in section 3.1.1, the plane waves have been removed in this ideal case, leaving only the edge waves. This can be explained with reference to figures (2.4.2a) and (2.5.1a), which show how the pressure and transmit-receive waveforms for a target on the axis of a conventional uniformly-excited transducer are modelled. If the initial rise in the velocity potential impulse response ϕ_i (figure (2.4.2a)) is not calculated, then the pressure impulse response P_i will not have the positive-going impulse, just the negative-going one. When this is convolved with itself (figure (2.5.1a)) to obtain the transmit-receive echo impulse response, and convolved with the transducer velocity, only one pulse remains in the echo waveform. Because there is now no plane wave to interfere with the edge waves, the waveforms are of constant amplitude on axis, and off axis, there is a small response straight ahead of the edge. This is due to the eccentric directivity of the edge waves being strongest straight ahead of the edge (Weight, 1982a), figure (3.1.4.1). This edge response is a quarter of the size of the axial response (12dB smaller) and so could lead to misinterpretation. Fortunately, this is not a problem with the physically-realizable non-

uniformly-excited edge-wave-only transducer (below). The overall pulse width has also been reduced, since there is now only one component pulse in the waveform. Thus the range resolution is now vastly improved.

The ideal non-uniformly-excited edge-wave-only transducer (figure (3.1.5.1c)) also has the echo waveforms concentrated along the axis of propagation, as would be expected from the ideal edge-wave-only case, although they are not as constant with range or simple in shape, but are certainly short enough to give a good range resolution. Off axis, there is very little response, even straight ahead of the edge, which is about 20dB smaller than on axis.

The ideal non-uniformly-excited plane-wave-only transducer of figure (3.1.5.1d) has waveforms concentrated in a beam along the axis of propagation. At the larger ranges on axis, the amplitude is less constant than for the conventional transducer (figure (3.1.5.1a)), but overall the waveforms are simpler. At close ranges, the conventional transducer gives results which have the familiar three-pulse structure (figure (2.5.1)), but the plane-wave-only transducer has shorter waveforms of almost one pulse, resulting. The consequences of waveform shape and length on overall resolution will be discussed more fully in section 4.1.

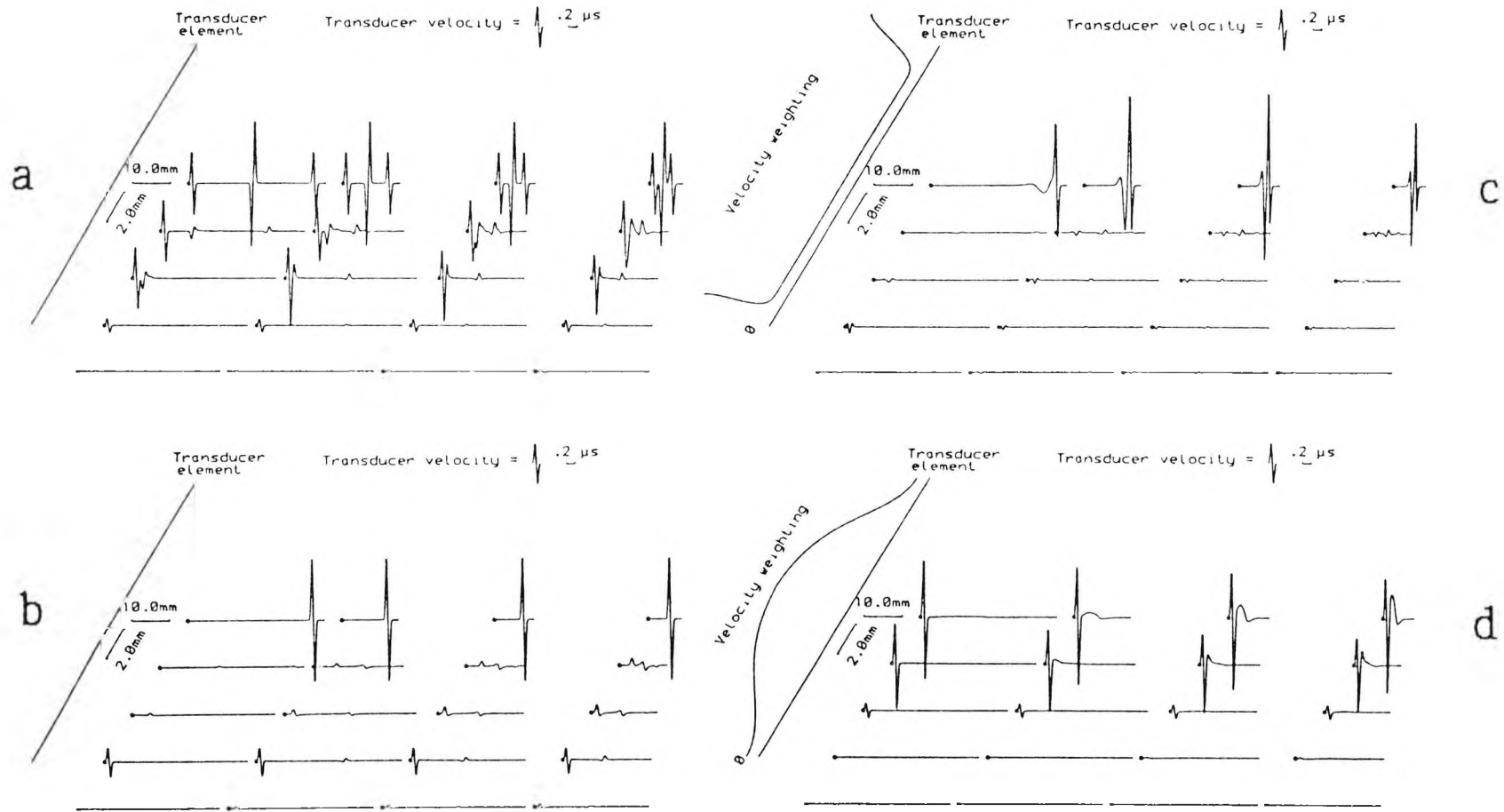


Figure (3.1.5.1): Transmit-receive echo responses when interrogating a point target (\cdot) in water, for:
a: conventional ideal uniformly-excited transducer,
b: ideal edge-wave-only transducer,
c: ideal non-uniformly-excited edge-wave-only transducer,
d: ideal non-uniformly-excited plane-wave-only transducer.

3.1.6 Transmit-receive beam profiles

Beam profiles corresponding to the transmit-receive echo waveforms of figure (3.1.5.1) have been obtained, figure (3.1.6.1). They assume full-wave detection has been used, since the method of detection has been shown to have a marked effect on the shape of the beam profile (Weight, 1984b).

Similar figures have already been published showing beam profiles for conventional and edge-wave-only transducers (Weight, 1982b, 1984a, 1984b). Beam profiles for non-uniformly-excited plane-wave-only transducers have only been presented in an internal report (Weight and Gatcombe, 1986) and a thesis (McLaren, 1987) and have yet to be published (Brittain and Weight, 1990, and Gatcombe and Weight, 1990).

As is well known for the uniformly-excited case (figure (3.1.6.1a)) the beam profiles are very broad (of the same order as the width of the source) and of a complicated shape. The large, central peak on axis, occurs due to the large, double amplitude pulse as shown in the transmit-receive echo waveforms, figure (3.1.5.1a). This peak remains at a constant size while the plane- and edge-wave components of the waveform are separated, and when the components merge together the amplitude of the peak changes. Because the beam profiles are broad, the lateral resolution (defined in section 2.6) is poor. This is because a point target in any lateral position in front of the transducer will produce a large response wherever it is, and so making the detection of two close targets difficult, if not impossible.

As figure (3.1.5.1b) shows, the ideal edge-wave-only transducer generates waveforms mainly on axis, and this shows in the beam

profiles of figure (3.1.6.1b), as a narrow, constant amplitude peak along the axis. This gives the transducer (were it physically possible) a very good lateral resolution. Two targets close together laterally (say 2-3mm apart) can now be resolved with this transducer, whereas with the conventional transducer, the two targets would have to be a transducer's diameter apart (19mm). The one drawback with this transducer is the small response straight ahead of the rim of the transducer. If the transducer were to be physically realisable, then this rim response could lead to misinterpretation of results, as explained previously in section (3.1.5). With a practical version of the transducer, this response straight ahead of the edge is greatly reduced (see below).

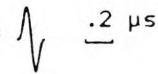
The non-uniformly-excited edge-wave-only transducer (figure (3.1.6.1c)) has similar properties to the ideal edge-wave-only transducer, viz. a narrow peak, centred on the transducer's axis. The amplitude of these central peaks are not constant with range however, resulting in a reduced operational range compared to the ideal edge-wave-only transducer. The small response straight ahead of the edge is now much reduced compared to the ideal edge-wave-only transducer.

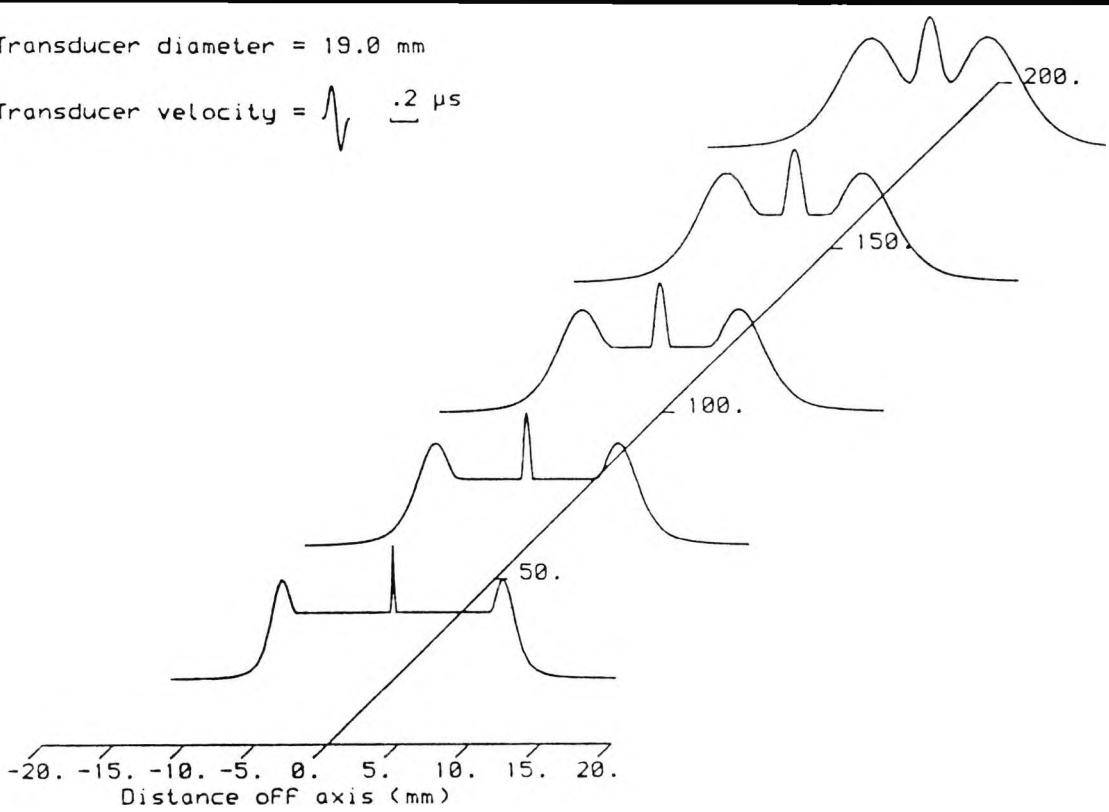
The non-uniformly-excited plane-wave-only transducer, figure (3.1.6.1d) has beam profiles which are almost as broad as those of the conventional transducer (figure (3.1.6.1a)), giving only a slight improvement in lateral resolution over the conventional transducer. They are however, much smoother and more constant in shape with range. Compared to the edge-wave-only transducers (figures (3.1.6.1b-c)), the broad beam profiles mean a poorer lateral resolution for the plane-wave-only transducer.

The effect of the beam profile shape, along with the transmit-receive echo waveforms of section 3.1.5, on the transducers ultimate resolution, will be discussed further in section 4.1.

a

Transducer diameter = 19.0 mm

Transducer velocity =  .2 μ s



b

Transducer diameter = 19.0 mm

Transducer velocity =  .2 μ s

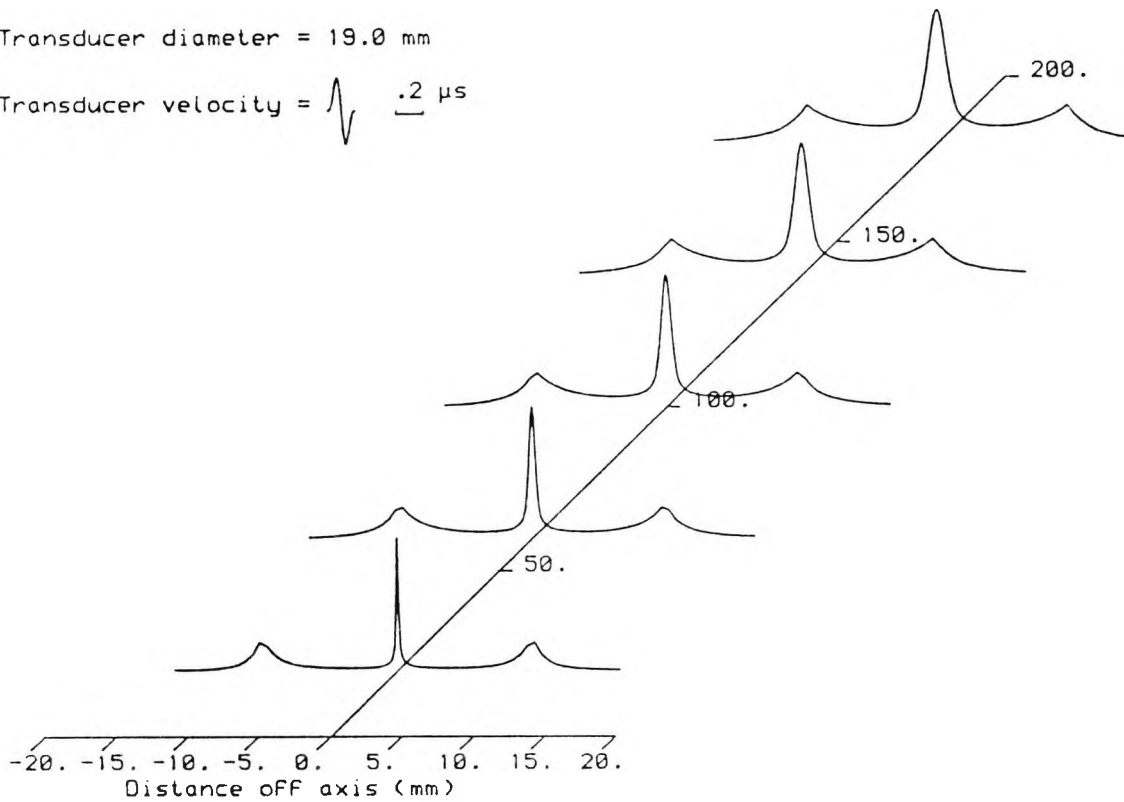


Figure (3.1.6.1): Transmit-receive beam profiles when interrogating a point target in water for:
a: conventional ideal uniformly-excited transducer,
b: ideal edge-wave-only transducer.

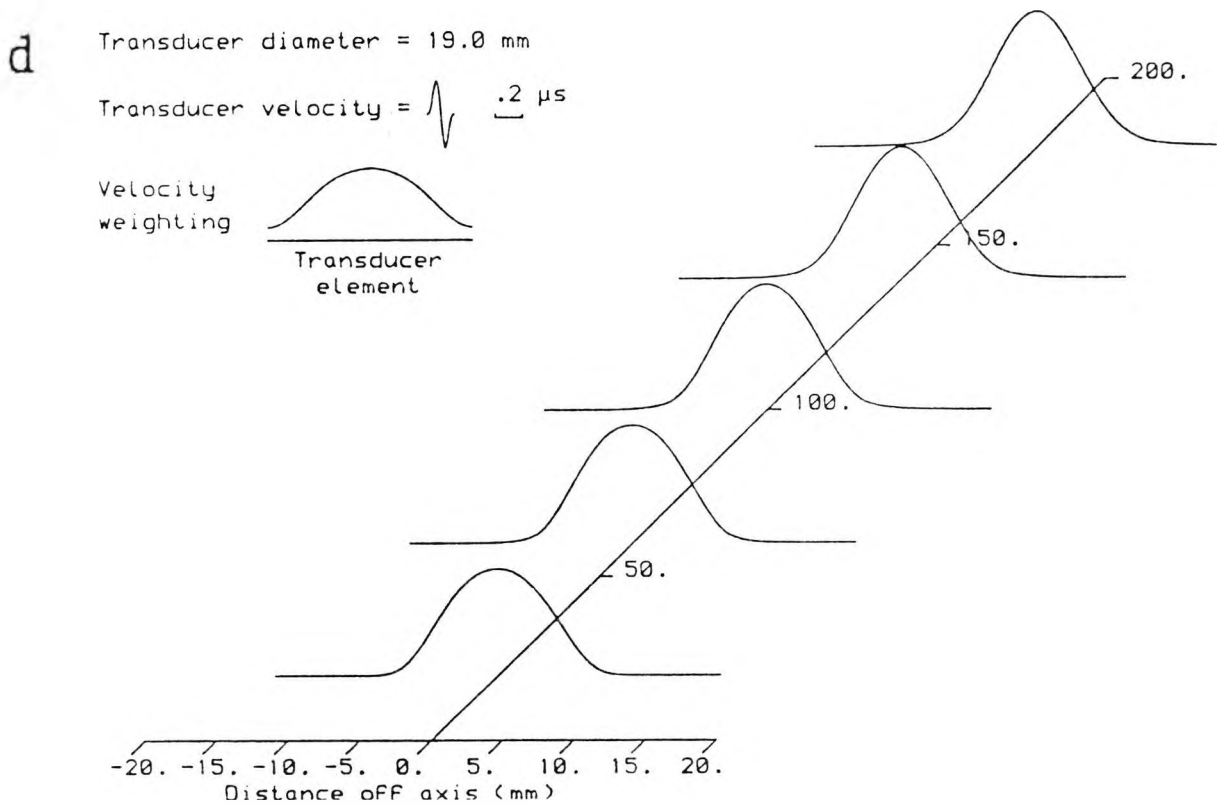
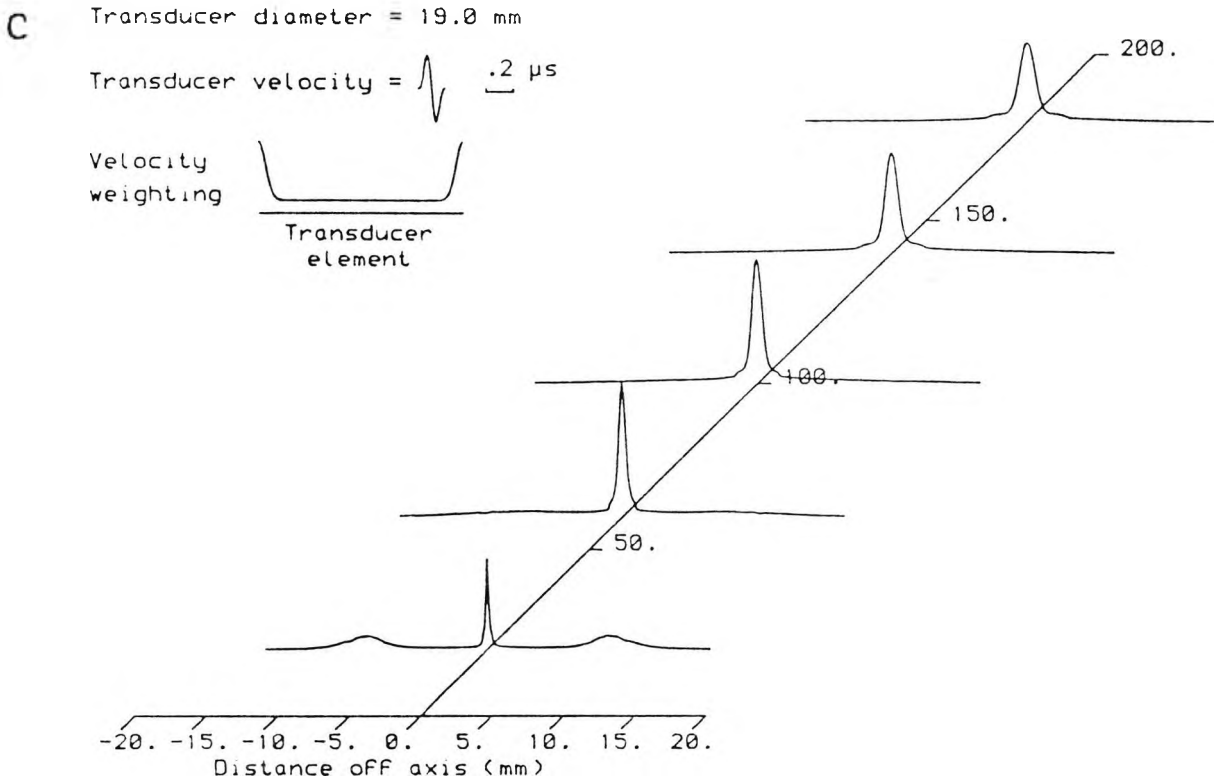


Figure (3.1.6.1): (continued)

c: ideal non-uniformly-excited edge-wave-only transducer,
 d: ideal non-uniformly-excited plane-wave-only transducer.

3.2 Computed results for finite-size targets

This section presents computed results for finite-size targets. The target sizes used were 0.8mm diameter, which is the smallest size it is practical to machine, and 4mm diameter. The same four transducers were modelled as for the point targets in section 3.1. Transmit-receive impulse responses and waveforms are shown, and from the waveforms it has been possible to generate some velocity potential impulse responses using the method described in section 2.9.

3.2.1 0.8mm diameter target

This target is of wavelength order across at the centre frequency ($c = 1500\text{m/s}$, $f = 5\text{MHz}$, $\lambda = c/f = 0.3\text{mm}$), and so it behaves almost like a point target. Impulse responses are shown first in figure (3.2.1.1), and then the transmit-receive echo responses are shown in figure (3.2.1.2).

For the conventional, uniformly-excited transducer of figure (3.2.1.1a), the on-axis impulse responses show a good agreement to those of Ueda and Ichikawa (1981). When convolved with the transducer's velocity function to obtain the transmit-receive echo responses, figure (3.2.1.2a), there is still the three-pulse structure on axis. Compared with the point target case of figure (3.1.5.1a), the three pulses now have different relative amplitudes, since the now finite size of the target allows the plane wave component (the first pulse) to be reflected strongly. The edge wave components are smeared out across the target's face, and so the latter two pulses are of reduced amplitude. It is interesting to note that the impulse response has an apparently large response straight ahead of the edge,

while the transmit-receive waveform is small. This seemingly contradictory result is because the impulse response consists of two delta functions close together, each of opposite sign. Because the time separation between the two impulses is less than the length of the source driving function (a single cycle sine wave), after convolution the effect is to reduce the total amplitude of the waveform.

For the case of the ideal edge-wave-only transducer, figures (3.2.1.1b) and (3.2.1.2b) show a large response on axis and a smaller response directly ahead of the edge, just as for the point target case (figure (3.1.5.1b)). The only difference is that for the point target case, the on axis waveforms have a constant amplitude, and for the finite-size target the amplitudes increase with range (over the range shown in the figure). This can be explained by considering ray paths from the edge of the transducer, to the centre and edge of the target. At far ranges, the paths are almost the same length, so the reflected pulses from the target are almost completely in phase, so the resultant echo signal is large. Closer to the transducer, the paths are very different lengths and so the reflected pulses tend to cancel each other, resulting in a smaller echo signal.

For the non-uniformly-excited transducers (figures (3.2.1.1c-d) and (3.2.1.2c-d)), the echo waveforms are almost exactly the same as the point target cases as in figures (3.1.5.1c-d).

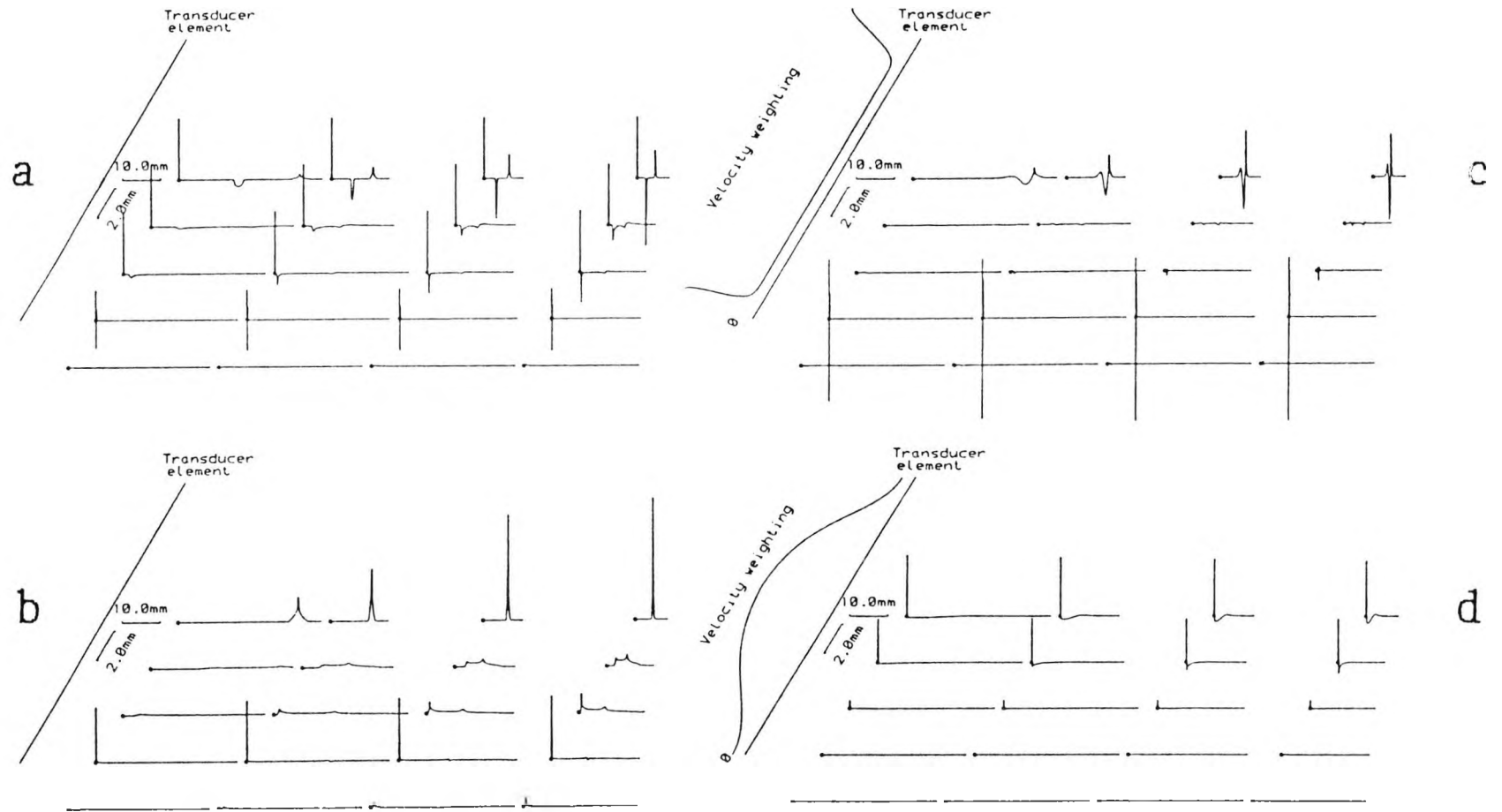


Figure (3.2.1.1): Transmit-receive impulse responses of a 0.8mm diameter target (·) in water, for:
a: conventional ideal uniformly excited transducer,
b: ideal edge-wave-only transducer,
c: ideal non-uniformly-excited edge-wave-only transducer,
d: ideal non-uniformly-excited plane-wave-only transducer.

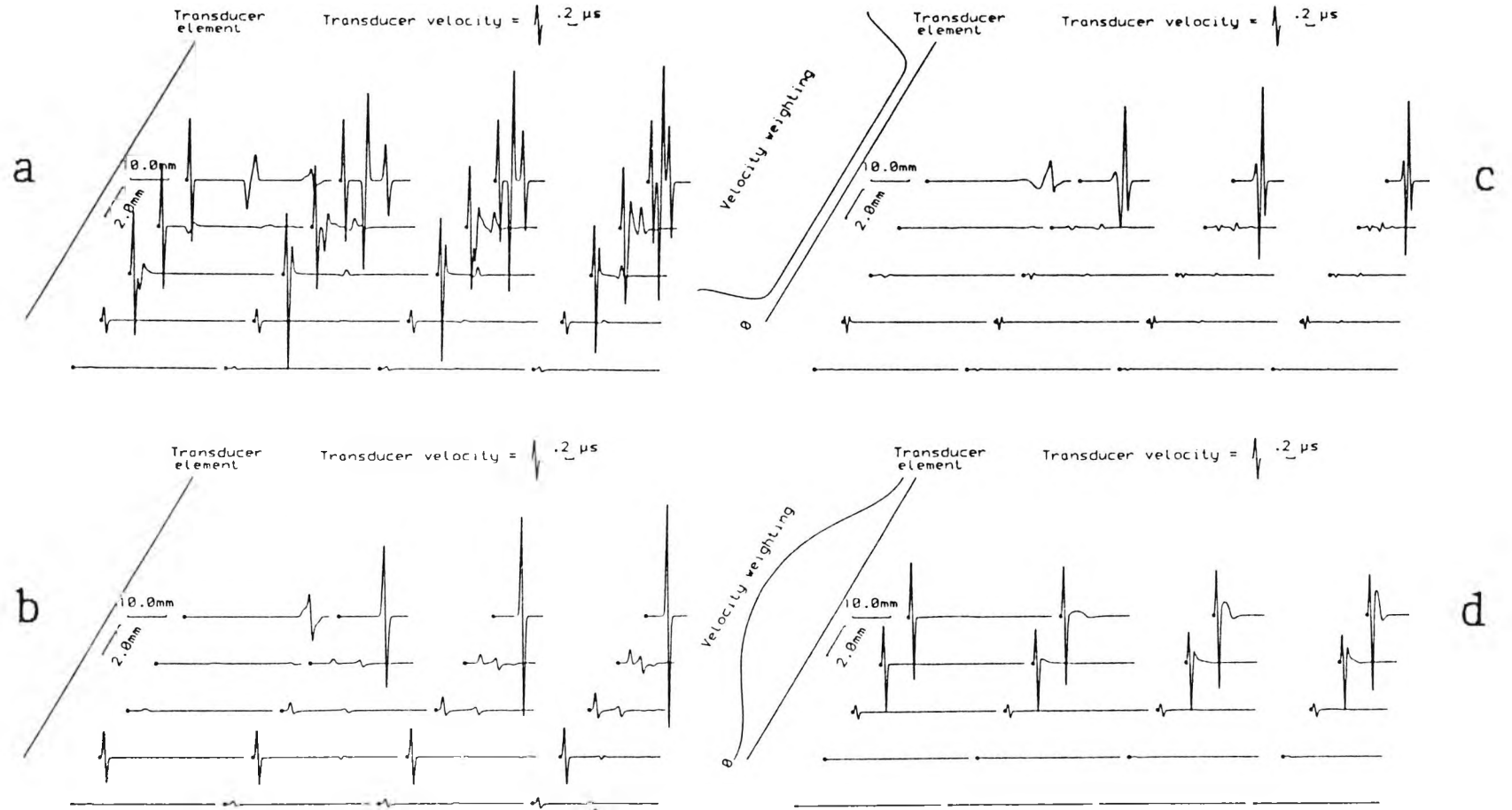


Figure (3.2.1.2): Transmit-receive echo responses when interrogating a 0.8mm diameter target (•) in water, for:
a: conventional ideal uniformly-excited transducer,
b: ideal edge-wave-only transducer,
c: ideal non-uniformly-excited edge-wave-only transducer,
d: ideal non-uniformly-excited plane-wave-only transducer.

3.2.2 4mm diameter target

This target is about 13 wavelengths across. Impulse responses and transmit-receive echo waveforms are shown in figures (3.2.2.1) and (3.2.2.2).

Again, the impulse responses on axis for the conventional uniformly-excited transducer (figure (3.2.2.1a)) agree with Ueda and Ichikawa (1981). The three-pulse structure of the point target case (figure (3.1.5.1a)) is now no longer visible, since the front face of the target reflects back so much of the plane wave, that it dwarfs the other components.

For the ideal edge-wave-only transducer (figures (3.2.2.1b) and (3.2.2.2b)), there is still a large response on axis, as for the 0.8mm target (figure (3.2.1.2b)). The response straight ahead of the edge is now much larger, and is comparable in size to the axial response. As can be deduced from the edge-wave directivity (figure (3.1.4.1)), the larger the target, the greater this edge response will become.

The non-uniformly-excited transducers (figures (3.2.2.1c-d) and (3.2.2.2c-d)) have almost identical behaviour as for the smaller targets (figures (3.2.1.1c-d) and (3.2.1.2c-d)) in all respects.

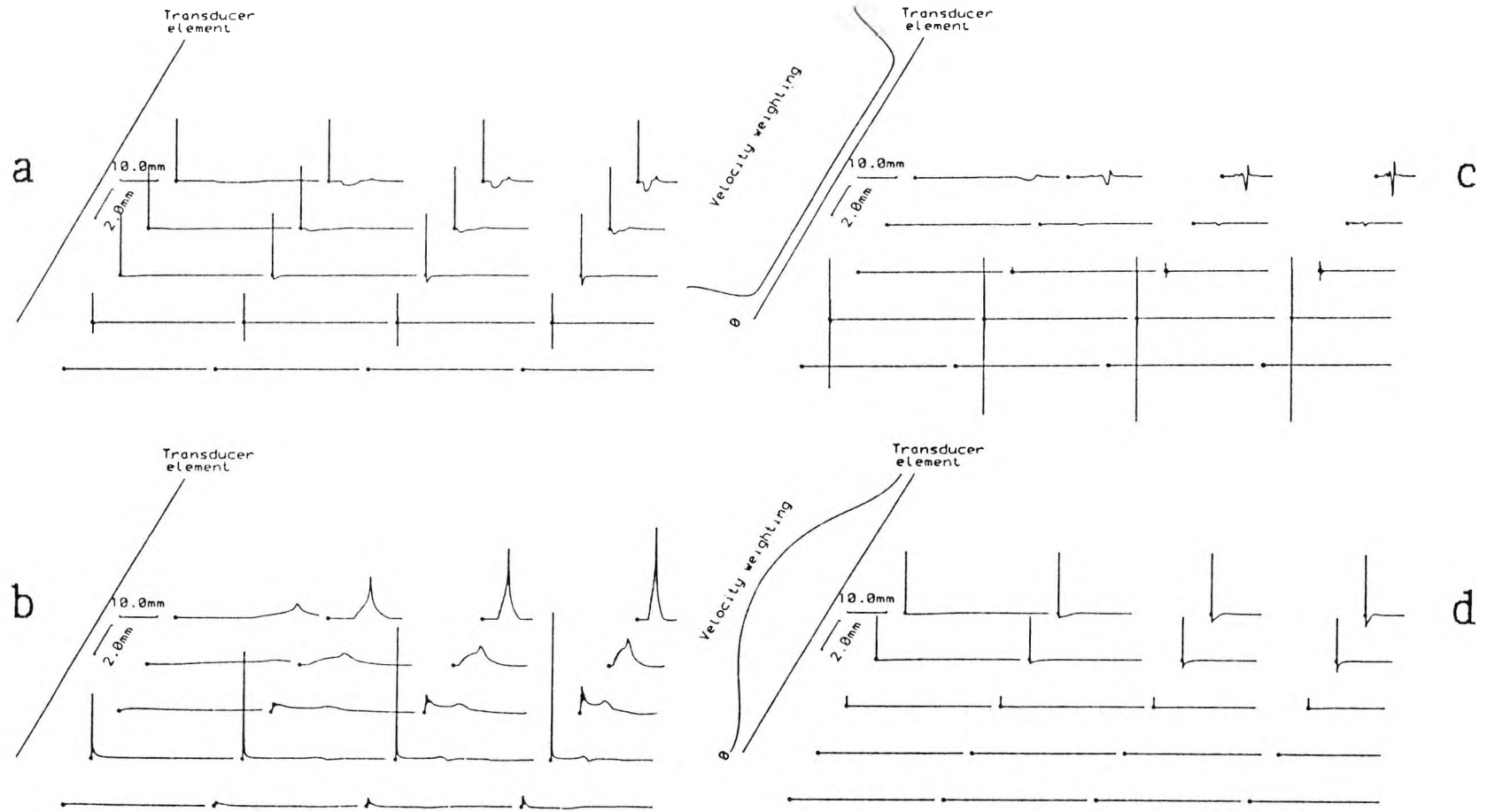


Figure (3.2.2.1): Transmit-receive impulse responses of a 4mm diameter target (·) in water, for:
a: conventional ideal uniformly-excited transducer,
b: ideal edge-wave-only transducer,
c: ideal non-uniformly-excited edge-wave-only transducer,
d: ideal non-uniformly-excited plane-wave-only transducer.

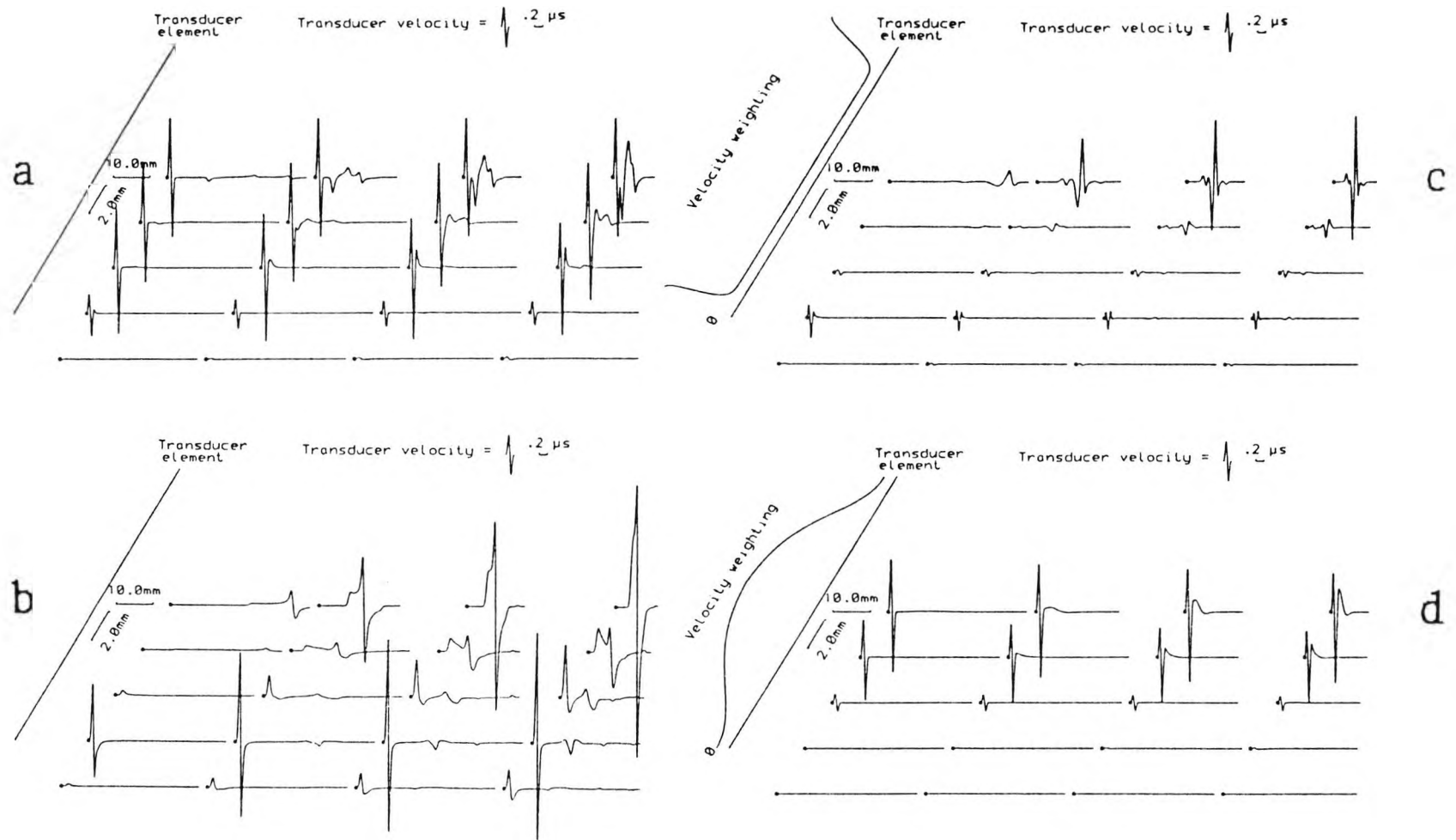


Figure (3.2.2.2): Transmit-receive echo responses when interrogating a 4mm diameter target (\cdot) in water, for:
 a: conventional ideal uniformly-excited transducer,
 b: ideal edge-wave-only transducer,
 c: ideal non-uniformly-excited edge-wave-only transducer,
 d: ideal non-uniformly-excited plane-wave-only transducer.

3.2.3 Velocity potential impulse responses

Velocity potential impulse responses have been obtained by working backwards from the transmit-receive waveforms shown in figures (3.2.1.2) and (3.2.2.2). The methods used to do this have already been described in section 2.9.

Currently only the conventional, uniformly-excited transducer and the non-uniformly-excited plane-wave-only transducer have been dealt with, using the same size targets as before, namely 0.8mm and 4mm diameter. Figures (3.2.3.1) and (3.2.3.2) show the velocity potential impulse responses for these cases. Comparing these figures with the point target cases (figures (3.1.1.1a) and (3.1.1.1d)), they are obviously very similar. The only difference is that as the target size increases, the trailing edges of the velocity potential impulse responses broaden. It is this broadening of the trailing edge which causes the reduction in the amplitude of the other component pulses in the transmit-receive echo waveforms of figures (3.2.1.2) and (3.2.2.2). This is because the differentiation of this trailing edge is responsible for generating the impulse which ultimately produces the edge-wave components of the waveforms (section 2.4). It follows that, as the trailing edge broadens, so its differential decreases, and so does the amplitude of the subsequent edge-wave components.

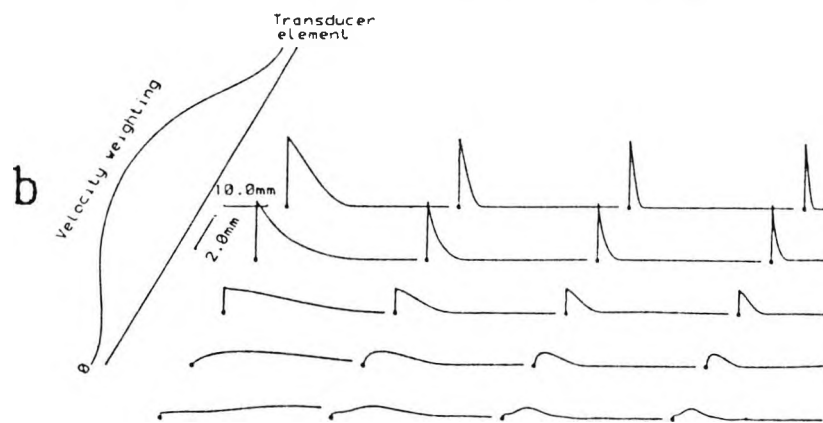
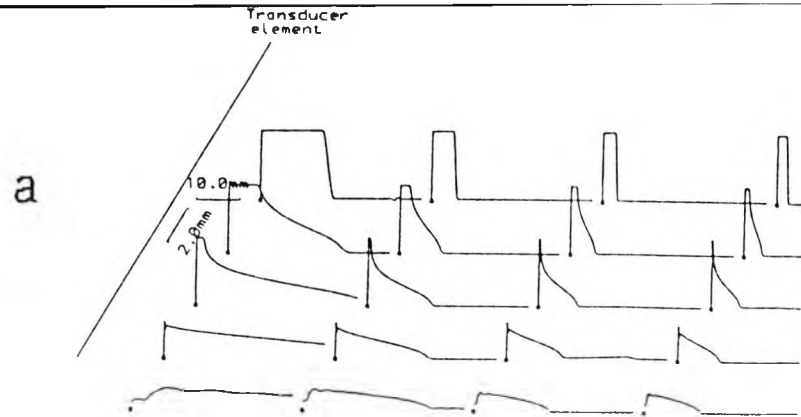


Figure (3.2.3.1): Velocity potential impulse responses for 0.8mm diameter targets at points (·) in the field of:
 a: conventional ideal uniformly-excited transducer,
 b: ideal non-uniformly-excited plane-wave-only transducer.

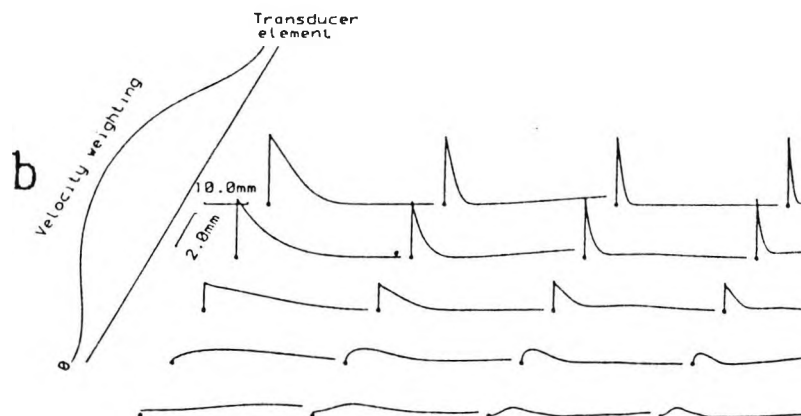
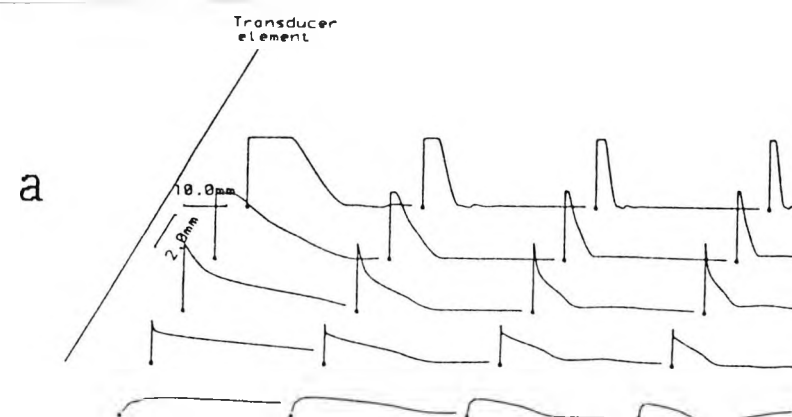


Figure (3.2.3.2): Velocity potential impulse responses for 4mm diameter targets at points (·) in the field of:
 a: conventional ideal uniformly-excited transducer,
 b: ideal non-uniformly-excited plane-wave-only transducer.

3.3 Experimental results for point targets

This section shows experimental transmit-receive echo waveforms and beam profiles obtained using a 0.8mm diameter brass rod for a target, immersed in a large water tank. This particular target is used because it is a strong reflector and will give large, well-defined echo signals. The size was chosen because it is the smallest that can be made in our workshops, and as it is of wavelength order across, should behave like a point target.

The transducers used to obtain the experimental results were a conventional transducer, commercially available from Panametrics (type V3829), and non-uniformly-excited transducers made in our laboratory. At the time of writing, a prototype plane-wave-only transducer had only just been made, and so only one set of experimental results have been obtained with this new transducer.

For each set of experimental results in this section, the laboratory equipment settings were kept constant, so that direct comparisons could be made between the calculated and measured results in each figure.

As the aim of this section is to compare calculated results and experimental results, a suitable function had to be used in the programs for the transducer's motion. There are several ways to obtain this function, depending on the circumstances.

With conventional transducers, if it is possible to get a miniature probe or small target close enough to the transducer so that the component pulses are separated, then it is easy to obtain sample values from just the plane-wave component of the waveform. Weight and Hayman (1978) have shown that the plane-wave component of the waveform

is proportional to the source velocity.

For the non-uniformly-excited transducers, there are no pure plane-wave components, so a different method must be used. As was stated in section 2.6, the far-field on-axis responses are the differentials of the transducer velocity function for pressure waveforms, and the second differential for transmit-receive echo waveforms (figure (2.6.1)). To obtain the transducer velocity function, a far-field axial pressure waveform is sampled, and must be numerically integrated (integrated twice in transmit-receive mode) before it can be used in the programs.

3.3.1 Conventional transducer

Transmit-receive echo responses have already been obtained for the conventional uniformly-excited transducer (Weight, 1982b), and for completeness, the relevant figure is reproduced here as figure (3.3.1.1).

The agreement between the calculated and measured results is generally very good. There are a few exceptions for the nearer ranges, where the amplitude of the edge-wave components differ slightly. There are two effects which cause this. The first is that the target does not behave like an ideal point target. The finite-size of the target means that when it is perfectly aligned to the transducer the target acts like a plane reflector. This means that the reflected plane wave is not spherical as was the case for a point target (section 2.5), but is more plane-like. This in turn means a greater contribution to the plane wave component upon reception back at the transducer, relative to the edge waves. Head waves are another factor affecting the relative amplitudes of the edge-wave components pulses at close ranges. These are caused by plate waves travelling radially across the surface of the transducer, generating the head waves (Hayman and Weight, 1979, and Harris et. al., 1983), which can interfere with the edge waves. At further ranges, the calculated and measured waveforms are virtually identical. Moving 2mm off axis, the calculated and measured results agree well at all ranges, since the above effects only cause problems near the transducer, and close to the axis of propagation.

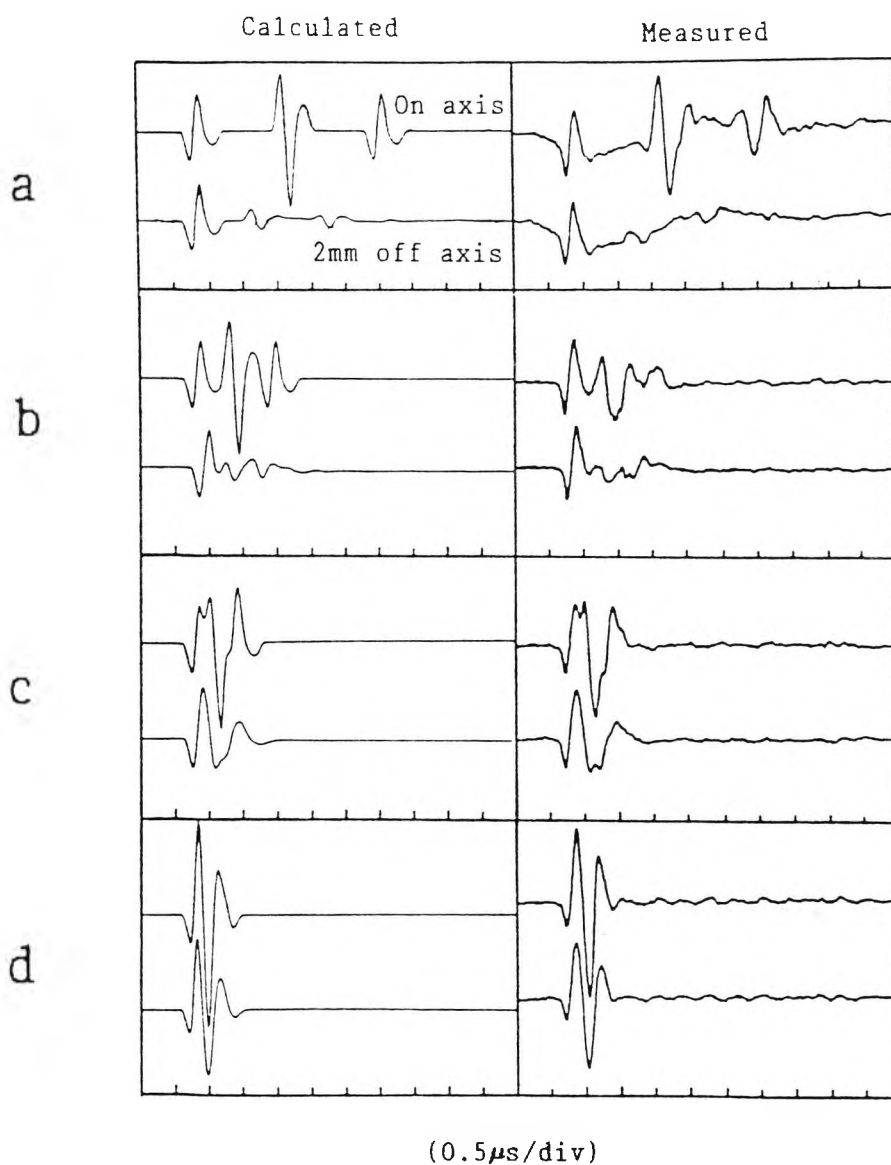


Figure (3.3.1.1): Calculated (*left*) and measured (*right*) transmit-receive echo responses when interrogating a 0.8mm diameter point-like target in water. Each figure shows an on-axis result (*top*) and a 2mm off-axis result (*bottom*). Ranges are: a: 20mm, b: 50mm, c: 100mm, d: 200mm.

3.3.2 Edge-wave-only transducer

Moving to the non-uniformly-excited edge-wave-only transducer, similar transmit-receive echo results were obtained. On-axis results are shown in figure (3.3.2.1), with 2mm off-axis results in figure (3.3.2.2).

For the on-axis results, the measured and calculated results agree well, except at the closest range, figure (3.3.2.1a), where the agreement is poor. This is again thought to be caused by the interaction of head waves as mentioned in section 3.3.1 for the conventional transducer. This effect is more pronounced with the non-uniformly-excited edge-wave-only transducer than with the conventional transducer since there is now no plane-wave component to dominate the waveform.

Comparing off-axis results with on-axis results, just 2mm off-axis, the results are much reduced in amplitude, ranging from 17dB at the closest range of 30mm, to 14dB at the furthest range of 140mm.

This off-axis reduction is made even more apparent in the beam profiles, shown in figures (3.3.2.3-4), the calculated and measured cases showing an almost identical, sharp response centred on the axis. For the closest range shown in the figure, 30mm, it is just possible to see a small response straight ahead of the edge of the transducer, although as this is about 30dB smaller than the central peak, it can be safely neglected. For the further ranges in the figure, this edge response is too small to show. It is precisely this narrow beam width (as predicted in section 3.1.6) that gives this type of transducer a vastly superior lateral resolution as compared to conventional transducers. This will be discussed further in section 4.1.

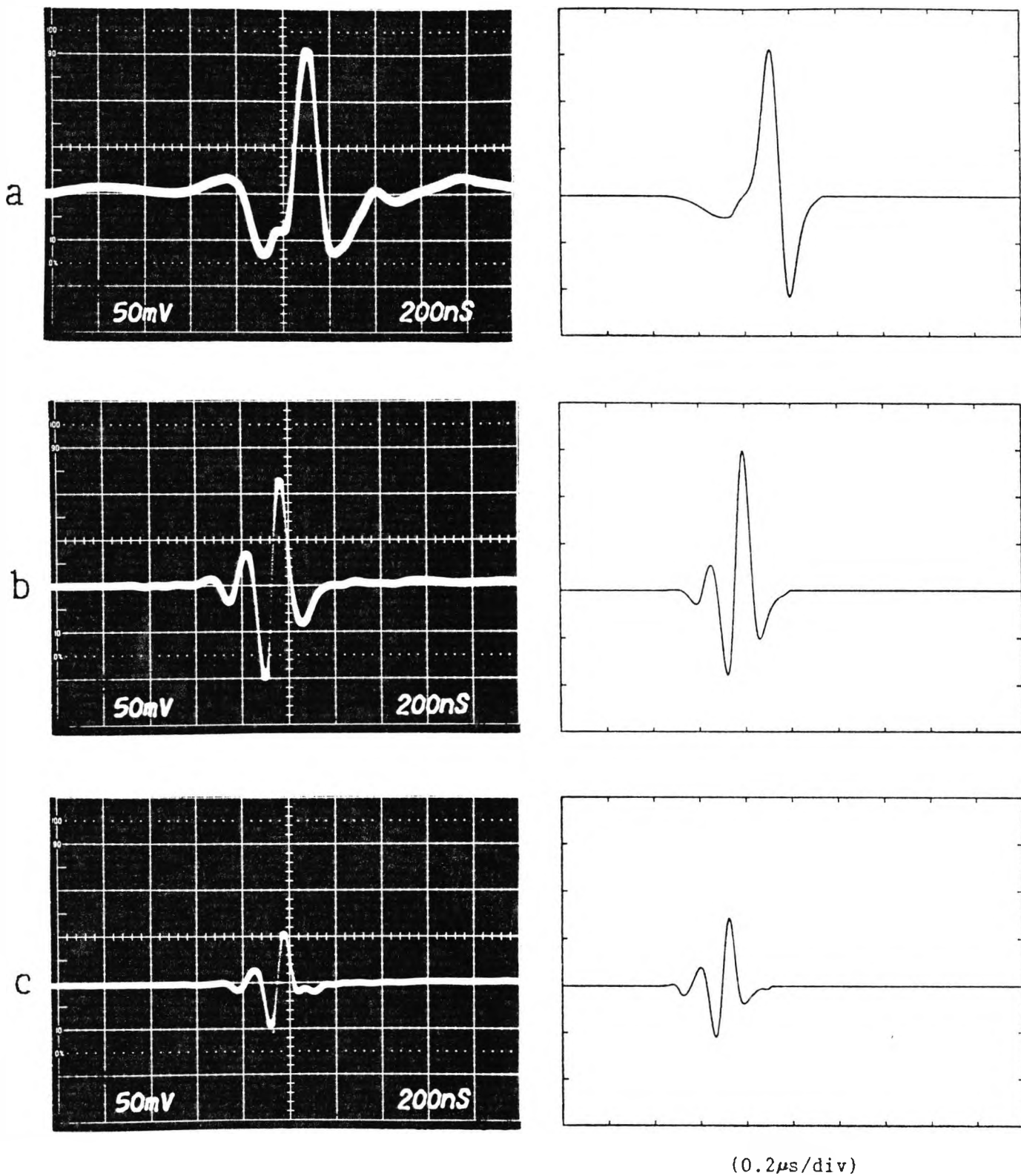


Figure (3.3.2.1): Measured (*left*) and calculated (*right*) transmit-receive echo responses when interrogating a 0.8mm diameter point-like target on axis, in water with an edge-wave-only transducer. Ranges are: a: 30mm, b: 70mm, c: 140mm.

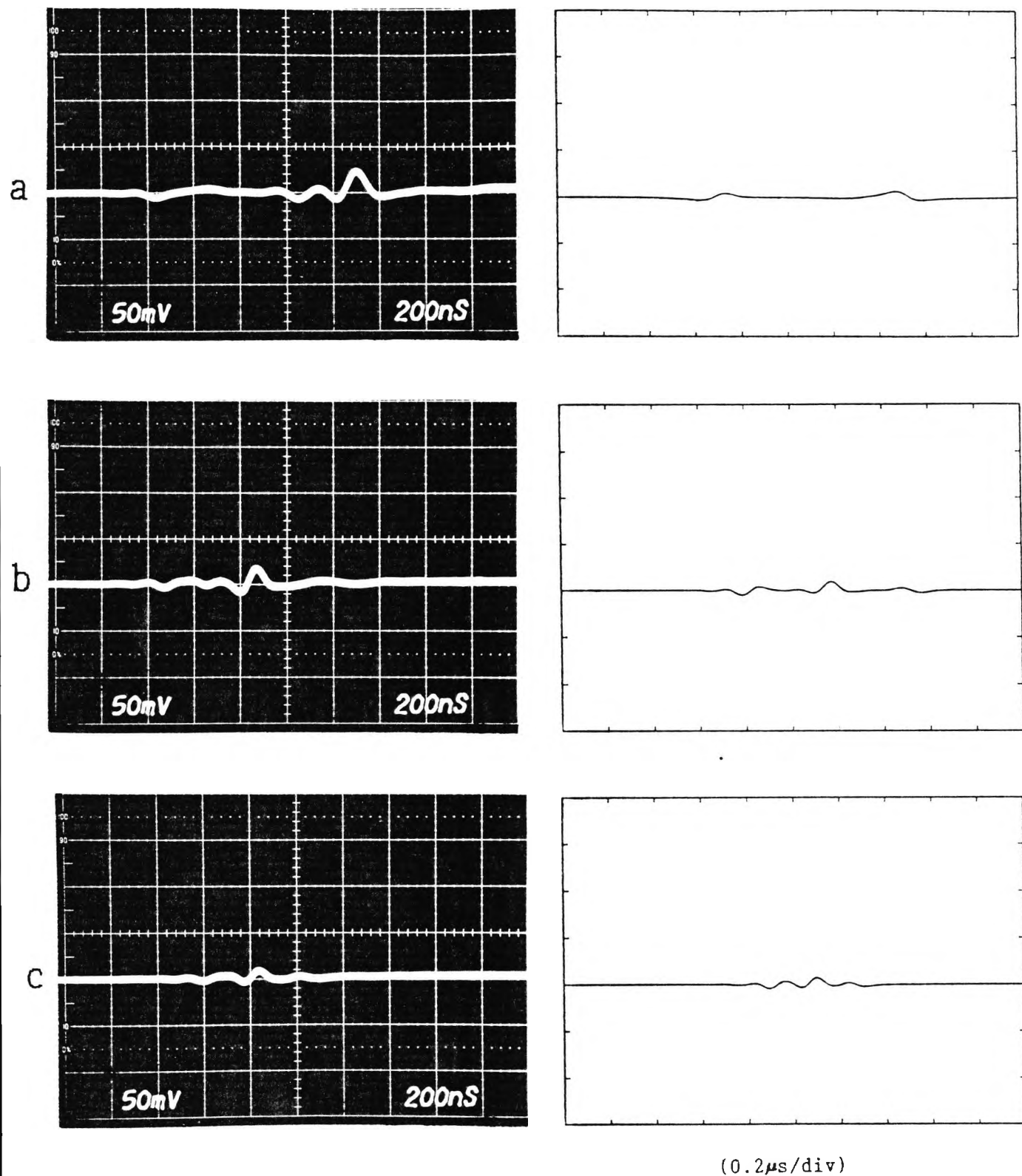
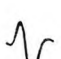
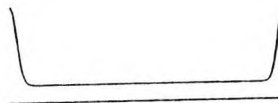


Figure (3.3.2.2): Measured (*left*) and calculated (*right*) transmit-receive echo responses when interrogating a 0.8mm diameter point-like target 2mm off axis, in water with an edge-wave-only transducer. Ranges are: a: 30mm, b: 70mm, c: 140mm.

Transducer diameter = 19.0 mm

Transducer velocity =  .5 μs

Velocity weighting 
Transducer element

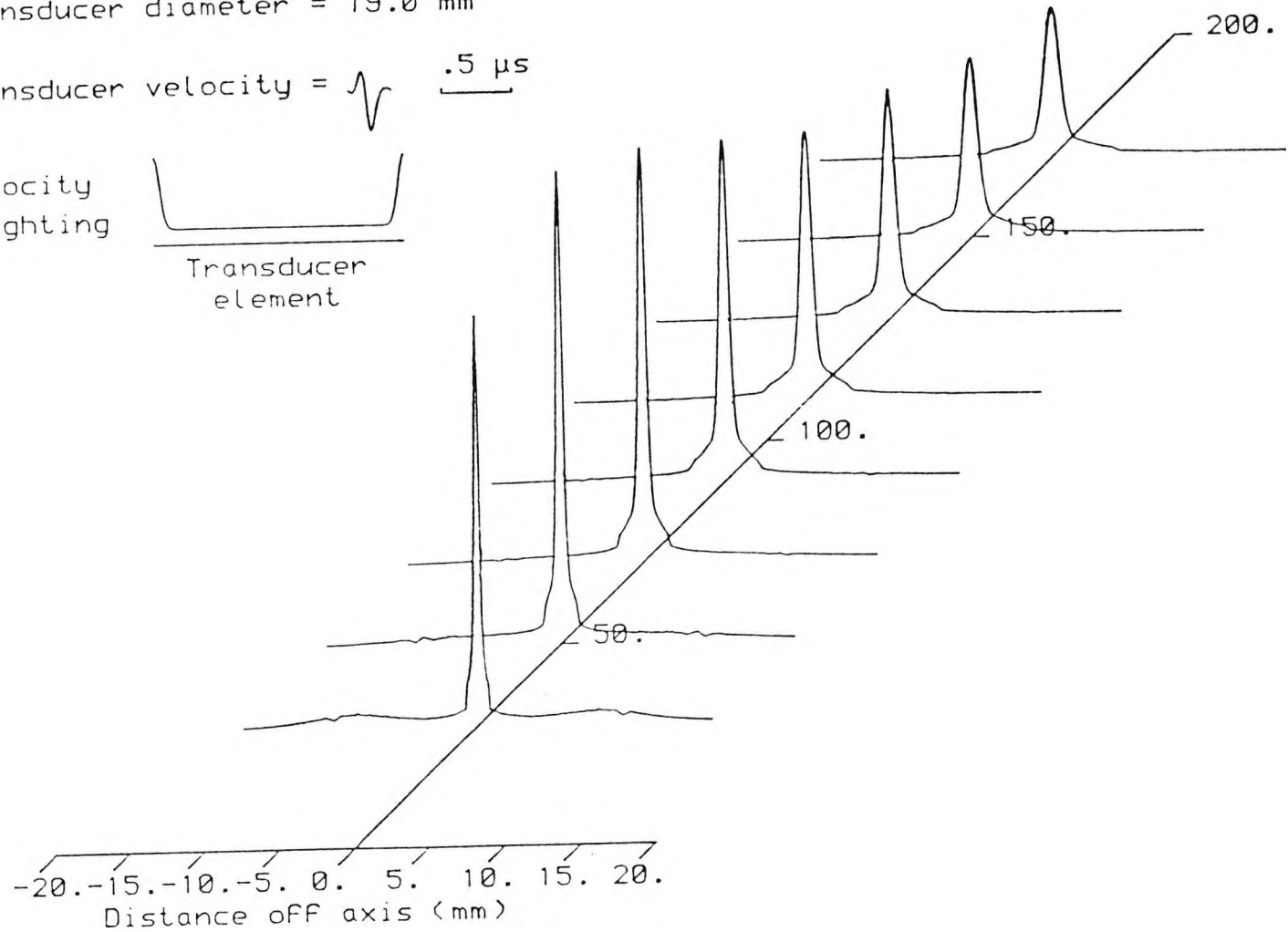


Figure (3.3.2.3): Calculated transmit-receive beam profiles when interrogating a point target in water, with a non-uniformly-excited edge-wave-only transducer.

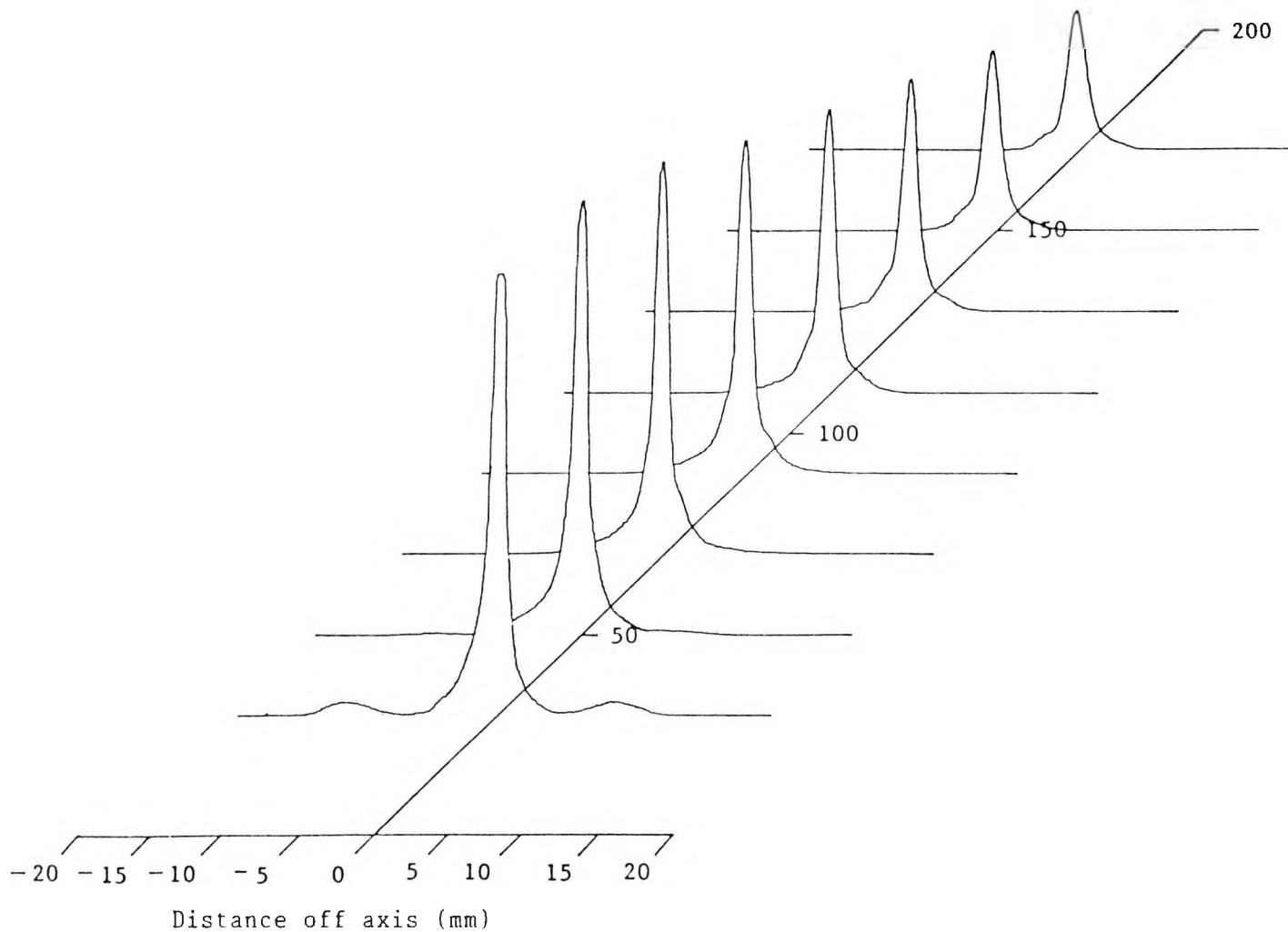


Figure (3.3.2.4): Measured transmit-receive beam profiles when interrogating a 0.8mm diameter point-like target in water, with an edge-wave-only transducer.

3.3.3 Plane-wave-only-transducer

Transmit-receive echo results have been obtained recently with one of our new non-uniformly-excited plane-wave-only transducers. These results are compared with some theoretical waveforms in figure (3.3.3.1).

Overall, the results of figure (3.3.3.1) show much simpler waveforms than for the conventional transducer of figure (3.3.1.1). The plane wave-only transducer produces a consistently short pulse echo waveform when interrogating a small target, whereas the conventional transducer produces a three-pulse echo waveform for a small target at close range (figure (3.3.1.1a)), but a single, short pulse at the furthest range (figure (3.3.1.1d)). This shows that two targets closely spaced in range would generate two short pulses when interrogated with the plane-wave only transducer. If a conventional transducer was used, the resulting multi-pulse structure would be very difficult, if not impossible to interpret.

At the closest range of 25mm (figure (3.3.3.1a)), there is evidence of some small pulses following the main pulse. There are two main causes of the generation of these extra pulses. The first is that the transducer is manufactured using a series of concentric ring electrodes to form the required velocity weighting function, as described in section 2.10.2. Currently, only a small number of electrode rings are used, resulting in a coarse approximation to the velocity weighting function which was used in the modelling. The second cause is the existence of head waves caused by the non-ideal motion of the transducer's piezo-electric element. This was observed for the other transducers, in sections 3.3.1-2.

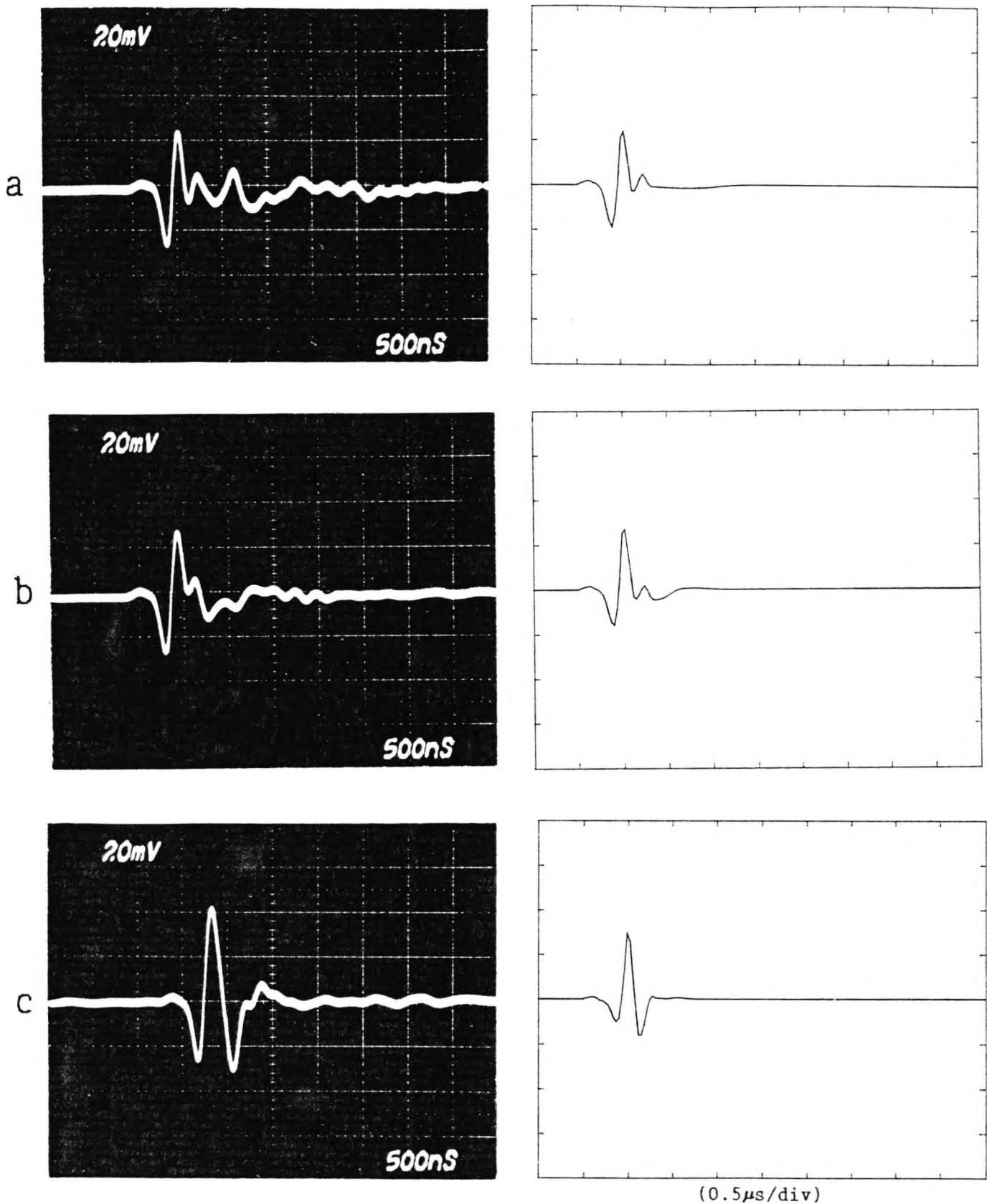


Figure (3.3.3.1): Measured (*left*) and calculated (*right*) transmit-receive echo responses when interrogating a 0.8mm diameter point-like target on axis, in water, with a plane-wave-only transducer. Ranges are: a: 25mm, b: 50mm, c: 100mm.

3.4 Experimental results for finite-size targets

As the aim of ultrasonic NDT is to be able to determine target characteristics from echo responses, one of the first steps is to be able to predict the responses theoretically. This section presents experimental and calculated transmit-receive echo responses from larger targets (where "larger" means bigger than the 0.8mm diameter target used to obtain the "point" results of the previous section) interrogated with the conventional transducer. The targets were machined from brass as before, in 2mm, 4mm and 10mm diameters. Each width of target was also machined with a cone-shaped front face, as described in section 2.12. The front face angles (with respect to the target's axis) were 90° (i.e. a flat face as before), 85°, 75°, 60° and 45°. Thus 15 different targets were made.

A set of experimental results have already been obtained using the 4mm diameter flat-faced target at various ranges (McLaren and Weight, 1987), and is included here to confirm calculated results. A second set of experimental results have subsequently been taken for the non-planar targets described above, to compare with the calculated waveforms obtained using the new modelling method described in section 2.12.1. These targets are a more difficult case to model theoretically than the flat-faced targets, since this is related to the case of a flat-faced target which is not normally aligned to the transducer.

3.4.1 Flat targets

Figure (3.4.1.1) shows measured and calculated transmit-receive waveforms for the 4mm diameter flat-faced target, being interrogated by a conventional transducer.

As the theory predicted (figure (3.2.2.2a)), close to the transducer there is a large plane wave response, followed by two much smaller pulses. As was stated in section 3.3.1, the extra large plane wave response is due to the face of the target causing a large specular reflection of the incident plane wave component. As the constituent pulses of the waveform close up with increasing range (figures (3.4.1.1b-d)), the resulting waveform again shows the double differentiation effect as described in section 2.6. The head wave effect mentioned in sections 3.3.1 2, does not appear to have any effect in these results. As these head waves only cause problems close to the transducer's axis, their influence taken over the area of a finite-sized target is small.

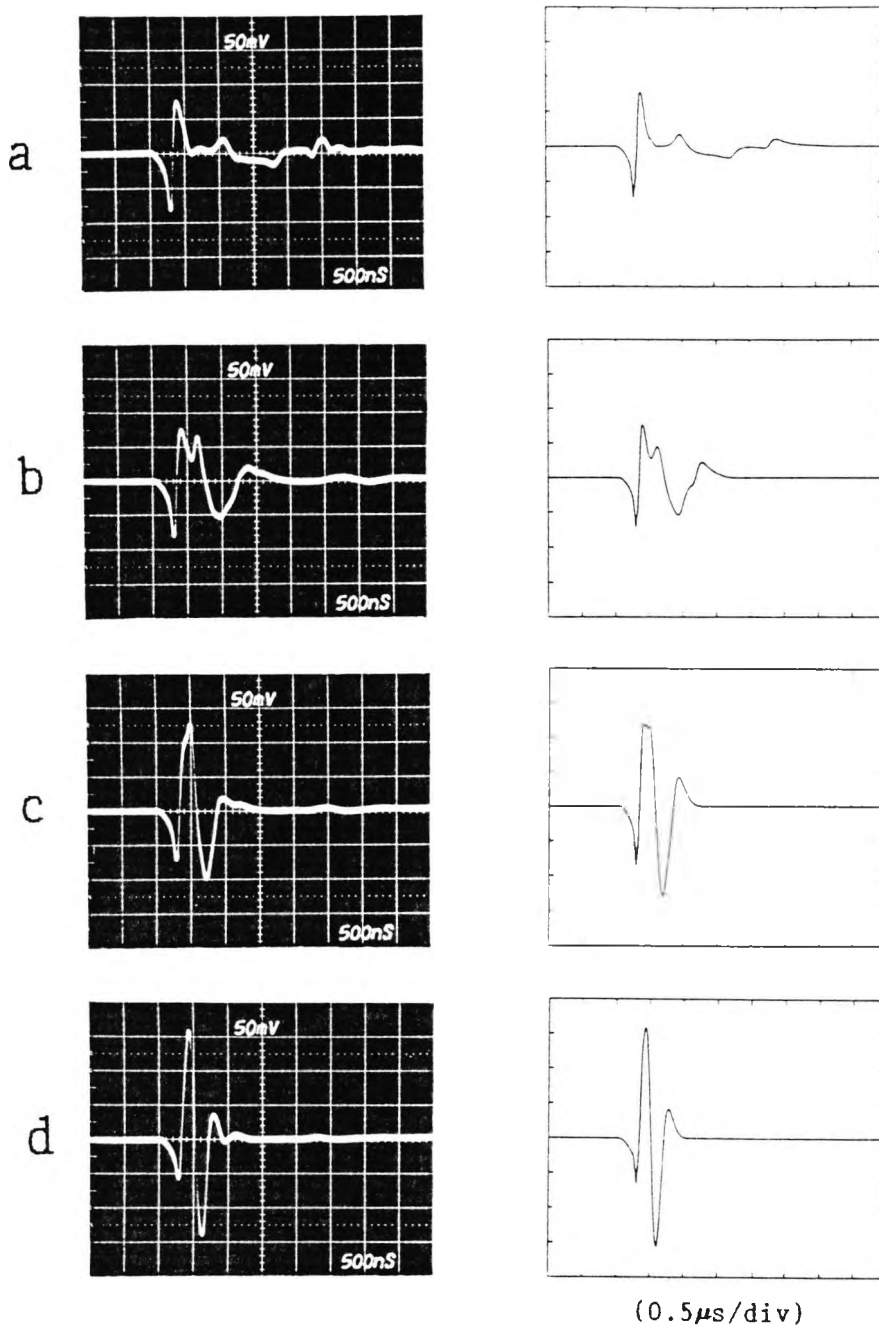


Figure (3.4.1.1): Measured (*left*) and calculated (*right*) transmit-receive echo responses from a 4mm diameter flat-faced target in water, with a conventional transducer. Ranges are: a: 30mm, b: 70mm, c: 120mm, d: 180mm.

3.4.2 Cone-shaped targets

Figures (3.4.2.1-6) show measured and calculated transmit-receive echo waveforms obtained by interrogating various cone-shaped targets, at two different ranges, using a conventional transducer. The targets were 2mm, 4mm and 10mm in diameter, and their front face angles were 90° (a flat front face), 85°, 75°, 60° and 45°. The targets were positioned on axis, at ranges of 35mm (in the near field) and 120mm (in the far field). Each figure shows a set of results for a given diameter target, at a given range, for all the front face angles.

The first figure shows results for the 2mm diameter targets at 35mm range, figure (3.4.2.1). For the 90° target (the completely flat face), the results are as predicted before, with three distinct pulses. As the target face angle decreases (i.e. the target becomes more pointed), there is a reduction in the amplitude of the waveforms. (Note that the decibel settings on each figure represent the amount of gain required to make each waveform big enough to be seen clearly.) For the 85° target, there is a slight (2dB) reduction in amplitude, although the overall shape of the waveform is virtually unchanged. For the more pointed targets there is further attenuation. This is due to the plane wave component becoming relatively smaller, as the more pointed targets serve to reflect more of the transmitted plane wave away, which results in less returning to the transducer. The comparison between the measured and calculated waveforms is good when comparing the shapes of the waveforms. In terms of amplitudes, the comparison is not as good for the more pointed 60° and 45° targets.

At the further range of 120mm, figure (3.4.2.2), similar effects

are seen. Again, as the targets become more pointed, the match between the measured and calculated waveforms becomes poorer.

As the target size increases (figures (3.4.2.3) and (3.4.2.5)), the usual three-pulse structure, which occurs for the smaller targets, disappears leaving a single pulse for the 10mm diameter target (figure (3.4.2.5)). This has been explained previously, in section 3.3.1 as being due to the target acting as a plane reflector, reflecting a larger proportion of the incident plane wave back to the transducer. As the targets become more pointed, this plane wave pulse very quickly disappears leaving small pulses due to the remaining edge-wave components. The far-field results of figures (3.4.2.4) and (3.4.2.6) show similar effects to the above.

The reason for the calculated and measured results not matching in terms of amplitude, is due to deficiencies in the modelling, which neglects such things as mode conversion, and multiple scattering and reflections inside the tip of the target. Also, the target's dimensions are subject to uncertainties. Experimentally, the appropriate gain setting was determined by looking at the far-field result and adjusting the gain so that the overall amplitude (measured in divisions on the oscilloscope screen) approximately matched the calculated result. The same gain setting was used to obtain the near field result. This means that relative amplitudes of near- and far-field experimental results can be easily compared. Any discrepancies with the calculated results must therefore be due to the modelling.

These results emphasise the importance of correct alignment when making experimental measurements. The pointed targets (here representing misaligned flat-faced targets) show just how much the

amplitude and shape can vary, even using the simple model of section 2.12. This will be discussed further in section 4.2.

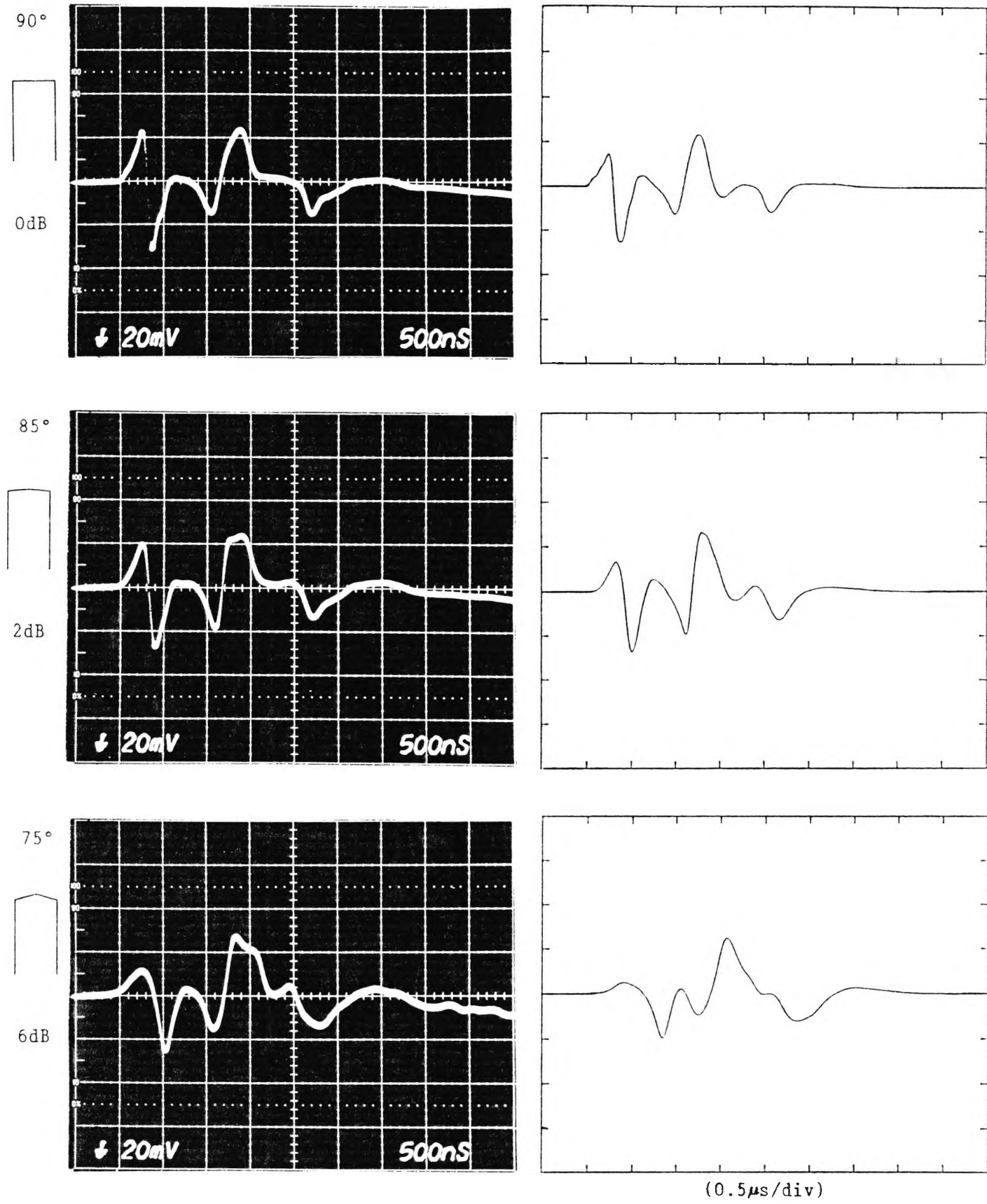
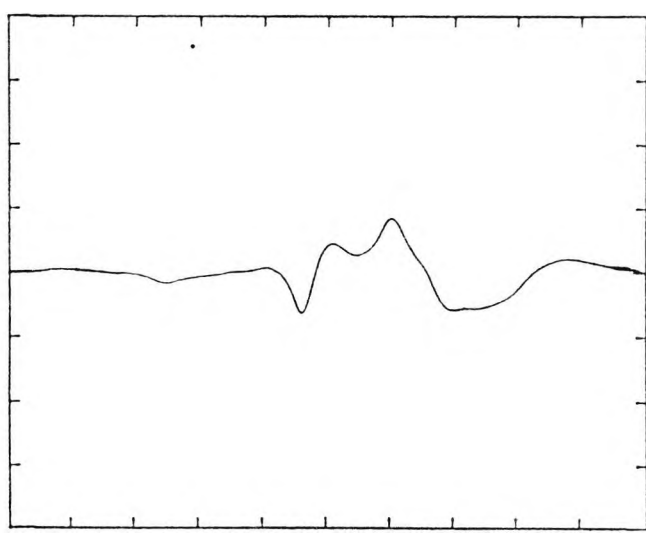
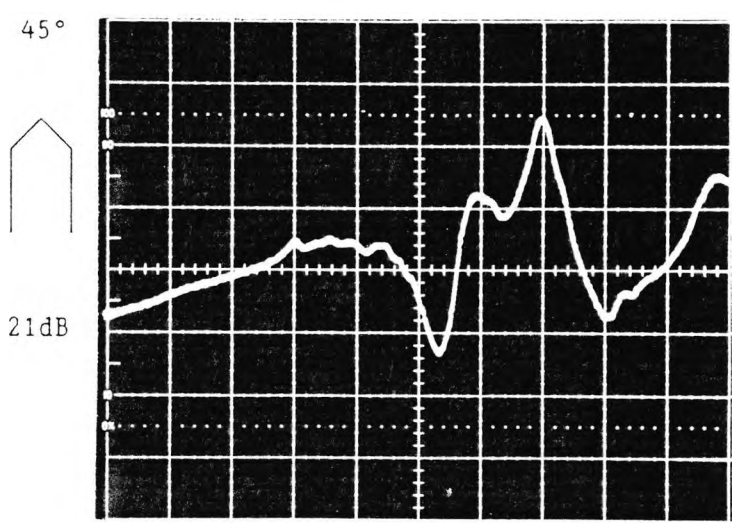
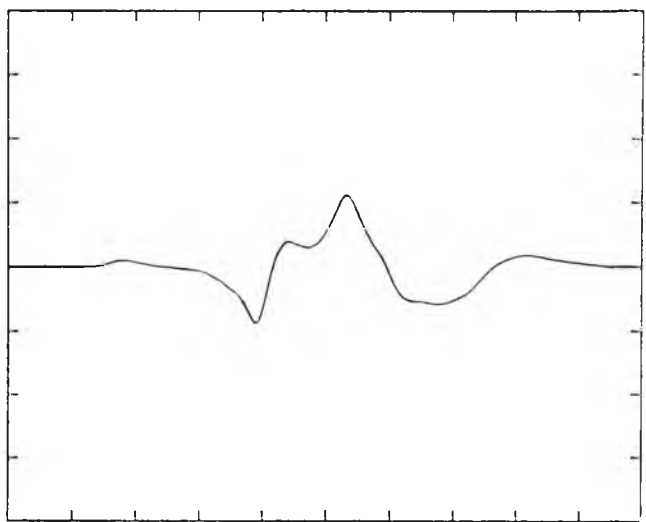
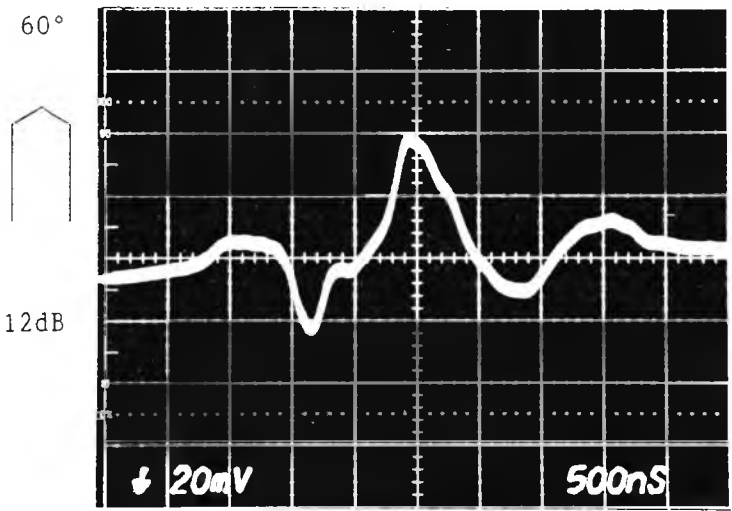


Figure (3.4.2.1): Measured (*left*) and calculated (*right*) transmit-
 receive echo responses from cone-shaped 2mm diameter
 targets, on axis at 35mm range. Front face angles
 are 90° (flat), 85°, 75°. Decibel settings represent
 relative gain.



(0.5 μ s/div)

Figure (3.4.2.1): (continued)
 Front face angles are 60°, 45°.

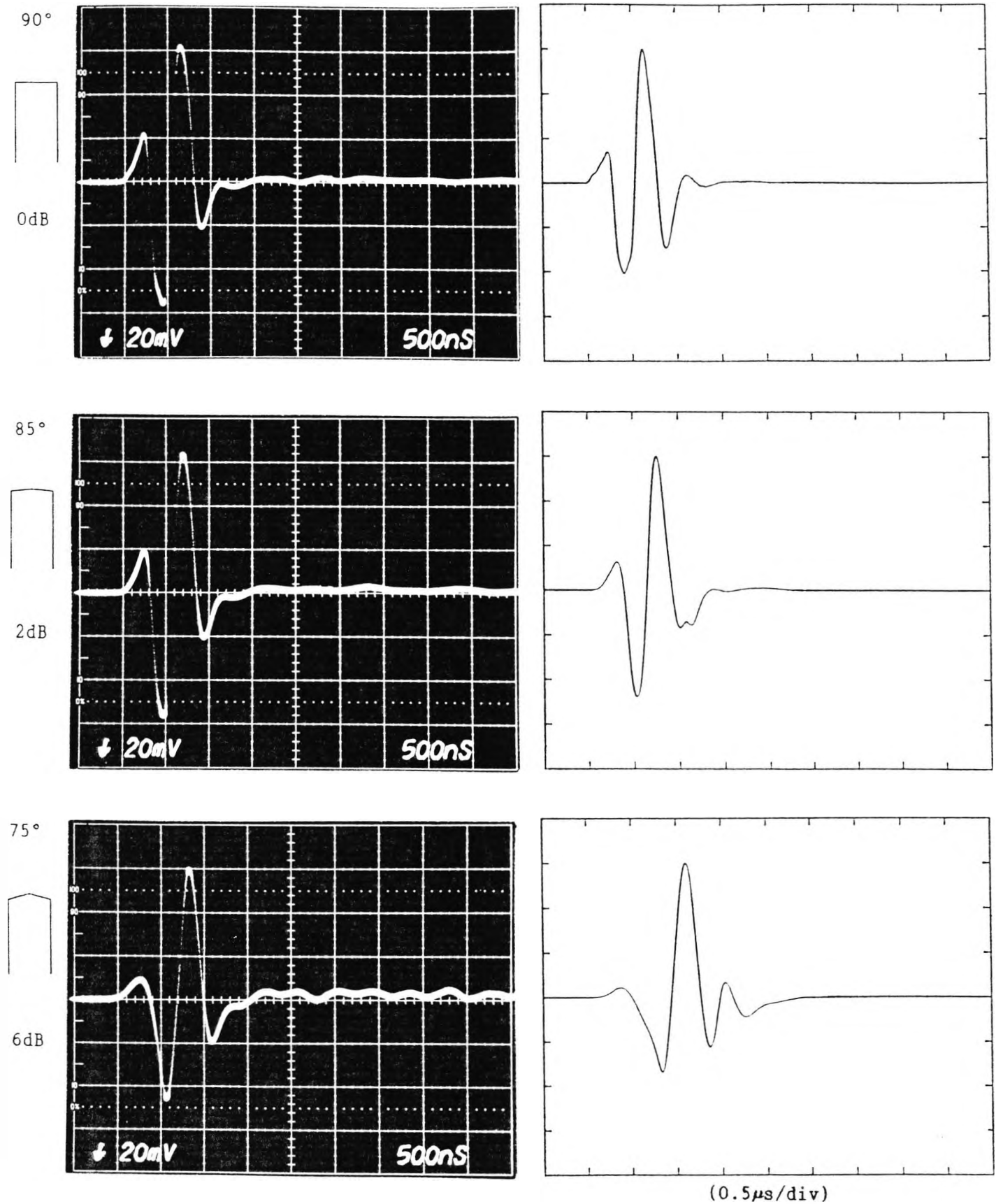
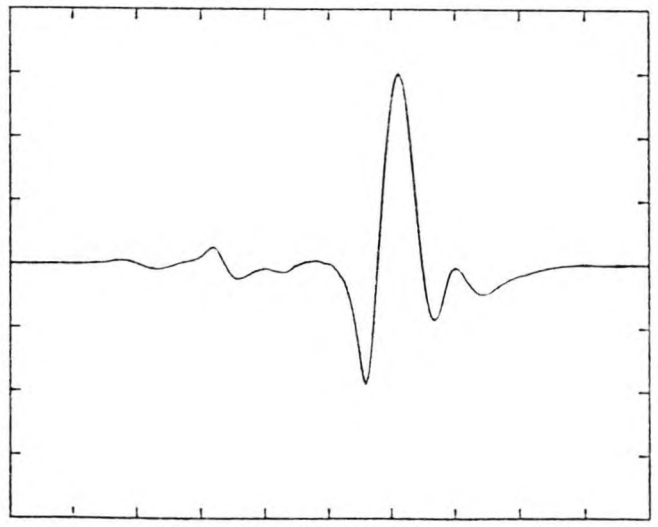
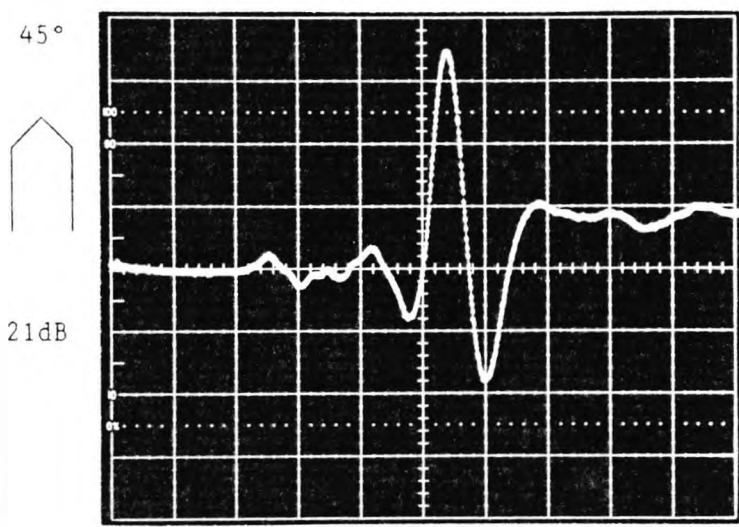
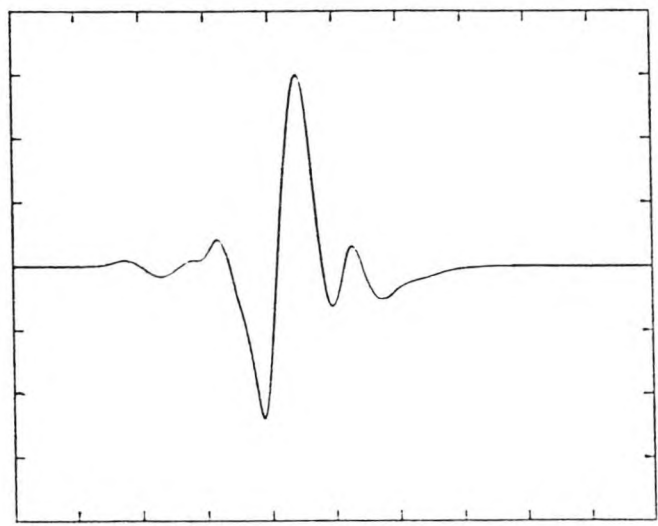
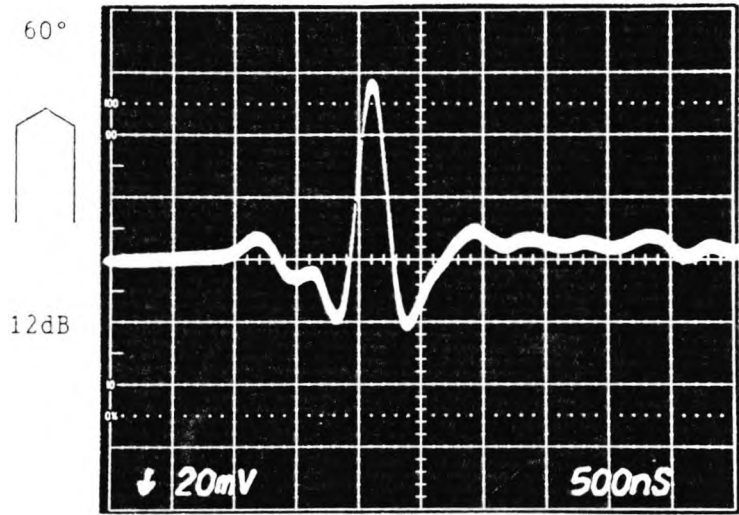


Figure (3.4.2.2): As figure (3.4.2.1), except targets are at 120mm range.



(0.5μs/div)

Figure (3.4.2.2): (continued)

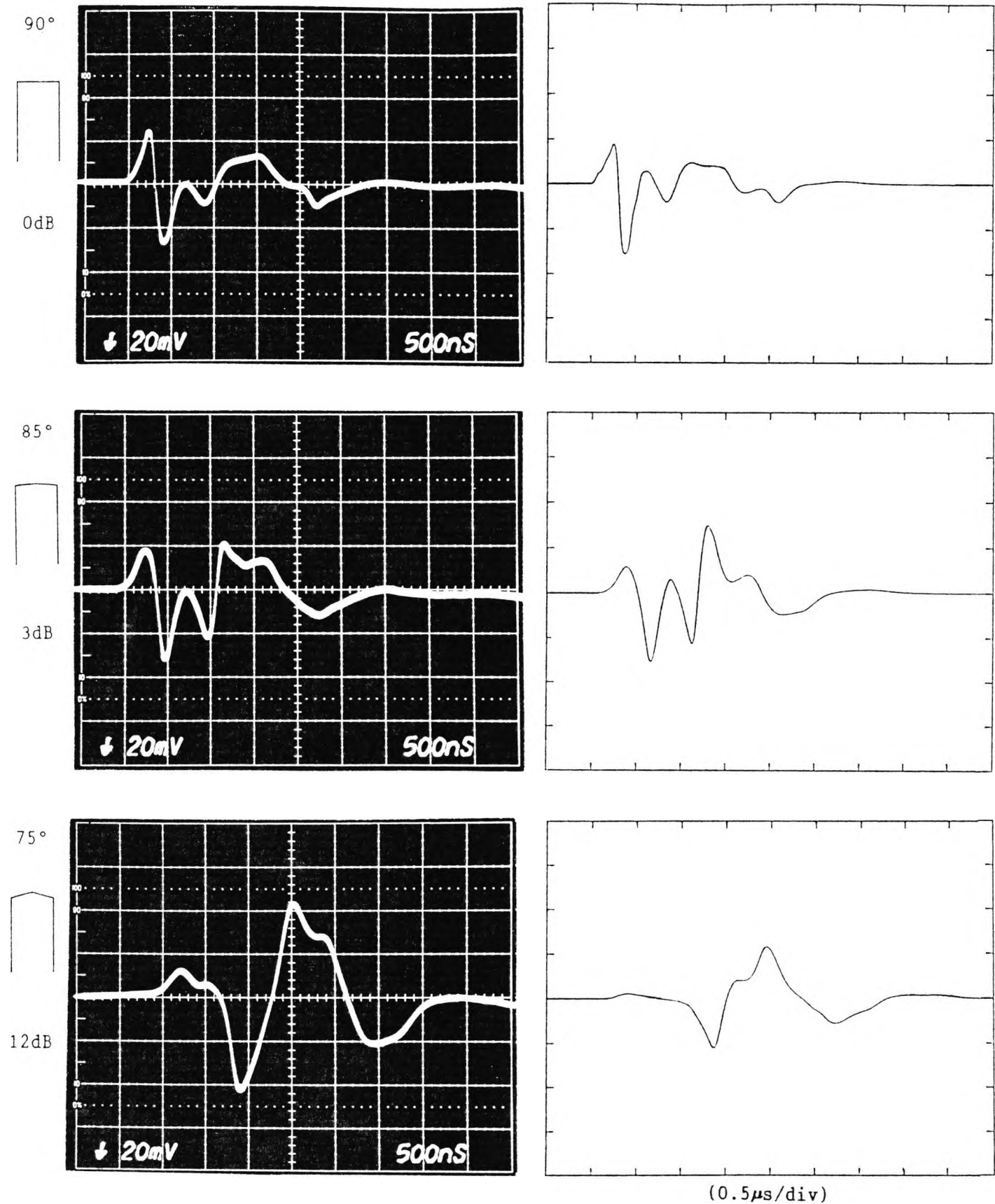


Figure (3.4.2.3): Measured (*left*) and calculated (*right*) transmit-receive echo responses from cone-shaped 4mm diameter targets, on axis at 35mm range. Front face angles are 90° (flat), 85°, 75°. Decibel settings represent relative gain.

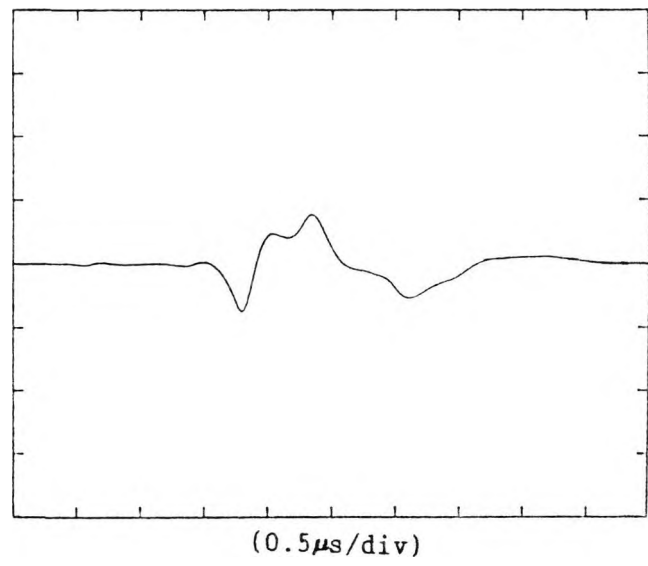
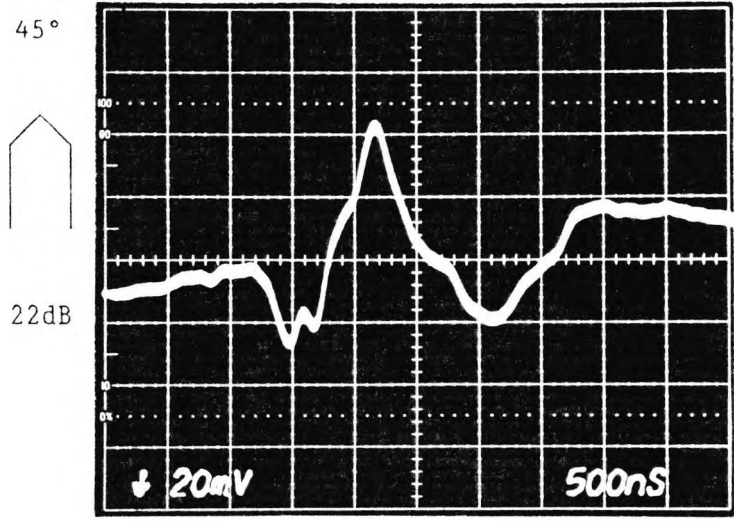
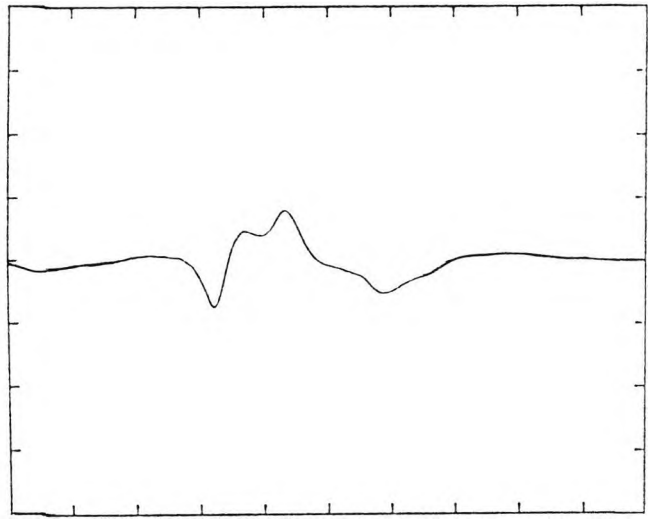
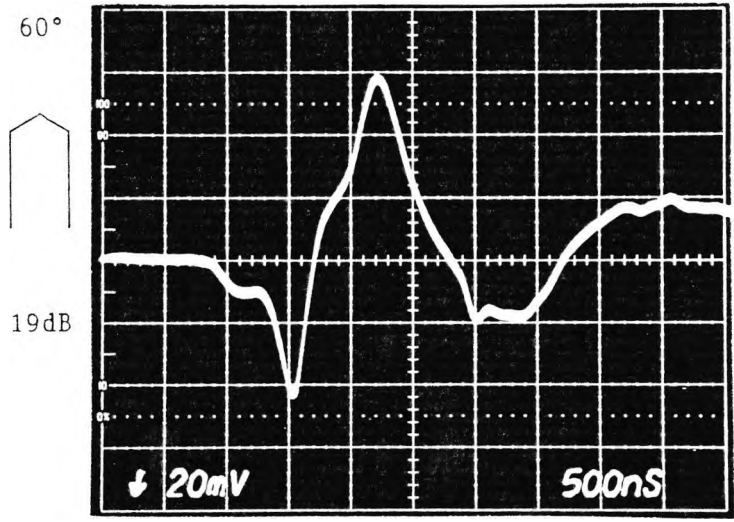


Figure (3.4.2.3): (continued)
 Front face angles are 60°, 45°.

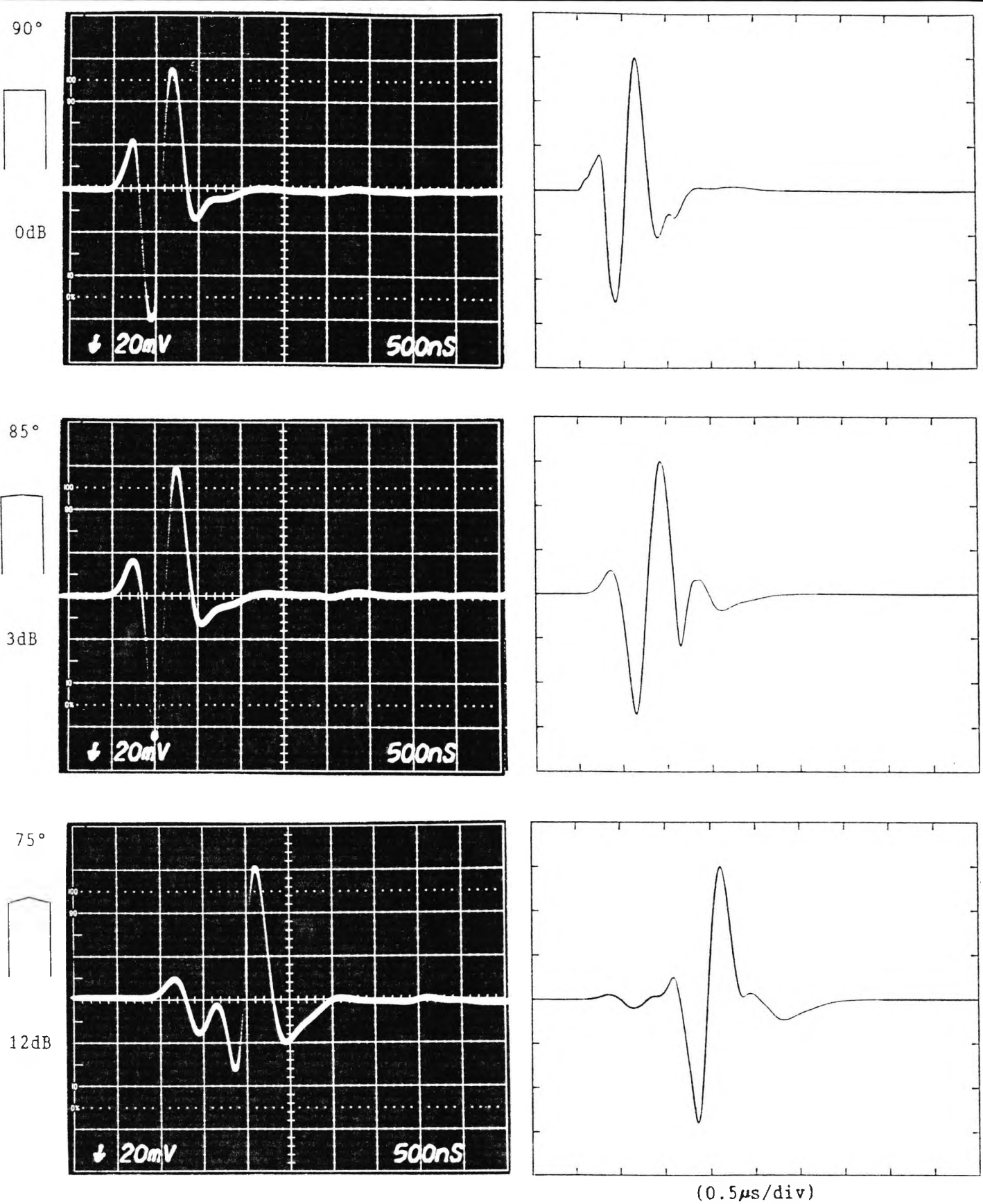
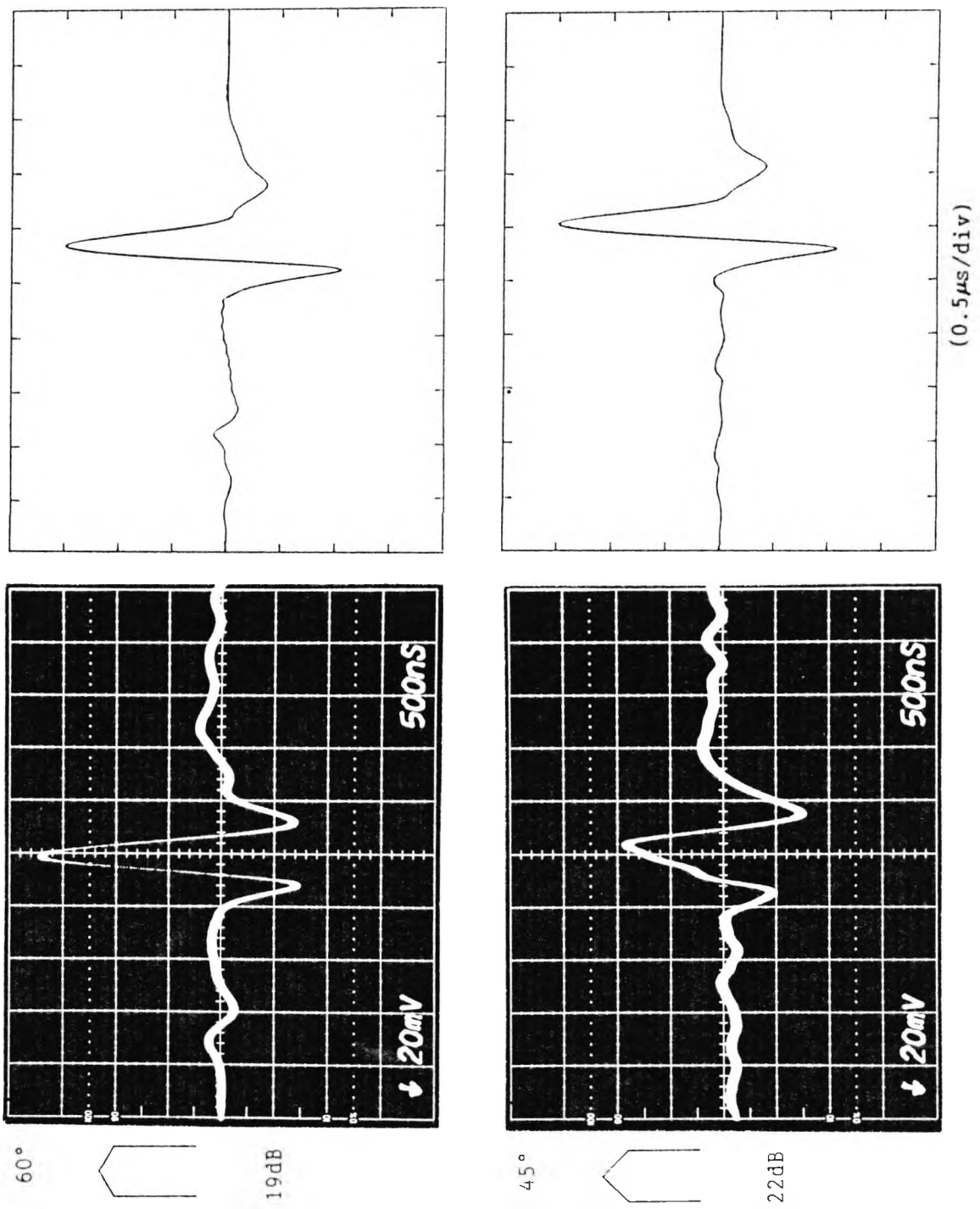
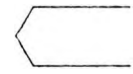


Figure (3.4.2.4): As figure (3.4.2.3), except targets are at 120mm range.

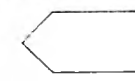


60°



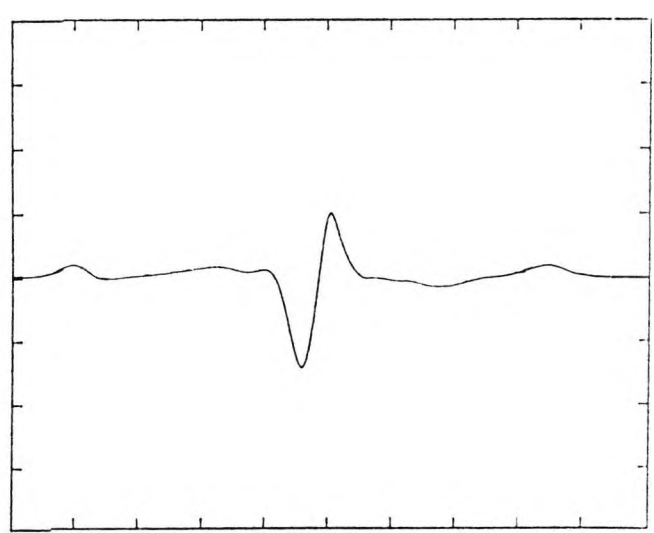
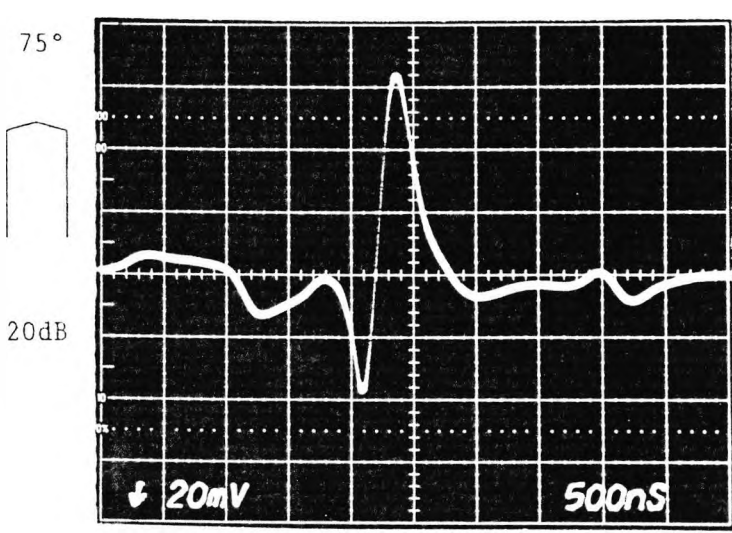
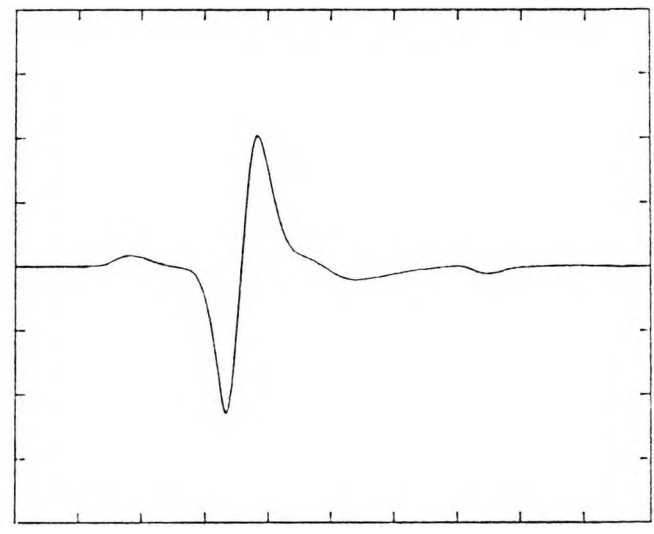
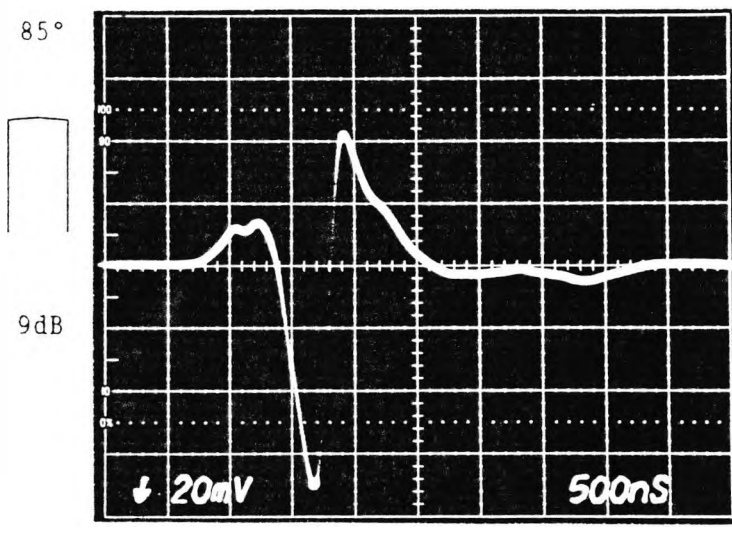
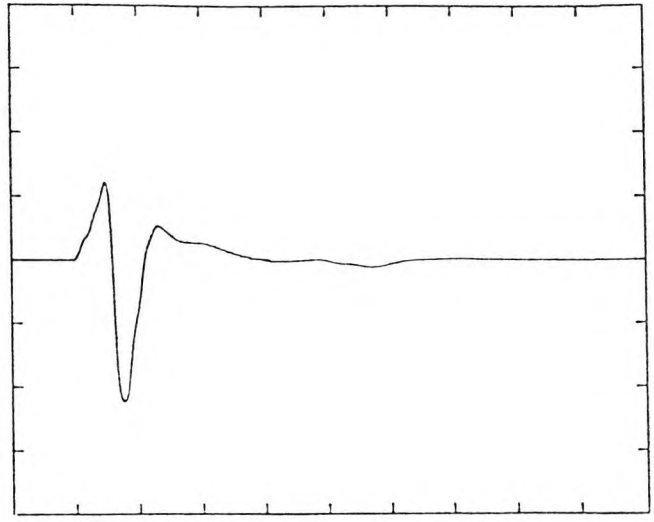
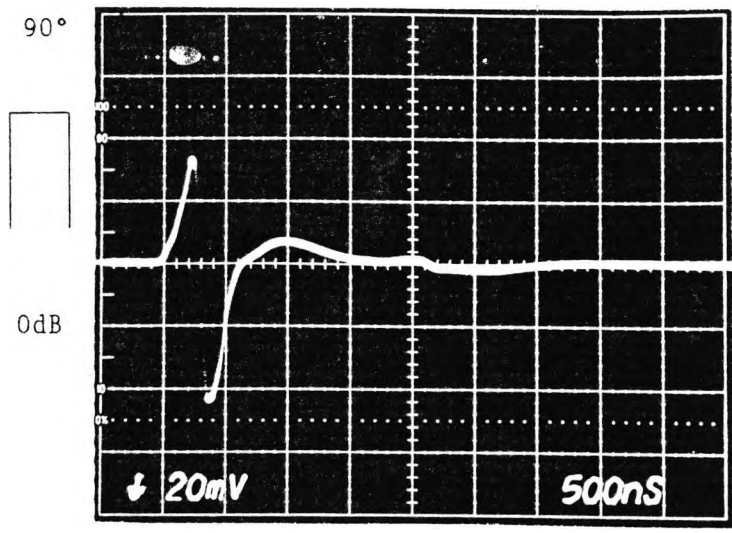
19dB

45°



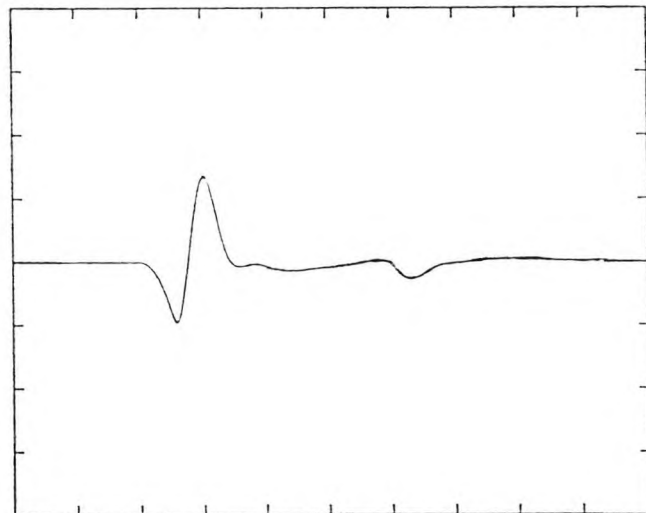
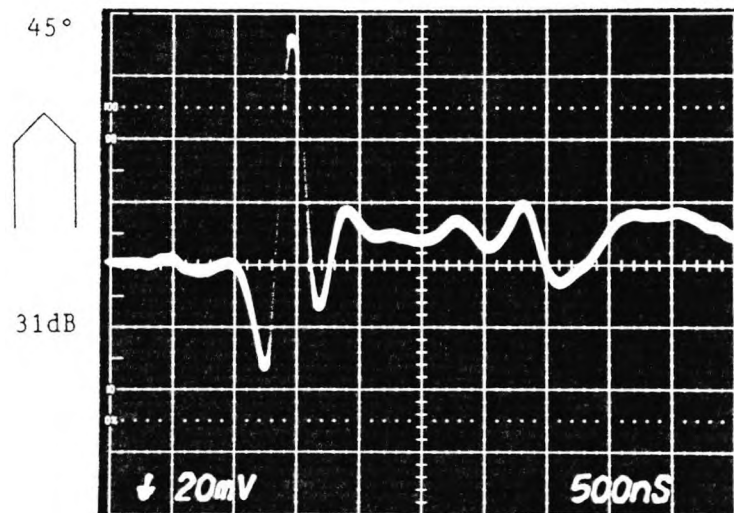
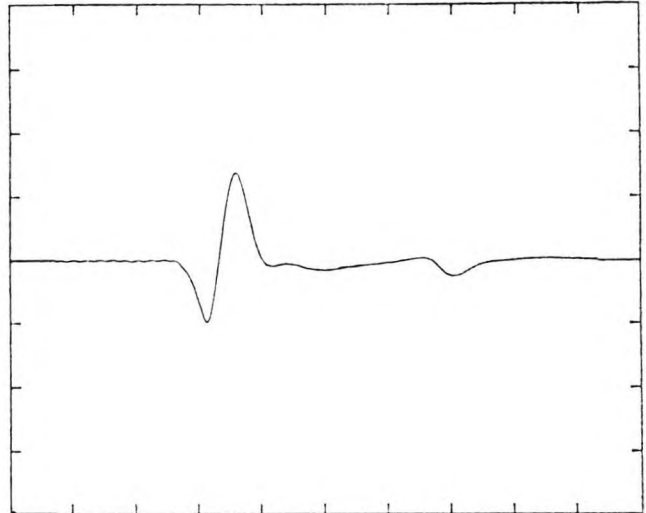
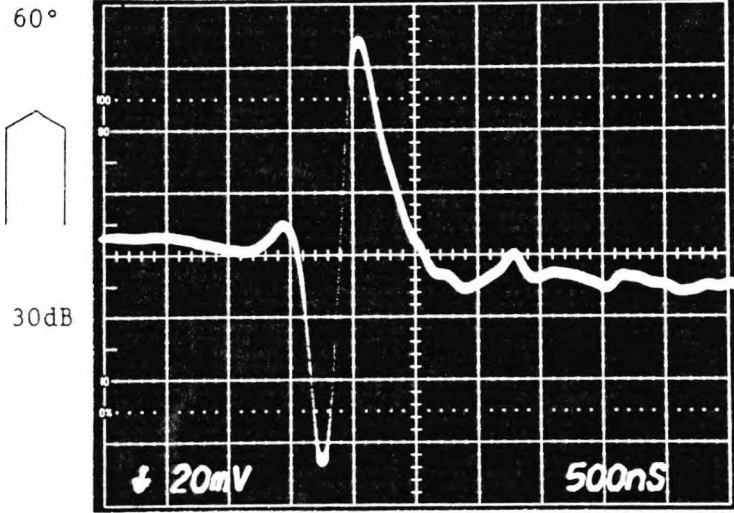
22dB

Figure (3.4.2.4): (continued)



(0.5μs/div)

Figure (3.4.2.5): Measured (*left*) and calculated (*right*) transmit-echo responses from cone-shaped 10mm diameter targets, on axis at 35mm range. Front face angles are 90° (flat), 85°, 75°. Decibel settings represent relative gain.



(0.5μs/div)

Figure (3.4.2.5): (continued)
 Front face angles are 60°, 45°.

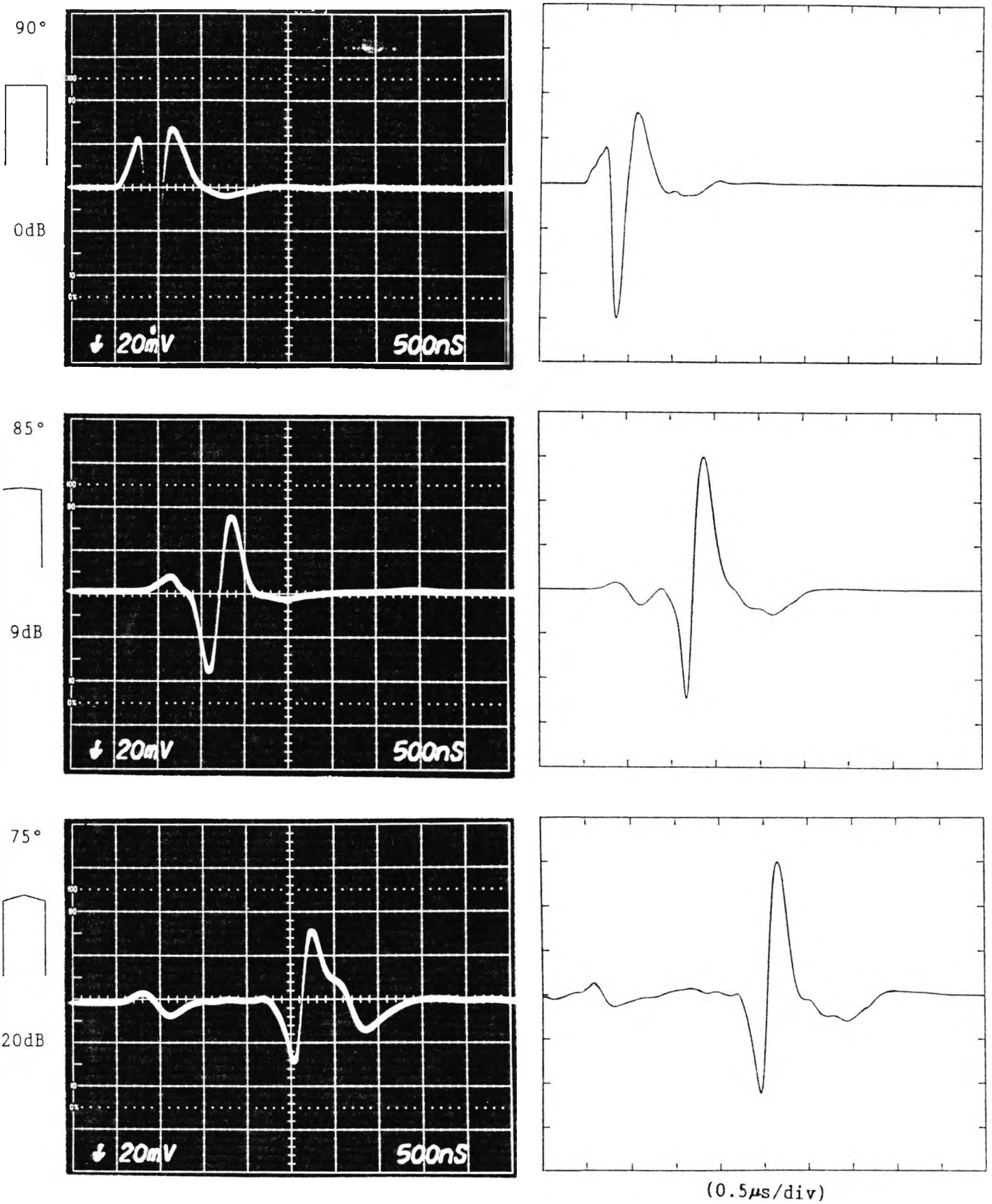


Figure (3.4.2.6): As figure (3.4.2.5), except targets are at 120mm range.

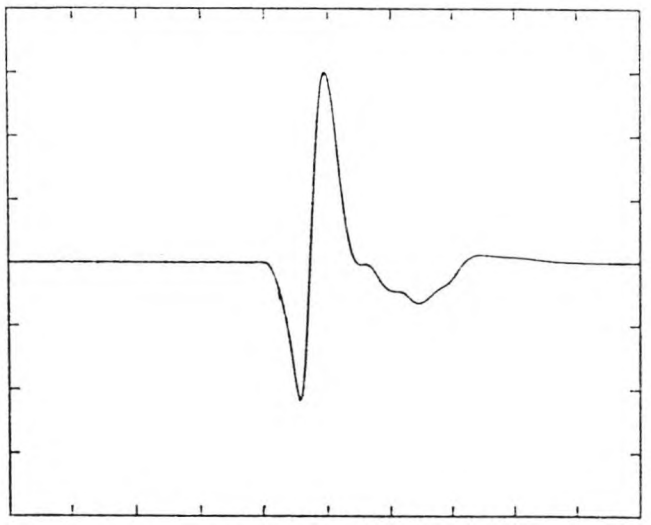
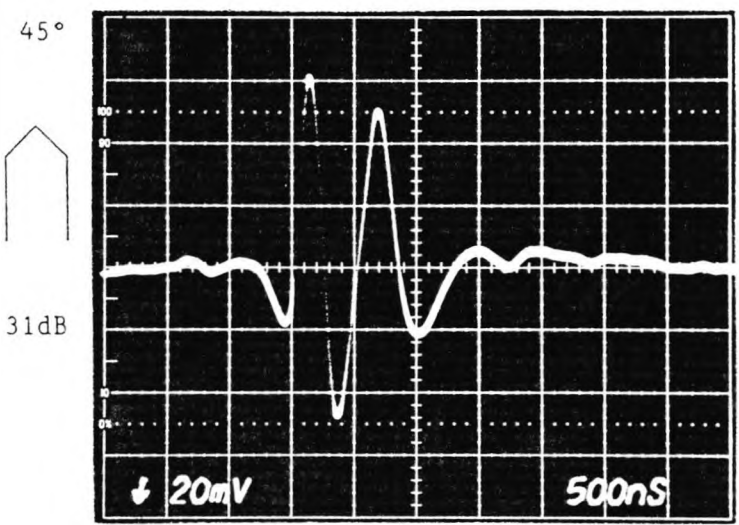
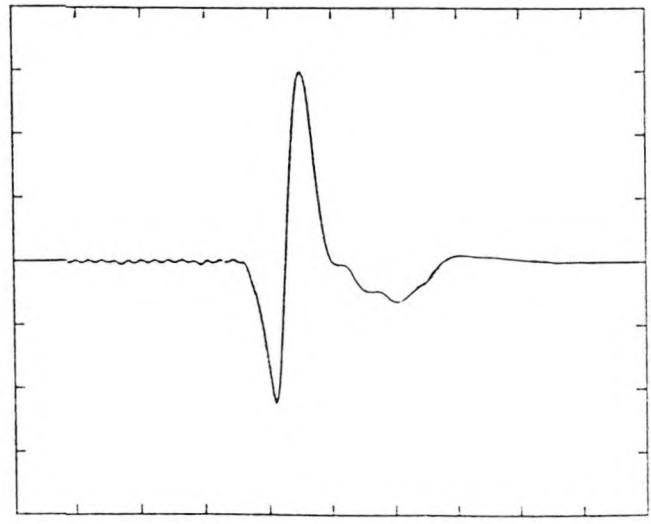
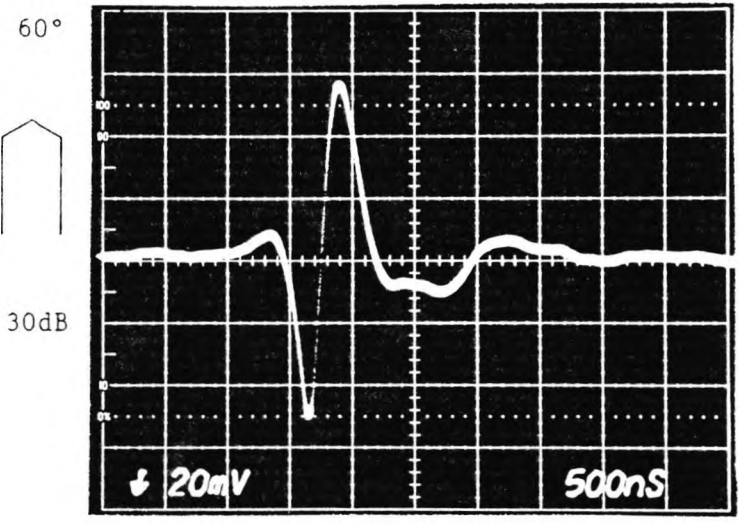


Figure (3.4.2.6): (continued)

3.5 B-scan imaging results

This section shows B-scan results obtained by using the conventional, uniformly-excited transducer, and comparing them with results obtained with a non-uniformly-excited edge-wave-only transducer. Two specially-made test targets were used to obtain the results, which, as they are B-scans, appear as a longitudinal section through the targets. Although these results have been seen before (Brittain and Weight, 1987 and McLaren, 1987), they are included as practical examples of just how well a non-uniformly-excited edge-wave-only transducer performs when compared to a conventional uniformly-excited transducer.

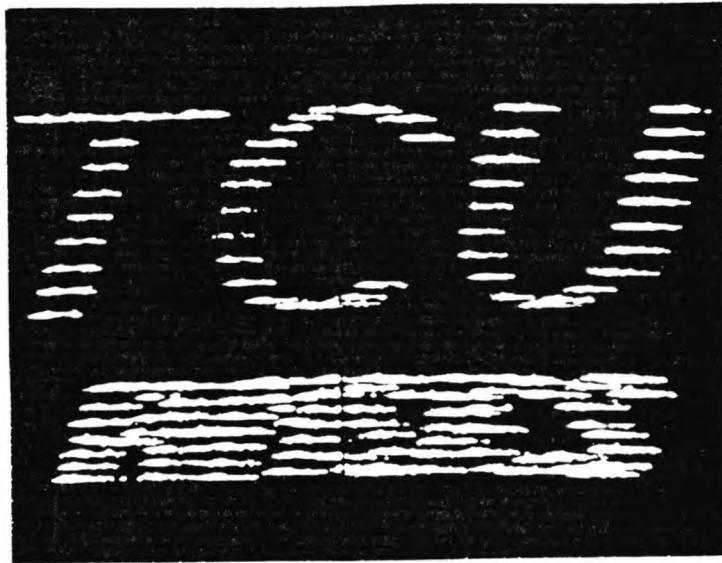
The first target to be imaged was an array of 0.2mm diameter nylon threads, in water, forming a dot-matrix pattern of letters. It was imaged using a conventional uniformly-excited transducer (figure (3.5.1a)) and a non-uniformly-excited edge-wave-only transducer (figure (3.5.1b)).

When imaged with the conventional transducer, figure (3.5.1a), the shortcomings of this device are immediately obvious. The image of each thread is not a small dot, but spread out laterally, and gets worse with range. This spreading out also means that for threads close together horizontally, the images merge together, showing the poor lateral resolution of this transducer. The top word can just about be read, but the lower word is almost impossible to read.

When using the edge-wave-only transducer, (figure (3.5.1b)), these problems are overcome, and each thread is now clearly visible as a single dot image. The lateral resolution is obviously vastly improved. As this target is wholly in water, the images give

completely accurate positional information, as there is no refraction effect (section 2.10.3) to take into account.

a



b

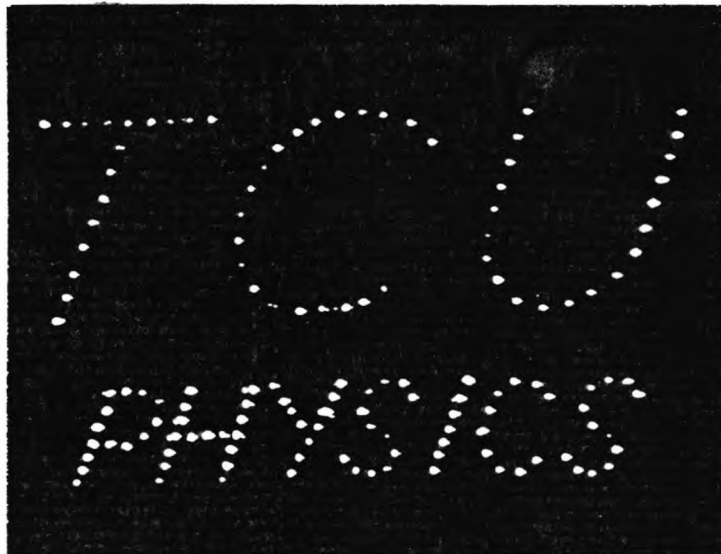


Figure (3.5.1): B-scans of a test target of 0.2mm diameter nylon threads in water.
a: B-scan using a conventional uniformly-excited transducer,
b: B-scan using a non-uniformly-excited edge-wave-only transducer.

The second target was an aluminium block with some perpendicularly drilled, 2mm diameter holes. This is shown schematically in figure (3.5.2a).

When imaged with the conventional transducer, figure (3.5.2b), the holes are imaged as lines as before. Internal reflections also cause spurious images to appear, and holes lying below the main diagonal line of holes, are not well imaged. The range resolution is good, however, since the transducer is capable of imaging the deepest hole in the target block. It should be pointed out that in this figure, echoes from the top and bottom surfaces of the target are displayed as horizontal lines at the top and bottom of each image.

With the edge-wave-only transducer, figure (3.5.2c), the improvement is obvious, and it can now image the holes lying below other holes. It should be noted that there is an inherent inaccuracy present in the actual position of the imaged holes, due to the refraction of ultrasound at the top surface of the block, as described in section 2.10.3. This may need to be taken into account in more accurate work. Here, this error is only of millimetre order, with a coupling range of about 30mm. Such errors in position can be safely neglected here, because with the specified coupling range, only the nearest holes have any error, and this tends to be masked by the size of the image on the display.

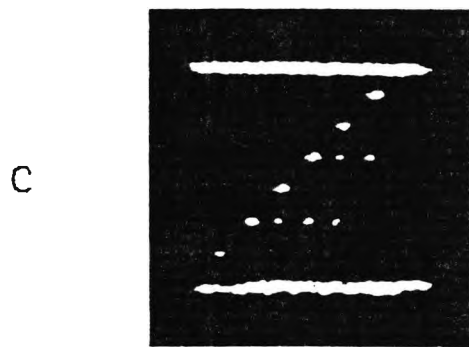
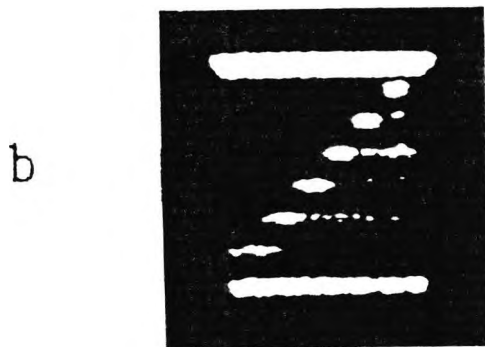
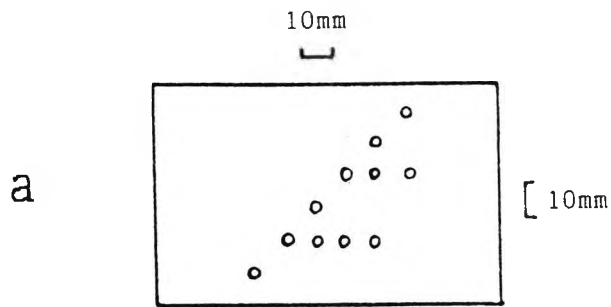


Figure (3.5.2): B-scans of a metal block with holes drilled in.
 a: Schematic diagram of block,
 b: B-scan using a conventional uniformly-excited transducer,
 c: B-scan using a non-uniformly-excited edge-wave-only transducer.

4 Discussion

This chapter discusses the results which were presented in the previous chapter, with particular reference to how the overall resolution of an ultrasonic pulse-echo system is influenced by the type of transducer being used.

Also discussed, are the effects of the target's size and front face shape on the received echo response, and the implications for characterisation techniques.

4.1 Resolution

This was defined in section 2.6 as the ability of a transducer to resolve two targets closely spaced laterally ("lateral resolution") or longitudinally ("range resolution").

As was shown in sections 3.1.5-6, the range resolution is limited by the effective pulse length, as shown in figure (3.1.5.1), and the lateral resolution is limited by the width of the beam, as shown in figure (3.1.6.1).

With the conventional uniformly-excited transducer, figure (3.1.5.1a), close to the transducer, on axis, the echo response from the target comprises three distinct pulses. This could lead to misinterpretation, making one think that there were three equally spaced targets. Overall, the total pulse length is greater than the direct transmit-receive time between the transducer and target, which means that echoes from two closely spaced targets would be interspersed, leading to further confusion about what targets are actually present. At further ranges, where the total pulse length decreases to a more or less constant value, it is easier to interpret

results.

Moving off axis, each edge wave component splits into two smaller pulses of reduced amplitude, leaving the plane wave component unchanged. In such cases, a target in any lateral position will produce echo responses of similar maximum amplitudes. This is shown clearly in the beam profiles of figure (3.1.6.1a), and demonstrated in the B-scans of figures (3.5.1a) and (3.5.2b), which show images of small targets as lines rather than as dots.

With the three other kinds of transducer, figure (3.1.5.1b-d), the problem of the multi-pulse echo structure is greatly reduced, since the total pulse length is now of the same order as the driving pulse width, and so the simpler echo responses make interpretation easier.

The ideal edge-wave-only transducer figures (3.1.5.1b) and (3.1.6.1b), would seem to be an excellent device if only it were physically realisable, with a simple response on axis, giving a good range resolution, and a sharp, narrow beam width, giving a good lateral resolution. Further off axis, straight ahead of the transducer's rim, there is, however, a small response which could lead to misinterpretations of echo results. Fortunately, the non-uniformly-excited edge-wave-only transducer, figures (3.1.6.1c) and (3.3.2.3), does not have this "rim response" (except very close to the transducer), even when interrogating a real point-like target, figure (3.3.2.4). The structure of the echo waveforms is much simpler when compared with the conventional transducer, each waveform being fairly short in duration, figure (3.1.5.1c). As in the ideal edge-wave-only transducer, the echo waveforms are concentrated along the

transducer's axis, figure (3.1.6.1c). The short pulse structure and narrow beam width result in a transducer with good range and lateral resolution. The excellence of this transducer shows in the B-scans of figures (3.5.1b) and (3.5.2c), where the images are properly resolved.

The non-uniformly-excited plane wave-only transducer also has simple and short waveforms, figure (3.1.5.1d), giving a good range resolution, but beam profiles are broad, figure (3.1.6.1d), giving a poorer lateral resolution than the non-uniformly excited edge-wave-only transducer. It would, however, appear to be better than the conventional transducer of figure (3.1.6.1a), since the latter has much broader beam profiles.

4.2 Target size and front face shape

For the conventional, uniformly-excited transducer, as the target size increases, the amplitude of the plane wave component increases, swamping all the other components. This can be seen in the sequence of figures (3.1.5.1a), (3.2.1.2a) and (3.2.2.2a), for the theoretical cases of a point target, and 2mm and 4mm diameter targets, respectively. This effect occurs because as the target size increases, it behaves more like a large flat reflector, and so allows more of the transmitted plane wave to be reflected back as a locally plane wave, as described in section 3.3.1. This is also seen in the experimental results of figures (3.3.1.1) and (3.4.1.1).

For the ideal edge-wave-only transducer, figures (3.1.5.1b), (3.2.1.2b) and (3.2.2.2b), as the target size increases, the response straight ahead of the transducer's edge becomes larger, relative to the axial response. For a point target, edge waves travel in a path from the edge of the transducer to the target and are reflected back to the edge of the transducer. As the target size increases, there is a new path to consider - from the transducer edge to the target edge and back to the transducer edge. As this new path is shorter than the path involving the centre of the target, the echo pulse due to the shorter path occurs first. As the target size approaches, and then exceeds, the size of the source, this "edge-to-edge" response becomes quite large, since the directivity (figure (3.1.4.1)) is maximum straight ahead of the edge. The reason that there is a large response straight ahead of the transducer's edge, when interrogating a large, axial target, but no response when a small target is positioned straight ahead of the transducer's edge, is that the large target

behaves as if it were a circular collection of point targets whose individual (small) responses build up to a large response.

For the non-uniformly-excited edge-wave-only transducer, figures (3.1.5.1c), (3.2.1.2c) and (3.2.2.2c), these effects are much smaller, as the experimental results in figures (3.3.2.1-2) confirm. For larger targets of the same order as the source, McLaren (1987) has shown experimental results confirming the existence of the extra pulses mentioned above. With changing target size, the overall response of the transducer stays very much the same.

This can also be said for the non-uniformly-excited plane wave-only transducer, figures (3.1.5.1d), (3.2.1.2d) and (3.2.2.2d). The waveforms keep the same shape and relative amplitude with changing target size.

One of the most common methods of estimating the size of a target was proposed by Krautkrämer (1959). This consists of a collection of curves relating echo response amplitudes and target range, to the size of a target. The DGS diagrams (distance-gain-size) are derived assuming a perfectly flat and circular reflecting target in a fluid medium, at right angles to the field radiated by the transducer. The target is assumed to be in the far-field, since the derivations assume steady-state behaviour (ie. cw.). Krautkrämer has also shown that for pulses consisting of a few cycles, there are deviations from the theoretically predicted cw. cases. For short wideband pulses the deviations become even greater. Despite their limitations, DGS diagrams can be used successfully in many cases. It has been shown by McLaren and Weight (1987) that the finite-sized target model described in sections 2.8-9 can be used to derive theoretical DGS diagrams for

arbitrary pulse shapes.

As the size of the target greatly affects the amount of plane-wave component which is received back at the transducer, there are implications for the shape of the velocity potential impulse response. As was mentioned in section 2.4, the sharp steps are responsible for the mathematical generation of the plane- and edge-wave components. Thus, as the plane-wave component becomes larger with increasing target size (and the edge-wave component becomes smaller), so the trailing step of the velocity potential impulse response spreads out, becoming less sharp. This is shown for the conventional transducer in figures (3.1.1.1a), (3.2.3.1a) and (3.2.3.2a). For the non-uniformly-excited plane-wave-only transducer, as little or no edge waves are generated anyway, this means that the trailing edge of the velocity potential impulse response is always spread out, and there is little change with target size, figures (3.1.1.1d), (3.2.3.1b) and (3.2.3.2b). If a way could be found to get an expression for the velocity potential impulse response directly (as is done for point targets, see eqn. (2.4.10)), this would have an obvious advantage of requiring less computing time to calculate the echo impulse response. This is because for the finite-size target case, the echo impulse response consists of a convolution within an integral (eqn. (2.9.2)). This however, is left for future work.

The correct alignment of the target with respect to the transducer becomes important as the target size increases. If the target is misaligned, the front face of the target reflects the plane wave away, so that less is received back at the transducer. This effect can be seen in the near-field results (so that the constituent

pulses are well separated) for the cone-shaped targets, in figures (3.4.2.1), (3.4.2.3) and (3.4.2.5). With the smallest target, figure (3.4.2.1), the usual three-pulse structure is evident for the less pointed targets, but as the targets become more pointed, the first pulse, which is due to the plane wave, becomes smaller in comparison to the other component pulses. For the most pointed target, the plane-wave component has virtually disappeared. With the larger targets, figures (3.4.2.3) and (3.4.2.5), the initially much bigger plane-wave component drops much more rapidly with increasing pointedness of the target. This can be seen by looking at the gain settings recorded by the experimental results, and noting that, much more gain needs to be applied as the target size increases.

4.3 Non-uniform relationship between range and time

The non-uniform relationship between range and time which exists for edge-wave type transducers, discussed in section 2.10.3, really only applies when refraction occurs between liquid and solid interfaces, where the targets are embedded in a solid medium. The only such result presented here is the B-scan of the metal block with the perpendicularly drilled holes, figure (3.5.2). As figure (2.10.3.2) shows, there is one particular depth within the target block at which the error in position is a maximum, assuming zero error at the front and rear faces of the block. In the example shown in the latter figure, at a depth of 20mm in the target block, the expected positional error is about 2mm. In the experimental result of the former figure, these errors have to be taken into account during the interpretation. To overcome this error would mean having an oscilloscope with a non-linear timebase, which would seem to be impractical. However, modern microcomputer controlled instrumentation would probably be able to carry out the necessary correction automatically. A simpler alternative would be to calculate a series of "correction curves" for the target configuration being studied.

5 Conclusions

This thesis has shown how the radiated sound field emitted by a circular ultrasonic transducer in a fluid, can be described in terms of a plane wave radiating within the geometric region straight ahead of the source, and a spreading edge wave radiating from the periphery of the source. Interaction between these two different types of wave cause variations in amplitude to occur in the transmit-receive echo responses, depending on the position of the target being interrogated.

Computer modelling has shown that non-uniformly-excited transducers have advantages over conventional, uniformly-excited transducers. The non-uniform excitation is described by a weighting profile which either varies smoothly from maximum at the centre of the source to zero at the edge, or maximum at the edge to zero in the centre. The former type tends to reduce the edge-wave components, leaving the plane-wave component, hence the name 'plane-wave-only transducer'. The latter type reduces the plane-wave component, leaving the edge-wave component, hence the name 'edge-wave-only transducer'.

Edge-wave-only transducers have been shown to emit an ultrasound beam which is concentrated in a narrow region along the axis of the transducer. This results in a vast improvement in lateral resolution when compared to the conventional transducer. The echo responses are much shorter than with the conventional transducer, resulting in a great improvement in range resolution. The advantages of this transducer are clearly demonstrated by comparing B-scan images taken with this transducer and a conventional transducer. All the targets are clearly resolved with the edge-wave-only transducer, but the conventional transducer has great difficulty resolving closely spaced

targets.

For the case of an edge-wave-only transducer interrogating a solid block with embedded targets, immersed in a fluid, it was explained how refraction occurring at the fluid/solid interface causes the echo pulses from the targets to be shifted in time. This time shift and hence error in perceived position, has been modelled using an iterative method. Such errors have been shown to be small.

The plane-wave-only transducer has also been shown to have useful properties. The short pulse length gives an excellent range resolution, like the edge-wave-only transducer, and has a much more constant shape throughout the field. Compared to a conventional uniformly excited transducer where the echo response varies greatly with target position, this is an important advantage.

The impulse response method is well suited to computer modelling, since after calculating the echo impulse response, the actual echo waveform received by the transducer can be calculated by convolution with the transducer's motion. This allows the echo response to be calculated for any arbitrary motion of the transducer. The core of all the modelling programs calculate impulse responses for uniformly excited transducers interrogating point targets at any position in the radiated field.

A way of adapting the model to allow non-uniformly-excited transducers to be included was presented. This treats the source as if it were a collection of coincident sources of decreasing diameter, the echo response of each weighted according to the desired weighting profile, and superposed to give the total echo response.

Incorporating the method of Ueda and Ichikawa (1981) (and

extending their method to off-axis targets) then gives the model the ability to handle circular targets of any finite size.

Thus, the overall modelling scheme described in this thesis is capable of calculating an echo response for any axisymmetric, non-uniformly-excited transducer, interrogating a flat, circular target placed at any position in the field, such that the faces of the transducer and target are parallel.

Circular targets are used in the modelling so as to take advantage of the inherent circular symmetry. However, the model can deal with non-circular targets, as McLaren (1987) has shown, with results for square and triangular targets.

Using the echo response for the finite-size target case, it has been possible to derive equivalent velocity potential impulse responses. It is hoped that further analysis of the velocity potential impulse responses will lead to simple expressions being obtained for them, as is done for point targets. This will considerably reduce the computer run-times required.

Detailed calculations have been made, along with experimental verification, of the properties of the different kinds of transducer, and their performance when interrogating different size targets in water. The results presented here show a very good agreement between calculated and experimentally measured results, proving the validity of the model.

An attempt has been made to model targets which are not flat, but pointed, as the first stage in the problem of target misalignment. Although the pointed target model is inaccurate for the most pointed targets, due to the assumptions made, the less pointed targets show

good matches between theory and experiment. For the smallest target there is only a 2dB reduction in amplitude between the flat (90°) target and the 85° target, and the waveform's shape is virtually unchanged. As the target diameter increases, so becoming a bigger reflector, this amplitude reduction also increases, and the waveform's shape changes drastically. This indicates that for small targets, the flatness of the face of the target doesn't seem to matter, whereas for larger targets, a few degrees of unevenness dramatically alters both the shape and size of the echo response.

In summary, this thesis has described a general model for circular ultrasonic transducers interrogating circular targets in fluids. Non-uniformly-excited edge wave-only and plane-wave-only transducers have been modelled, and these results have compared well with results obtained from real transducers made in our laboratory. Both types of transducer give better resolution than conventional, uniformly excited transducers.

6 Future work

The main area requiring further research concerns modifications to the modelling. Currently the model can only cope with flat targets, or pointed targets to a limited degree, which are perfectly aligned; ie. the axes of the transducer and target are parallel. It would be desirable to improve the model for pointed targets, and extend it to allow for more general non-flat targets.

It would be advantageous to develop formulations for the velocity potential impulse response for the case of finite-size targets. This would considerably reduce the computer run-times involved in calculating the echo impulse responses.

Finally, the next major step would be to incorporate all the results discussed in this thesis into the case of targets in solid materials, which is made more complicated by the presence of shear waves, and mode conversion.

Appendix

Calculation of frequency responses for finite-sized targets

In section 2.8 it is necessary to obtain expressions for the frequency response of the total scattering medium, in terms of changes of velocity and changes of density, separately. First assume that there are velocity fluctuations only, i.e. $\Delta\rho$ is zero. The scattering strength $Q(\underline{r},t)$ from eqn. (2.8.3) becomes:-

$$Q(\underline{r},t) = \left[\frac{2\Delta c}{c^3} \right] \left[\frac{\partial^2 P_{in}(\underline{r},t)}{\partial t^2} \right] . \quad (A.1)$$

The incident wave is given by eqn. (2.8.4):-

$$P_{in}(\underline{r},t) = u(t) * \rho \frac{\partial \phi(\underline{r},t)}{\partial t} , \quad (A.2)$$

or, since

$$\phi(\underline{r},t) = e^{j\omega t} , \quad (A.3)$$

so

$$\frac{\partial \phi(\underline{r},t)}{\partial t} = j\omega \phi(\underline{r},t) , \quad (A.4)$$

$$P_{in}(\underline{r},t) = \rho u(t) * j\omega \phi(\underline{r},t) . \quad (A.5)$$

If this is written as an inverse Fourier transform:-

$$P_{in}(\underline{r},t) = \rho \frac{1}{2\pi} \int_{-\infty}^{\infty} U(\omega) j\omega \Phi(\underline{r},\omega) e^{j\omega t} d\omega . \quad (A.6)$$

Differentiating twice with respect to time:-

$$\frac{\partial^2}{\partial t^2} P_{in}(\underline{r}, t) = \frac{\rho}{2\pi} \int_{-\infty}^{\infty} U(\omega) j\omega \Phi(\underline{r}, \omega) \left[\frac{\partial^2}{\partial t^2} e^{j\omega t} \right] d\omega, \quad (A.7)$$

$$= \frac{\rho}{2\pi} \int_{-\infty}^{\infty} U(\omega) j\omega \Phi(\underline{r}, \omega) (j\omega)^2 e^{j\omega t} d\omega. \quad (A.8)$$

Thus the scattering strength, eqn. (A.1), becomes:-

$$Q(\underline{r}, t) = \left[\frac{2\Delta c}{c^3} \right] \left[\frac{\rho}{2\pi} \int_{-\infty}^{\infty} U(\omega) j\omega \Phi(\underline{r}, \omega) (j\omega)^2 e^{j\omega t} d\omega \right]. \quad (A.9)$$

The scattered wave is given by eqn. (2.8.2):-

$$P_{sc}(\underline{r}, t) = \int_V \frac{Q(\underline{s}, t - |\underline{r} - \underline{s}|/c)}{4\pi|\underline{r} - \underline{s}|} dv, \quad (A.10)$$

$$= \int_V \frac{\left[\frac{2\Delta c}{c^3} \right] \left[\frac{\rho}{2\pi} \int_{-\infty}^{\infty} U(\omega) j\omega \Phi(\underline{s}, \omega) (j\omega)^2 e^{j\omega[t - |\underline{r} - \underline{s}|/c]} d\omega \right]}{4\pi|\underline{r} - \underline{s}|} dv. \quad (A.11)$$

$$= \int_{-\infty}^{\infty} \int_V \frac{\Delta c (j\omega)^3 \rho U(\omega) \Phi(\underline{s}, \omega) e^{j\omega t} e^{-j\omega[t - |\underline{r} - \underline{s}|/c]} }{(2\pi)^2 c^3 |\underline{r} - \underline{s}|} d\omega dv . \quad (\text{A.12})$$

The echo signal is proportional to the integral of the scattered wave across the transducer surface:-

$$e_c(t) \propto \int_S P_{sc}(\underline{r}, t) ds , \quad (\text{A.13})$$

and since

$$\Phi(\underline{r}, \omega) = \frac{1}{2\pi} \int_S \frac{e^{-j\omega[t - |\underline{r} - \underline{s}|/c]} }{|\underline{r} - \underline{s}|} ds , \quad (\text{A.14})$$

eqn. (A.13) becomes:-

$$e_c(t) \propto \int_{-\infty}^{\infty} \int_V \frac{\Delta c (j\omega)^3 \rho U(\omega) \Phi(\underline{s}, \omega) e^{j\omega t} \Phi(\underline{r}, \omega)}{2\pi c^3} d\omega dv . \quad (\text{A.15})$$

Eqn. (A.15) can be made an equality by inserting a constant $T(\omega)$, which takes into account the behaviour of the transducer on reception:-

$$e_c(t) = \int_{-\infty}^{\infty} \left[\int_V \frac{\Delta c (j\omega)^3 \rho U(\omega) T(\omega) \Phi(\underline{s}, \omega) e^{j\omega t} \Phi(\underline{r}, \omega)}{2\pi c^3} dv \right] d\omega \quad (A.16)$$

The echo signal can be expressed as an inverse Fourier transform:-

$$e_c(t) = \frac{1}{2\pi} \int_{-\infty}^{\infty} \left[\int_V \frac{\Delta c (j\omega)^3 \rho U(\omega) T(\omega) \Phi(\underline{s}, \omega) \Phi(\underline{r}, \omega)}{c^3} dv \right] e^{j\omega t} d\omega \quad (A.17)$$

or as a convolution:-

$$e_c(t) = \rho u'(t) * \frac{\partial f_c(t)}{\partial t} \quad (A.18)$$

where $u'(t)$ is the inverse Fourier transform of $U(\omega)T(\omega)$, $f_c(t)$ is the velocity potential impulse response, and $\partial f_c(t)/\partial t$ is the pressure impulse response.

Comparing eqns. (A.17) and (A.18):-

$$\frac{\partial f_c(t)}{\partial t} = \frac{1}{2\pi} \int_{-\infty}^{\infty} \left[\int_V \frac{\Delta c (j\omega)^3 \Phi(\underline{s}, \omega) \Phi(\underline{r}, \omega)}{c^3} dv \right] e^{j\omega t} d\omega \quad (A.19)$$

$$f_c(t) = \int e^{j\omega t} dt \frac{1}{2\pi} \int_{-\infty}^{\infty} \left[\int_V \frac{\Delta c (j\omega)^3 \phi(\underline{s}, \omega) \phi(\underline{r}, \omega)}{c^3} dv \right] d\omega, \quad (\text{A.20})$$

$$= \frac{1}{2\pi} \int_{-\infty}^{\infty} \left[\int_V \frac{\Delta c (j\omega)^2 \phi(\underline{s}, \omega) \phi(\underline{r}, \omega)}{c^3} dv \right] e^{j\omega t} d\omega, \quad (\text{A.21})$$

Thus, the frequency response, for velocity fluctuations only, is:-

$$F_c(\omega) = \int_V \frac{\Delta c (j\omega)^2 \phi(\underline{s}, \omega) \phi(\underline{r}, \omega)}{c^3} dv. \quad (\text{A.22})$$

The above procedure is used to obtain the frequency response for density fluctuations only, i.e. where Δc is zero:-

$$F_\rho(\omega) = \int_V \frac{-\phi(\underline{r}, \omega) \nabla(\Delta\rho) \cdot \nabla\phi(\underline{s}, \omega)}{2\rho} dv. \quad (\text{A.23})$$

References

BEAVER W.L.

"Sonic nearfields of a pulsed piston radiator."

J. Acoust. Soc. Am. 56, pp1043-1048, 1974.

BRACEWELL R.N.

The Fourier transform and its applications.

Mc.Graw-Hill, 1978. 2nd edition, Chapter 3.

BRITTAİN R.H. and WEIGHT J.P.

"Fabrication of non-uniformly excited wide-band ultrasonic transducers."

Ultrasonics 25 (2), pp100-106, 1987.

BRITTAİN R.H. and WEIGHT J.P.

"Non-uniformly excited wide-band ultrasonic transducers with improved pulse shapes."

(In preparation, 1990.)

DEHN S.

"Interference patterns in the near field of a circular piston."

J. Acoust. Soc. Am. 32, pp1692-1696, 1960.

GATCOMBE C.P. and WEIGHT J.P.

"Axisymmetric transducers and finite-sized targets in fluid media."

(In preparation, 1990.)

GRAFF K.F.

Wave motion in elastic solids.

Clarendon Press, 1975. Chapter 6.

GUYOMAR D. and POWERS J.

"Transient radiation from axially symmetric sources."

J. Acoust. Soc. Am. 79 (2), pp273-277, 1986.

HARRIS G.R.

"Transient field of a baffled planar piston having an arbitrary vibration amplitude distribution."

J. Acoust. Soc. Am. 70 (1), pp186-204, 1981b.

HARRIS G.R., CAROME E.F. and DARDY H.D.

"An analysis of pulsed ultrasonic fields as measured by PVDF spot-poled membrane hydrophones."

IEEE Trans. SU 30 (5), pp295-303, 1983.

HARRISON G.H. and BALCER-KUBICZEK E.K.

"Experimental demonstration of Fourier synthesis of an annular ultrasonic intensity distribution."

Ultrasonics 25 (3), pp172-174, 1987.

HAYMAN A.J.

"Schlieren visualisation of focused ultrasonic images."

PhD Thesis, The City University, London, 1977.

HAYMAN A.J. and WEIGHT J.P.

"Transmission and reception of short ultrasonic pulses by circular and square transducers."

J. Acoust. Soc. Am. 66 (4), pp945-951, 1979.

HUNTER J.L.

Acoustics.

Prentice-Hall, 1957. Chapter 4.

HUTCHINS D.A., MAIR H.D., PUHACH P.A. and OSEI A.J.

"Continuous-wave pressure fields of ultrasonic transducers."

J. Acoust. Soc. Am. 80 (1), pp1-12, 1986.

JACQUINOT P. and ROIZEN-DOSSIER B.

"Apodisation."

In: Progress in optics, (Editor: WOLF E.).

North Holland Publishing Company, 1964. Volume 3, Section 2.

KINSLER L. and FREY A.

Fundamentals of acoustics.

Wiley, 1962. 2nd edition, Chapter 7.

KRAUTKRÄMER J.

"Determination of the size of defects by the ultrasonic impulse echo method."

Brit. J. App. Phys. 10, pp240-245, 1959.

McLAREN S.

"High resolution ultrasonic non-destructive testing."

PhD thesis, The City University, London, 1987.

McLAREN S. and WEIGHT J.P.

"Transmit-receive mode responses from finite-sized targets in fluid media."

J. Acoust. Soc. Am. 82 (6), pp2102-2112, 1987.

MARTIN F.D. and BREAZEAL M.A.

"A simple way to eliminate diffraction lobes emitted by ultrasonic transducers."

J. Acoust. Soc. Am. 49, pp1668-1669, 1971.

MILES J.W.

"Transient loading of a baffled piston."

J. Acoust. Soc. Am. 25, pp200-203, 1953.

OBERHETTINGER F.

"On transient solutions of the baffled piston problem."

J. Res. Nat. Bur. Stan. 65B, pp1-6, 1961.

RAYLEIGH, LORD (J.W. STRUTT).

The theory of sound.

Macmillan, 1896. Volume 2, Chapters 11, 14.

ROBINSON D.E., LEES S. and BESS L.

"Near-field transient radiation patterns for circular pistons."

IEEE Trans. ASSP 22 (6). pp395-403, 1974.

STACEY R.

"Analysis of echo signals from weak or uniform impurities."

(Submitted for publication, 1989.)

STEPANISHEN P.R.

"The time-dependent force and radiation impedance on a piston in a rigid infinite planar baffle."

J. Acoust. Soc. Am. 49 (2), pp841-849, 1971a.

STEPANISHEN P.R.

"Transient radiation from pistons in an infinite planar baffle."

J. Acoust. Soc. Am. 49 (2), pp1629-1638, 1971b.

STEPANISHEN P.R.

"Acoustic transients from planar axisymmetric vibrators using the impulse response approach."

J. Acoust. Soc. Am. 70 (4), pp1176-1181, 1981.

UEDA M. and ICHIKAWA H.

"Analysis of an echo signal reflected from a weakly scattering volume by a discrete model of the medium."

J. Acoust. Soc. Am. 70 (6), pp1768-1775, 1981.

WEIGHT J.P. and HAYMAN A.J.

"Observations of the propagation of very short ultrasonic pulses and their reflection by small targets."

J. Acoust. Soc. Am. 63, pp396-404, 1978.

WEIGHT J.P.

"Improved resolution transducers and systems for the transmission and/or reception of waves propagated by vibration."

UK Patent No. GB 2 094 100 A, 1982a.

WEIGHT J.P.

"The propagation and reception of wide-band ultrasonic pulses."

PhD thesis, The City University, London, 1982b.

WEIGHT J.P.

"New transducers for high-resolution ultrasonic testing."

NDT International 17 (1), pp3-8, 1984a.

WEIGHT J.P.

"Ultrasonic beam structures in fluid media."

J. Acoust. Soc. Am. 76 (4), pp1184-1191, 1984b.

WEIGHT J.P. and RESTORI M.

"Diffraction effects in the pulsed and continuous wave fields."

In: Conference Proceedings, Ultrasound in Medicine, Bath, UK, 1986.

The Institute of Acoustics, 1986. pp103-111.

WEIGHT J.P. and GATCOMBE C.P.

"High resolution ultrasonic instrumentation."

SERC final report (GR/B/9289.8), 1986.

WEIGHT J.P.

"A model for the propagation of short pulses of ultrasound in a solid."

J. Acoust. Soc. Am. 81 (4), pp815-826, 1987.

YOUNG T.

"On the theory of light and colours."

Phil. Trans. Roy. Soc. 20, pp12-48, 1802.

ZEMANEK J.

"Beam behaviour within the nearfield of a vibrating piston."

J. Acoust. Soc. Am. 49, pp181-191, 1971.